UNIVERSITÀ DEGLI STUDI DI MILANO

SCUOLA DI DOTTORATO
Scuola di Dottorato Terra, Ambiente e Biodiversità

DIPARTIMENTO
Scienze della Terra "Ardito Desio"

CORSO DI DOTTORATO
Scienze Naturalistiche e Ambientali
(XXVIII ciclo)

TESI DI DOTTORATO DI RICERCA

Applicazione di tecniche remote sensing per lo studio dell'evoluzione e della dinamica criosferica in aree remote e di alta quota

---

Remote sensing investigations to analyse evolution and dynamics of the cryosphere in remote and high elevation areas

S.F.D. GEO04 – Macroarea 04/A3

Dott. Umberto Minora
Matricola R10238

TUTOR
Prof. Claudio Smiraglia

CO-TUTOR
Prof. Mauro Guglielmin
Prof Guglielmina Diolaiuti
Prof. Daniele Bocchiola

COORDINATORE DOTTORATO
Prof. Nicola Saino

A.A. 2014/2015

Contents

Abstract....1
Riassunto....4
Chapter 1....7
Introduction....8
1.Aims....8
2.Remote sensing of the cryosphere....9
3.Thesis organization....12
References....13
Chapter 2....15
Glacier area stability in the Central Karakoram National Park (Pakistan) in 2001–2010 — the "Karakoram Anomaly" in the spotlight....16
Abstract....16
1.Introduction....17
2.Study site....18
3.Materials and methods....20
3.1The CKNP glacier inventory....20
3.2Supraglacial debris mapping....21
3.3Glacier outline and error assessment....21
3.4Snow cover data....23
3.5Climate data analysis....24
4.Results....26
4.1Glacier changes during 2001–2010....26
4.2Snow cover validation and variability....32
4.3Climate trends....37
5.Discussion....40
5.1The relation between climate change and glacier stability in the CKNP....41
5.2Difference between debris-free and debris-covered glaciers in the CKNP....42
5.3The contribution of the surging events to the CKNP glacier area change....43
5.4Comparison with the other glacier inventories....44
6.Conclusions....46
References....47
Chapter 3....56
A simple model to evaluate ice melt over the ablation area of glaciers in the Central Karakoram National Park, Pakistan....57
Abstract....57
1.Introduction....58
2.Study site....60
3.Methods....62
3.1Distribution of the meteorological parameters....63
3.2Distribution of the debris thickness....64
3.3Melt over debris-covered areas....67
3.4Melt over debris-free areas....68
4.Results....69
5.Discussion....75
6.Conclusions....80

References....81
Chapter 4....87
2008–2011 snow covered area (SCA) variability over 18 watersheds of the central Chile through MODIS data....88
Abstract....88
1.Introduction....89
2.Study site....89
3.Materials and methods....90
4.Results and discussions....92
4.1Northern zone....94
4.2Central zone....95
4.3Southern zone....95
5.Conclusions....96
References....96
Chapter 5....98
Remote sensing and interdisciplinary approach for studying glaciers....99
Abstract....99
1.Introduction....100
2.Remote sensing for the study of mountain glaciers. A literary review and some didactical considerations....101
3.Miage glacier....108
3.1Analysis of the Miage glacier satellite images....109
4.Freney glacier....113
4.1Analysis of the Freney glacier satellite images....114
5.Kilimanjaro glaciers....115
5.1Analysis of Kilimanjaro glacier satellite images....116
6.Harding Icefield....118
6.1Analysis of Harding Icefield satellite images....119
7.Aletsch glacier....120
7.1Analysis of the Aletsch glacier satellite images....121
8.Drygalski ice tongue....124
8.1Analysis of the Drygalski ice tongue satellite images....125
References....127
Chapter 6....134
Conclusions....135
References....138
Curriculum Vitae....139
List of Publications....140

Abstract

Glaciers are sensitive climate indicators because they adjust their size in response to changes in climate (e.g. temperature and precipitation). The attention paid by the scientists to mountain glacier change is increasing as there are robust evidence of a global glacier shrinkage over the past five decades, which in turn is the consequence of global warming. Understanding the glacier response to climate change is of tremendous importance not only for improving scientific knowledge, but also to predict and manage water resources and natural risks for the people living in mountain areas in the short (e.g. glacier lake outburst floods), and long term (e.g. droughts).

In this thesis are analysed different cryospheric elements (mainly glaciers and snow coverage) to describe their recent evolution and to look for relations, if any, with climate trends.

Firstly, the focus is put on the Karakoram glaciers. Although a general worldwide retreat of mountain glaciers has been acknowledged by the scientific community, the Karakoram region represents an exception in this sense. Indeed, the net mass balance of the glaciers here in the early twenty-first century was slightly positive, and even some are expanding and thickening. This anomalous behaviour is known as Karakoram Anomaly.

More precisely the study area is the Central Karakoram National Park (CKNP), a protected national park in Northern Pakistan representative of the glaciation of the whole Karakoram Range. The westerlies represent the dominant wind system and they occur during winter, while the neighbour Himalayan region is mainly influenced by the summer moonson. A comprehensive description of the state of the CKNP glaciers and of their recent evolution is presented. This was made after the compilation of the glacier inventory of the park for the years 2001 and 2010, which is also presented. Moreover, the analysis of the regional climate change in the recent years is also discussed and related to the actual glacier change, in order to understand the causes behind the Karakoram Anomaly. The glacier area change of the 711 glaciers mapped in the study zone during 2001–2010 was only -0.4 ± 202.9 km^2 (over 4605.9 ± 86.1 km^2 in 2001), evidencing a general stability. The climate analysis supports glacier stability in the area. A slight increase in late summer snow cover area during 2001–2010 was observed from MODIS snow data. At the same time, the available weather stations revealed an increase of snowfall events and a decrease of mean summer air temperatures since 1980, which would translate into more persistent snow cover during the melt season. These results support an enhanced glacier preservation in the ablation areas due to a long-lasting snow cover, and stronger accumulation at higher altitudes, pushing towards positive net balances.

The other major aim of the present work is to provide a simple model to evaluate ice melt at the glacier surface. As the supraglacial-debris cover can alter ice ablation close to the glacier surface depending on its thickness, the model was made up of two parts: one which computes the ice melt over the bare ice areas using an enhanced T-index formula; and one for the debris-covered areas

using a conductive heat flux module. For the debris-covered parts, the debris thickness map is produced and then provided to the model as input for the computation, other than the distributed shortwave incoming radiation. For the bare ice areas, the modeled air temperature and shortwave incoming radiation are derived from the automatic weather stations present in the CKNP and given to the model. The other model requirement is the digital elevation model. In particular, the meteorological input data were distributed starting from data acquired at Askole automatic weather station, located within the CKNP. The meteorological distribution was validated by comparison with data from other two AWS in the same park limits (Urdukas and Concordia). The modeled ablation data were in strong agreement with measurements collected in the field during 2011 on Baltoro glacier, which is representative of CKNP glaciers. Two sets of the same ablation dataset collected in the field in the CNKP area were used separately for calibration and validation. Snow melt was neglected since snow data in the study area was not systematically available.

The model was run against the peak ablation season (23 July–9 August 2011), when meltwater mainly comes from ice melt, with snow thaw playing a minor role in this region. The total freshwater from the ablation areas of CKNP glaciers estimated by the model was 1.963 km^3 (0.109 km^3 d^{-1} on average). The meltwater from the debris-covered parts was 0.223 km^3 (0.012 km^3 d^{-1} on average; min–max 0.006–0.016 km^3 d^{-1}), and 1.740 km^3 (0.097 km^3 d^{-1} on average; min–max 0.041–0.139 km^3 d^{-1}) from debris-free sectors. The estimated total freshwater corresponds to 14% of the water contained in a large strategic dam along the Indus River, of which all the CKNP glaciers are tributaries. The sensitivity tests suggest that any increase in the extent of debris coverage (which will likely occur due to augmented macrogelivation processes and rockfall events), will affect melt depending on new debris thickness, and melting will increase largely if summer air temperature increases.

The second major focus of this research is put on the snow cover variability of the Chilean Andes.

A parallel major aim of this research work is to implement a methodology based on remote sensing to study the snow cover variation on an acceptable spatio-temporal resolution. The MODIS sensor was chosen as the most suitable for this purpose and a methodology for deriving snow maps automatically from it is described and applied for analyzing the SCA variation over 18 watersheds of the central Andes in Chile during 2008–2011. The same methodology was then adopted for the climate analysis in the CKNP as mentioned.

The study area was divided into three sub-zones (Northern, Central, and Southern), for easing the computation of the snow analysis. Overall, SCA decreased during the four considered years. The maximum SCA was found in the Central Zone, while the topographic and climatic features (i.e. lower altitudes in the South, and a drier climate in the North), limited snow deposition elsewhere. The snow line was found higher in the Northern zone due to the presence of the plateau, while it decreases southwards. In the Northern Zone the minimum SCA was reached sooner than elsewhere, and it lasted for a longer period (November to March), probably because of the drier climate. West aspects showed the maximum of SCA in all zones throughout the study period.

Finally, some examples of application of remote sensing to glacier related studies is presented for glaciers of various typology, size, and localization. Six case studies are shown, amongst which there are three alpine glaciers (Miage, Freney, Aletcsh), equatorial glaciers (the Kilimanjaro glaciers), the Harding Icefield in Alaska, and an Antarctic glacier (the Drygalsky Ice Tongue).

Riassunto

I ghiacciai sono efficaci indicatori climatici poichè si modificano in risposta ai cambi del clima (es. temperatura e precipitazioni). L'attenzione sui ghiacciai di montagna sta aumentando tra la comunità scientifica per via del loro sempre più evidente arretramento a scala globale negli ultimi cinquant'anni. Ciò è conseguenza del riscaldamento globale. Comprendere il comportamento dei ghiacciai in risposta al cambio climatico è di enorme importanza non solo per arricchire la conoscenza scientifica, ma anche per poter meglio gestire in futuro le situazioni di rischio naturale che possono colpire le popolazioni che vivono nelle zone montuose, sia nel breve termine (es. GLOF), sia nel lungo (es. Siccità).

Questa tesi di dottorato analizza differenti aspetti della criosfera (ghiacciai e neve) per descriverne la variabilità recente e le relazioni con la dinamica climatica.

Inizialmente ci si è concentrati sul Karakorum. Questa è un’area particolare per gli studi criosferici, che non segue i trend globali di regresso; infatti, in questa zona il bilancio di massa netto dei ghiacciai nei primi anni del ventunesimo secolo è stato leggermente positivo, con anche taluni casi di espansione. Questa eccezionale situazione è riconosciuta con il nome di Anomalia del Karakorum (*Karakoram Anomaly*).

Più precisamente il presente elaborato si focalizza sulla zona del *Central Karakoram National Park* (CKNP), un'area protetta nel nord del Pakistan, rappresentativa della glaciazione dell'intera catena del Karakorum. In questa regione, i venti occidentali rappresentano il sistema di venti dominante e sono presenti nella stagione invernale, mentre la confinante regione Himalayana è sotto l'influenza predominante dei monsoni, che sono venti estivi. Il presente lavoro descrive in maniera completa lo stato dei ghiacciai del CKNP e la loro recente evoluzione. Ciò è stato possibile a seguito della compilazione del catasto glaciale del parco per gli anni 2001 e 2010, a sua volta descritto nel dettaglio nel presente elaborato. Inoltre è discussa l'analisi dei cambiamenti climatici poi messa in relazione con quelli glaciali, per poter comprendere le cause dietro l'Anomalia del Karakorum. Il cambiamento areale dei 711 ghiacciai mappati nell'area di studio è stato -0.4 ± 202.9 km^2 (su 4605.9 ± 86.1 km^2 nel 2001), il che evidenzia una generale situazione di stabilità. Anche l'analisi climatica supporta tale condizione di stabilità. Durante il periodo 2001–2010 si è osservato grazie ai dati del sensore MODIS un leggero aumento delle aree coperte da neve a fine estate. Allo stesso tempo, dati meteo dalle stazioni disponibili hanno rivelato un aumento delle nevicate e una diminuzione della temperatura media dell'aria in estate fin dal 1980, il che si tradurrebbe in coperture nivali più persistenti durante la stagione ablativa. Questi risultati vanno a favore della preservazione glaciale nelle zone di ablazione dovuta a una copertura di neve più duratura, e un maggiore accumulo a quote più alte, presupponendo bilanci di massa netti tendenti al segno positivo.

L'altro principale obiettivo del presente elaborato di tesi è quello di fornire un modello di semplice

utilizzo per quantificare l'ablazione di ghiaccio alla superficie glaciale. Dal momento che una copertura detritica sopraglaciale è in grado di alterare la fusione del ghiaccio vicino alla superficie in funzione dello spessore, il modello tiene conto di due diversi casi: una parte stima l'ablazione per le aree di ghiaccio scoperto con un metodo definito *enhanced T-index*; l'altra stima la fusione per le zone coperte da detrito, utilizzando un modello di flusso di calore conduttivo. Per quanto concerne le parti coperte da detrito, è stata prodotta una mappa degli spessori detritici che è poi stata usata come input per il modello, assieme alla radiazione solare entrante distribuita. Per le aree scoperte da detrito, sono state derivate la temperatura dell'aria e la radiazione entrante distribuite attraverso i dati delle stazioni meteo automatiche presenti nell'area, in seguito usate come input. L'altro parametro necessario è un modello di elevazione del terreno. In particolare, la distribuzione degli input meteorologici è stata validata con dati di altre due stazioni presenti all'interno del CKNP (le stazioni di Urdukas e Concordia). L'ablazione modellata è risultata essere fortemente concorde con le misurazioni effettuate sul ghiacciaio del Baltoro nel 2011, ghiacciaio rappresentativo di tutto il CKNP. Due campioni dello stesso set di dati di fusione misurati su terreno sono stati usati ciascuno rispettivamente in sede di calibrazione e validazione. La fusione nivale è stata ignorata dal momento che mancavano dati di neve sistematici nell'area di studio.

Il modello è stato fatto girare durante il picco della stagione ablativa (23 luglio–9 agosto 2011), durante il quale l'acqua di fusione deriva primariamente dalla fusione glaciale, mentre quella nivale ha un ruolo decisamente minore in questa regione. Il modello ha calcolato un totale di acqua da fusione glaciale pari a 1.963 km^3 (0.109 km^3 al giorno in media). Quella derivante dalle parti coperte da detrito ammonta a 0.223 km^3 (0.012 km^3 al giorno in media; min–max 0.006–0.016 km^3 al giorno), mentre per le parti a ghiaccio scoperto è 1.740 km^3 (0.097 km^3 al giorno in media; min–max 0.041–0.139 km^3 al giorno). Tale quantità è paragonabile al 14% di tutta l'acqua contenuta in una grande diga strategica lungo il fiume Indo, di cui i ghiacciai del CKNP sono tributari. I test di sensitività del modello suggeriscono che un aumento delle superfici coperte da detrito sui ghiacciai (probabile per via dell'aumento di eventi di macrogelivazione e di frane) avrà un notevole impatto sulla fusione effettiva in funzione dei nuovi spessori detritici, e l'ablazione aumenterà sensibilmente se la temperatura dell'aria dovesse alzarsi.

Successivamente l'attenzione del presente elaborato di tesi è concentrata sulle Ande Cilene e sulla variabilità della copertura nevosa. Un obiettivo principale parallelo della presente ricerca è stato infatti quello di individuare una metodologia basata sul telerilevamento per studiare la variazione della copertura nevosa ad una risoluzione spazio-temporale accettabile. Il sensore MODIS si è rivelato il più idoneo allo scopo ed è stata implementata una metodologia che permettesse di estrarre mappe di copertura di neve in maniera automatica dalle informazioni raccolte dal sensore stesso. In particolare, sono stati studiati diciotto bacini idrografici di montagna delle Ande centrali in Cile durante il periodo 2008–2011. La stessa metodologia è stata esportata e adottata per l'analisi della neve nel CKNP come detto.

L'area di studio è stata divisa in tre sotto-zone (Settentrionale, Centrale, Meridionale), per

alleggerire il carico di calcolo dell'analisi. In generale, l'area coperta da neve è diminuita nel corso dei quattro anni di riferimento. I valori massimi sono stati ritrovati nella zona centrale, mentre fattori topografici e climatici (i.e. quote basse più a sud e un clima più arido nel nord), hanno limitato la deposizione della neve nelle altre zone. La linea della neve è più alta nella zona settentrionale a causa della presenza dell'altopiano, e si abbassa via via verso la zona merdionale. Nella zona settentrionale i minimi di copertura nivale vengono raggiunti prima che nelle altre zone e durano più a lungo (da novembre a marzo), probabilmente a causa del clima più arido. Durante l'intero periodo i valori massimi di copertura nevosa si ritrovano verso ovest.

Al termine dell'elaborato e pertinente al tema principale delle applicazioni del telerilevamento allo studio della criosfera, sono presentati alcuni esempi di analisi di ghiacciai di diversa tipologia, dimensione e area geografica. Si tratta di sei casi, fra cui sono presenti tre ghiacciai alpini (Miage, Freney, Aletcsh), ghiacciai equatoriali (i ghiaccia del Kilimajaro), l'Harding Icefield in Alaska e un esempio di ghiacciaio antartico (la Drygalsky ice Tongue).

Chapter 1

Introduction

1. Aims

The present research is about the application of remote sensing techniques to studying the state of glaciers —and in general of the cryosphere— in remote areas. In particular, the state of the glaciers of the Central Karakoram National Park (CKNP) in Pakistan, and the snow cover variability of the central Andes in Chile are the two major topics addressed and detailed here.

The research started with the continuation of the work carried out by the same author during his master thesis, when he and his tutors were dealing with the compilation of the glacier inventory of the CKNP. Therefore, the first aim was to provide a complete inventory, including the glacier outlines and their most important parameters (area, perimeter, length, elevation, etc.). In this phase, the images from the Landsat satellites were used as the basis for the glacier delineation which was performed with a geographic information system (GIS). The final CKNP glacier inventory includes 711 glacier bodies covering ~4600 km^2, and it refers to the year 2001. These same outlines were used against other Landsat images of 2010 and modified to fit the actual perimeter of this year, in order to produce a new dataset and permit the temporal analysis between the two reference years (2001 and 2010).

The second major objective was then to analyze the temporal evolution of the glaciers of the CKNP during 2001–2010. The choice of the study area (about 13,000 km^2 wide) is strategical, as i) it hosts the largest glaciers of the Karakoram Range, ii) it is widely covered by ice (for about the 40%), and iii) its glacierized area is ~30% of the total glacier surface of the Karakoram Range within Pakistan (total area from Bajracharya and Shrestha, 2011). For these reasons, the CKNP is representative of the whole Karakoram Range glaciation. The attention paid to this area has increased since the last decade, as it turns out to be one of the few regions in the world where glaciers are stable, in contrast to the general glacier retreat observed worldwide on average. This condition is also known with the name of “Karakoram Anomaly” (Hewitt, 2005).

The area change of the CKNP glaciers during 2001–2010 confirms the Karakoram Anomaly, being this difference smaller than 1km^2. The research then focused on the possible causes of the anomaly (third aim): first, the snow cover variation during the study period was analyzed through the Moderate Resolution Imaging Spectroradiometer (MODIS) snow data; second, a climate analysis was performed over the climate data of 1980–2009 from three meteorological weather stations in the area; finally, a supraglacial-debris was mapped for all the inventoried glaciers to understand the role of debris cover in the context of the Karakoram Anomaly. Indeed, debris can alter ice melting depending on its thickness (Mattson and others, 1993), grain size, lithology (Juen and others, 2013), moisture, and porosity (Nicholson and Benn, 2006).

On 2011 the group of glaciologists of the University of Milan carried out a field campaign on the Baltoro glacier (the largest glacier of the CKNP), during which they also measured supraglacial-

debris thickness at different sites. These measurements and the debris map of the CKNP glaciers derived through remote sensing were used as the basis to build up a model to calculate ice melt for the ablation areas of the glaciers in the park. The aim was to provide a distributed model which behaves differently whether the ice melt is calculated on a debris-free or on a debris-covered pixel. The two major outcomes of the model are: i) the estimation of the amount of freshwater derived from ice melt, and ii) the estimation of the rate of mitigation of a debris cover on the overall ice melt.

During the development of the research related to the CKNP area, a parallel work was conducted to carry on the analyses performed in Chile by the author and some colleagues just after earning the Master's degree. The aim was to analyze the snow cover variability (SCA) of the central Andes of Chile during 2008–2011 over eighteen watersheds. The methodology implemented to achieve the result was then adopted also for the CKNP area, and it is detailed in the following chapters. The results were then organized in the form of a scientific paper (Chapter 4).

Following is a list that summarizes the objectives of the present study:

1. Producing a detailed glacier inventory for the CKNP area for the years 2001 and 2010;
2. Studying the glacier changes occurred during 2001–2010 in the CKNP;
3. Relating the glacier and climate changes of the CKNP to the Karakoram Anomaly;
4. Producing an ablation model for the glaciers of the CKNP, to estimate the amount of ice melt and the influence of the supraglacial-debris cover;
5. Implementing a methodology to analyze the snow cover variability over the central Andes in Chile and over the Karakoram region.

2. Remote sensing of the cryosphere

Remote sensing is the science and art of obtaining information about an object, area, or phenomenon through the analysis of data acquired by a device that is not in contact with the object, area, or phenomenon under investigation (Lillesand and others, 2014).

Some data are acquired as photographs by cameras, others are collected from sensors as digital information and converted into images by a computer. Sensors can measure data in certain segments of the electromagnetic spectrum (EMS), and can be carried by various types of vehicle (e.g. an airplane), or can be on board satellites. The EMS describes the continuous spectrum of energy from gamma rays to radio waves (figure 1).

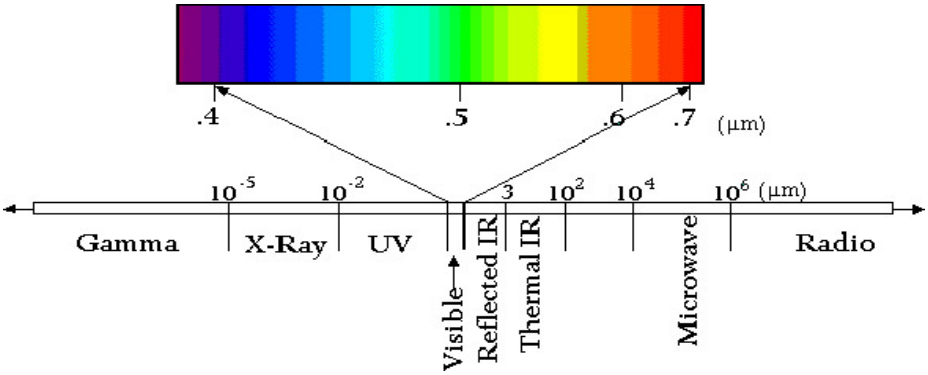

Figure 1: Electromagnetic Spectrum (source: landsat.usgs.gov)

Most, but not all, remote sensing systems used for snow and ice involves either measuring the emission of electromagnetic radiation from the surface (passive techniques) or the reflection or scattering of incident electromagnetic radiation from the surface (active techniques, Vaughan and Cracknell, 2013). In passive sensors, two important physical properties of snow and ice are:

- reflectivity or albedo, which is the fraction of incoming solar radiation which is reflected from the surface,adding together both the direct surface reflection and volume scattering from within the snow or ice;
- emissivity, the power emitted from a surface as a fraction of the power emitted at that frequency by a perfect black body of the same physical temperature.

In the present dissertation, two major passive multispectral sensors were used: the Enhanced Thematic Mapper + (ETM+, and its previous version Thematic Mapper, TM) on board the Landsat satellite, and the Moderate Resolution Imaging Spectroradiometer (MODIS) on board the Terra and Aqua satellites. As said, both are multispectral sensors, namely able to measure reflected energy within several specific sections (called bands). In particular, the ETM+ has seven bands (plus one panchromatic band): three bands collect data in the visible and near infrared fraction (VNIR, band 1 to 4); two in the shortwave infrared (SWIR, band 5 and 7); and one in the thermal infrared (TIR, band 6). The wavelength value for each Landsat band is shown in figure 2, together with another satellite, the Advanced Spaceborne Thermal Emission and Reflection Radiometer (ASTER).

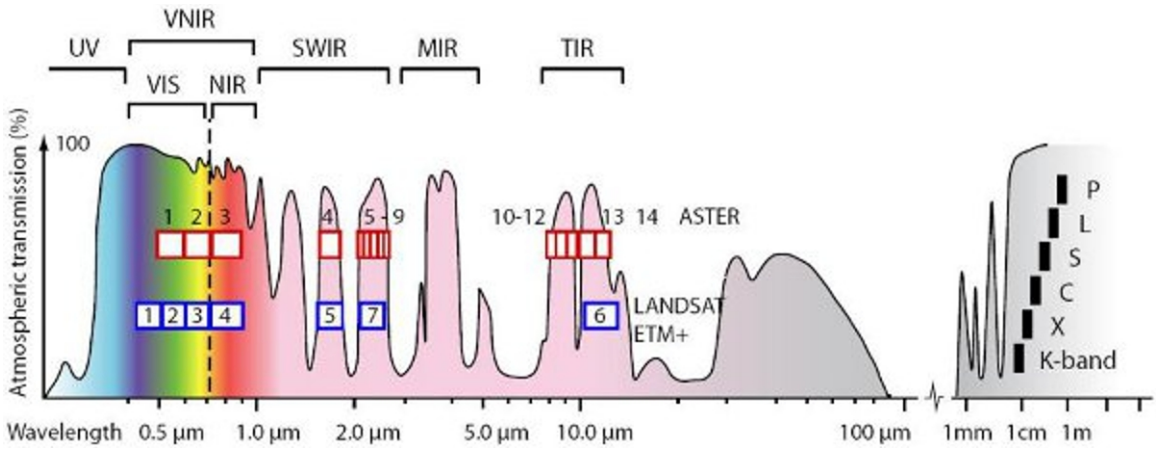

Figure 2: The Landsat and ASTER spectral bands (source: Duda and others, 2009)

By assigning any 3 spectral band into the trhee colors (red, green, blue), one can create a colored image that give the human eyes the ability to see data attributes that are not visible to them otherwise (e.g. SWIR, TIR).

Deriving glacier outlines from satellite data has become increasingly popular in the past decade (Paul and other, 2013). A number of accurate methods for automated mapping of clean ice (e.g., free of debris cover) and snow by means of multispectral classification is available, for example from thresholded ratio images with band 4/band 5 (e.g., Paul and others., 2002; Sidjak and Wheate, 1999; Williams and Hall, 1998). However, a wide range of issues have to be considered to delineate glaciers, for example the interpretation of seasonal and/or perennial snowfields, handling of glaciers covered (partly) by clouds, identification of drainage divides in the accumulation region, the correct delineation of debris-covered glaciers, the determination of the terminus for calving glaciers or those with dead ice, or the interpretation of invisible glacier boundaries in cast shadow (Paul and others, 2013). Thus, further manual correction may be needed in order to adjust the glacier outlines derived automatically to the actual limits. As regards the debris-covered glaciers, higher resolution images can lead to more precise delineation. Nevertheless, these limits are not easy to recognize even during manual digitization. In general, the higher the color contrast between features in the image, the easier it gets to recognize a glacier perimeter. Unfortunately, high-resolution images have in general fewer spectral bands than the medium- to low-resolution ones, and therefore it is not always possible to obtain a high detail and a good color contrast at the same time. The Landsat satellite has 30 meters of resolution, with the possibility to combine the panchromatic band to increase the resolution to 15 meters. Moreover, its temporal resolution is 16 days. This makes this satellite a valuable choice for glacier mapping.

The MODIS sensor on board the Terra and Aqua spacecrafts has a coarser resolution than Landsat, (2km, 1km, 500m, and 250m, depending on the band), but an almost daily temporal resolution, and 36 bands. Moreover, it has a swath width of 2330 km (cross track), against 185 km of the Landsat satellite. This makes this sensor preferable for large scale studies.

The National Snow and Ice Data Center (NSIDC) provides pre-processed snow and sea data derived from the same MODIS sensor. In particular, the MOD10A1 and MOD10A2 products contain snow cover, snow albedo, and fractional snow cover ready to use data. These datasets are based on a snowmapping algorithm that employs a Normalized Difference Snow Index (NDSI) and other criteria (Hall and others, 2006). A methodology which uses the MOD10A2 snow product was used by the author of this dissertation for assessing the snow cover variability during 2008–2011 in the central Andes of Chile. The procedure is described in the dedicated chapter.

3. Thesis organization

The present research pursued the aims listed and described in the above section. The progresses are documented in the next chapters in the form of scientific articles, most of which were published on international journals. In particular:

- aims 1, 2, and 3 are addressed in chapter 2 (“Glacier area stability in the Central Karakoram National Park (Pakistan) in 2001–2010 — the “Karakoram Anomaly” in the spotlight”);
- aim 4 is addressed in chapter 3 (“A simple model to evaluate ice melt over the ablation area of glaciers in the Central Karakoram National Park, Pakistan”);
- aim 5 is addressed in chapter 4 (“2008–2011 snow covered area (SCA) variability over 18 watersheds of the central Chile through MODIS data”).

Chapter 2 deals with the compilation of the CKNP glacier inventory, detailing the materials and methods which lead to the final product. Moreover, after describing the results derived from the same inventory, the analysis of the glacier area change during 2001–2010 is shown. As the temporal analysis suggests that no significant change occurred, the main focus of the rest of the chapter is put on investigating the causes of such stability, also known as Karakoram Anomaly. In particular, the SCA change occurred during 2001–2011 is analyzed through MODIS snow data. Then, the climate change occurred since 1980 was investigated by analyzing climate data from three automatic weather stations (AWS) of the Pakistan Meteorological Department (PMD).

In chapter 3, a model to evaluate ice melt over the ablation area of the same CKNP glaciers is described. It is a distributed model which computes ice melt for each pixel within the glacier outlines provided in the CKNP inventory. The model requires meteorological inputs to work (temperature and shortwave radiation from AWS). The supraglacial-debris coverage for each glacier is computed with a supervised classification (maximum likelihood algorithm) against Landsat images. The equations used to compute ice melt in the model are different for debris-free (Pellicciotti and others, 2005) and debris-covered pixels (Mihalcea and others, 2008). The final output is the sum between the ablation derived from the debris-free and the debris-covered areas, over the time window considered (23 July–9 August 2011).

Chapter 4 deals with the study of the SCA variation over the central Andes in Chile during 2008–2011. The study is conducted over eighteen mountain watersheds covering more than 200,000 km^2,

and furthers a previous study performed by the Direccíon General de Aguas of the Chilean Government (DGA, 2008). This chapter describes the implementation of a method which processes snow data derived from MODIS sensor to extract snow maps on a daily basis, discarding those days with too much cloud cover. The method combines a GIS with Python programming language for automation purposes.

An additional chapter (chapter 5) describing a work made in conjunction with the Sapienza University of Rome was also included in this thesis. It describes some case studies of remote sensing applied to glaciers of various typology, size, and localization (“Remote sensing and interdisciplinary approach for studying glaciers”).

First, three alpine glaciers are presented. The first is the Miage glacier, which is the largest debris-covered glacier in Italy; the second is the Freney glacier, which is an example of a small, steep-mountain alpine glacier located in the Mont Blanc massif (Graian Alps), next to Miage; the last one is the Aletsch glacier, a clean-ice glacier of the Berner Alps (Valais) in Switzerland, which is also the largest glacier found in the Alps.

Following, the Kilimanjaro glacier is described, the most emblematic example of the impact of the global warming on glaciers. Then, the Harding Icefiled, in the Kenay Mountains of Alaska is included in the chapter as the largest icefield entirely contained within the boundaries of the United States. Finally, an example from the Anctartic: the Drygalsky Ice Tongue. Here, the benefit from having a broad wavelength of the electromagnetic spectrum being registered by the OLI sensor of the Landsat 8 satellite is shown.

Eventually, chapter 6 summarizes the major outcomes and conclusions achieved in the present research work.

References

Bajracharya S.R., Shrestha B. (eds) (2011) The status of glaciers in the Hindu Kush-Himalayan region. Kathmandu: ICIMOD.

DGA, Direcciòn General de Aguas (2008) Dinámica de la cobertura nival entre las cuencas de los ríos Copiapó y Petrohue utilizando imágenes satelitales. Dirección General de Aguas, Unidad de Glaciología y Nieves, Santiago de Chile.

Duda K.A., Ramsey M., Wessels R. and Jonathan Dehn (2009) Optical Satellite Volcano Monitoring: A Multi-Sensor Rapid Response System. Geoscience and Remote Sensing, Chapter 22, Ed. Pei-Gee Peter Ho, DOI: 10.5772/8303.

Hall D.K., Salomonson V.V. and Riggs G.A. (2006) MODIS/Terra Snow Cover Daily L3 Global 500m Grid, Version 5. Boulder, Colorado USA. NASA National Snow and Ice Data Center Distributed Archive Center.

Hewitt K. (2005) The Karakoram Anomaly? Glacier expansion and the “elevation effect”,

Karakoram Himalaya. Mt. Res. Dev. 25: 332-340.

Juen M., Mayer C., Lambrecht A., Wirbel A. and Kueppers U. (2013) Thermal properties of a supraglacial debris layer with respect to lithology and grai size. Geografiska Annaler: Series A, Physical Geography, Vol. 95, Issue 3, 197–209.

Lillesand T., Kiefer R.W. and Chipman J. (2014) Remote sensing and image interpretation, Sevent Edition, Wiley ed.

Mattson L.E., Gardner J.S. and Young G.J. (1993) Ablation on debris covered glaciers: an example from the Rakhiot Glacier, Punjab, Himalaya. Snow and Glacier Hydrology, Proc. Kathmandu Symp. November 1992, edited by: Young, G. J., IAHS Publ. no. 218, IAHS Publishing, Wallingford, 289-296.

Mihalcea C., Brock B.W., Diolaiuti G., D'Agata C., Citterio M., Kirkbride M.P., Cutler M.E.J. and Smiraglia C. (2008) Using ASTER satellite and ground-based surface temperature measurements to derive supraglacial debris cover and thickness patterns on Miage Glacier (Mont Blanc Massif, Italy), Cold Regions Science and Technology, 52, pp. 341-354.

Nicholson L. and Benn D.I. (2006) Calculating ice melt beneath a debris layer using meteorological data. Journal of Glaciology 52: 178

Paul F., Kääb A., Maisch M., Kellenberger T. and Haeberli W. (2002) The new remote sensing derived Swiss glacier inventory. I: Methods. Annals of Glaciology, 34, 355 – 361.

Paul F., Barrand N.E., Baumann S., Berthier E., Bolch T., Casey K., Frey H., Joshi S.P., Konovalov V., Le Bris R., Mölg N., Nosenko G., Nuth C., Pope A., Racoviteanu A., Rastner P., Raup B., Scharrer K., Steffen S. and Windswold S. (2013) On the accuracy of glacier outlines derived from remote-sensing data. Ann. Glaciol. 54 (63).

Pellicciotti F., Brock B.W., Strasser U., Burlando P., Funk M. and Corripio J.G. (2005) An enhanced temperature-index glacier melt model including shortwave radiation balance: development and testing for Haut Glacier d'Arolla, Switzerland. J. Glaciol., 51, 573–587 (doi: 10.3189/172756505781829124)

Sidjak R.W. and Wheate R.D. (1999) Glacier mapping of the Illecillewaet Icefield, British Columbia, Canada, using Landsat TM and digital elevation data. International Journal of Remote Sensing, 20(2), 273 – 284.

Vaughan R.A. and Cracknell A.P. (2013) Remote Sensing and Global Climate Change, Springer Sciences & Business Media.

Williams Jr R.S., Hall D.K., Sigurdsson O. and Chien J.Y.L. (1997) Comparison of satellite-derived with ground-based measurements of the fluctuations of the margins of Vatnajökull, Iceland, 1973–1992. Annals of Glaciology, 24, 72–80.

Chapter 2

Glacier area stability in the Central Karakoram National Park (Pakistan) in 2001–2010 — the “Karakoram Anomaly” in the spotlight

Article under revision by: **Minora U.**, Bocchiola D., D'Agata C., Maragno D., Mayer C., Lambrecht A., Vuillermoz E., Senese A., Compostella C., Smiraglia C., Diolaiuti G.

Abstract

The Karakoram Range is one of the most glacierized mountain regions in the world, and glaciers therein are an important water resource for Pakistan. The attention paid to this area is increasing because its glaciers remained rather stable in the early twenty-first century, in contrast to the general glacier retreat observed worldwide on average. This condition is also known as “Karakoram Anomaly”. Here we focused upon the recent evolution of glaciers within the Central Karakoram National Park (CKNP, area: ~13,000 km^2), to assess their status in this region with respect to the described anomaly. A glacier inventory was produced for the years 2001 and 2010, using Landsat images. In total, 711 ice-bodies were detected and digitized, covering an area of 4605.9 ± 86.1 km^2 in 2001 and 4606.3 ± 183.7 km^2 in 2010, with abundant supraglacial debris cover. The difference between the area values of 2001 and 2010 is not significant (+0.4 ± 202.9 km^2), confirming the anomalous behavior of glaciers in this region. The causes of such anomaly may be various. The increase of snow cover areas from 2001 to 2011 detected using MODIS snow data, the reduction of mean summer temperatures, and the augment of snowfall events during 1980–2009 observed at meteorological stations and confirmed by the available literature are climatic factors pushing towards positive mass balances. Being the response of glacier area change to climate variation very slow for large glaciers, the presence of some of the largest glaciers of the Karakoram Range in this region might have delayed the effects of the climate change so far, or this latter was not sufficient to drive an actual area increase. In this context, understanding the role of debris cover, meltwater ponds, and exposed ice cliffs on debris-covered glaciers, and surging glaciers (which are found abundant here), is still an issue to clarify the mechanisms behind the Karakoram Anomaly.

1. Introduction

Glaciers are sensitive climate indicators because they adjust their size in response to changes in climate (e.g. temperature and precipitation). There is robust evidence of a global glacier shrinkage over the past five decades (Vaughan and others, 2013). This is also true on a regional scale, with some exceptions. The Hindu Kush Karakoram Himalaya (HKH from here on) displays a heterogeneous picture in this sense.

Recent observations of glacier fluctuations indicate that in the Eastern and Central HKH glaciers are subject to general retreat, and have lost a significant amount of mass and area in the second half of the 20th century (Salerno and others, 2008; Bolch and others, 2011). Rapid declines in glacier area are reported throughout the Greater Himalaya and most of mainland Asia (Bolch and others, 2012; Yao and others, 2012). However, observations of individual glaciers indicate that glacier retreat rates may vary strongly between different glacial basins, and even some advancing glaciers are observed in the Karakoram mountains (Hewitt, 2005; Scherler and others, 2011; Bhambri and others, 2013; Rankl and others, 2014). The Eastern part of the HKH is under the influence of the Indian monsoon, which brings precipitation during summer, while the Western (which includes the Karakoram range) receives most of the annual precipitation during winter and spring, as it is influenced primarily by the westerlies originating predominantly from Mediterranean and Caspian Sea regions (Fowler and Archer, 2006; Bookhagen and Burbank, 2010). This East-West variability in the predominant wind system leads to differences in glacier accumulation in the HKK, and might be one reason for the large spread in detected glacier changes within the region (Bolch and others, 2012; Kääb and others, 2012).

The estimated glacier mass balance budget in the Karakoram positively affected the 2003–2008 specific mass balance for the entire HKH region, which was calculated by Kääb and others (2012) into -0.21 ± 0.05 m yr^{-1} of water equivalent. This is significantly less than the estimated global average for glaciers and ice caps (Cogley, 2009; WGMS, 2013; Gardner and others, 2013). Gardelle and others (2012) show not only balanced to slightly negative mass budgets in the Karakoram Range, but even an expansion and thickening of some glaciers in the Central Karakoram since the early twenty-first century. Hewitt (2005) reported that 33 glaciers thickened (by 5 to 20 m on the lowest parts of their tongues) and advanced, or at least were stagnant in this region between 1997 and 2001. The same author defined the anomalous presence of stagnant and advancing glaciers in the Central Karakoram as Karakoram anomaly.

The climate-glacier relation in the Central Karakoram is still not well understood, and interactions between the cryosphere, the climate, and the hydrosphere in the lower latitudes are of great interest for both global and regional purposes. Glaciers here represent a major source of water for the Indus river, upon which agriculture, human consumption, and power production rely (Bocchiola and Diolaiuti, 2013). Observations of glacier coverage and evolution are then essential to understand the role of the cryosphere in influencing the regional hydrology and water resources in this region. An

in depth scientific understanding of glacier evolution in the Karakoram was hampered hitherto by the lack of systematic long-term field observations, due to the rugged topography and the complex climatology of the area. Therefore, the combination of remote sensing studies and data from field surveys is required for improving the understanding of glacier evolution in Karakoram.

In this contribution, we focused on the protected area of the Central Karakoram National Park (CKNP, ~13,000 km^2), to provide an updated picture of the glacier state in the Central Karakoram and to better characterize the Karakoram anomaly. To this regard, we produced the CKNP glacier inventory using Landsat images from 2001 and 2010. Although other glacier inventories covering the Karakoram region are available (Randolph Glacier Inventory, Arendt and others, 2014; ICIMOD glacier inventory, Bajracharya and Shrestha, 2011; GAMDAM glacier inventory, Nuimura and others, 2015), our work focuses on the specific area of the CKNP only, providing a high-resolution and very detailed inventory. We analyzed the glacier area and supraglacial debris cover change during 2001–2010. Moreover, we analyzed the snow cover area (SCA) change occurred during 2001–2011 using MODIS snow data. Eventually, we investigated the climate change occurred since 1980 by analyzing climate data from three automatic weather stations (AWS) of the Pakistan Meteorological Department (PMD).

2. Study site

The HKH stretches for more than 2000 kilometers in length from West to East, and hosts about 40,000 km^2 of ice bodies (glaciers, glacierets and perennial ice surfaces, http://rds.icimod.org/). The economy of the HKH regions relies upon agriculture, and it is highly dependent upon water availability and irrigation (Aggarwal and others, 2004; Kahlown and others, 2007; Akhtar and others, 2008). Likely more than 50% of the water in the Indus river originating from the Karakoram comes from snow and glacier melt (Immerzeel and others, 2010; Soncini and others, 2015).

In this study, we focus on the area of the CKNP, an extensive (~13,000 km²) protected area in the Northern Pakistan, in the main glaciated region of the Central Karakoram (Figure 1). It was established in 2009, and ~40% of this area is covered by ice. The CKNP hosts the largest glaciers of the Karakoram range (Baltoro, Biafo, and Hispar glaciers, amongst others).

The study area is under the influence of two wind systems: the moonsons in summer, and the westerlies in winter. Anyway, the North moving monsoon storms intrudes only little into the Karakoram because it is mitigated by the Nanga Parbat massif to the South. Therefore, the CKNP is mainly influenced by the westerlies (Bookhagen and Burbank, 2010).

Earlier investigations of Northern Pakistan climate displayed evidence of regional behaviour (Weiers, 1995; Winiger and others, 2005; Soncini and others, 2015). Most notably Bocchiola and Diolaiuti (2013), found three homogeneous climatic regions in Northern Pakistan, one of which was called Northwest Karakoram, which includes the CKNP (Figure 1). This region displays winter and occasional spring and summer rainfall, with precipitation increasing from 150–500 mm at 1500–

3000 m a.s.l. to more than 1700 mm at 5500 m a.s.l.. The winter precipitation provides the dominant nourishment for the glaciers of the HKH (Bocchiola and Diolaiuti, 2013). High elevation snowfall is still rather unknown, due to the diffculty of obtaining reliable measurements. Some estimates from snow pits above 5000 m a.s.l. range from 1000 mm to more than 3000 mm yr^{-1}, depending upon location (Wake and others, 1990; Winiger and others, 2005; Soncini and others, 2015). However, there is considerable uncertainty about the spatial distribution and the vertical gradient of precipitation at high altitudes.

The glaciers in the CKNP show a large variability in size, geometry, type, and surface conditions (i.e. buried and bare ice). They belong to the Shigar and Hunza drainage basins. These are high altitude catchments with summer and annual runoff that is truly governed mostly by glacier and snow melt (Archer, 2003).

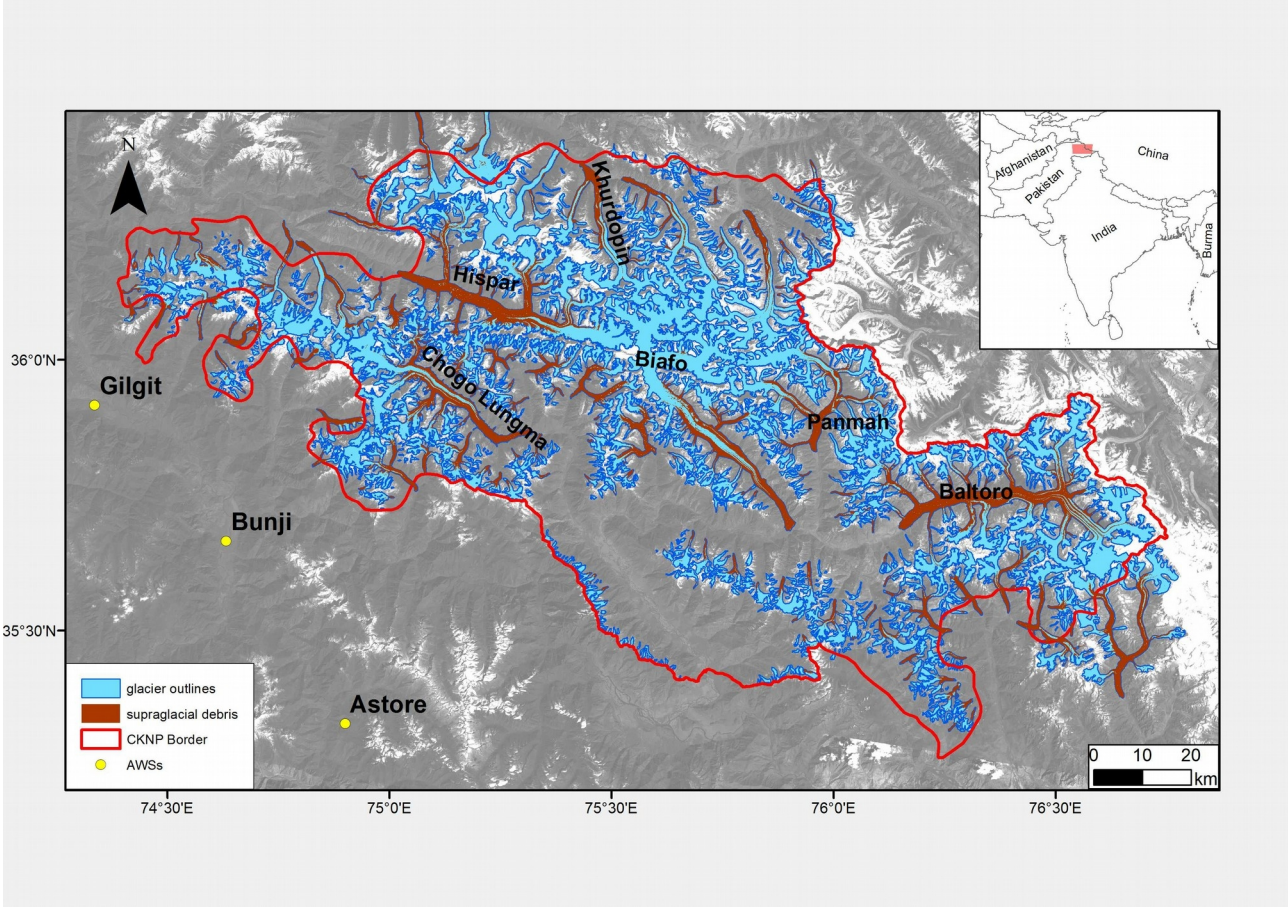

Figure 1: The CKNP, including the glacier outlines, the supra-glacial debris cover and the locations of the AWSs used in this study.

3. Materials and methods

3.1 The CKNP glacier inventory

For the compilation of the CKNP glacier inventory we followed the recommendations by Paul and others (2009), and we considered parameters such as identification code, coordinates, dates of acquisition of the image related to each glacier outline, area, length, minimum, maximum, mean and mean elevation, mean aspect, and slope. We used Level 1T Landsat ETM+ and TM scenes of 2001 and 2010 (Table 1) as the basis for glacier delineation.

Table 1: Landsat imagery used for the analysis. Star symbol (*) indicates the reference images used for glacier delineation, the other ones were used to cross-check the results. The band combination is 543, PAN-sharpened to 15 m for Landsat 7 using the Panchromatic band (band 8).

Date	Scene identification No.	Resolution [m]	Sensor	SCAN line error	Cloud cover over glaciers [%]
21/07/2001	LE71480352001202SGS00*	15	ETM+	No	0.0
30/09/2001	LE71490352001273EDC01*	15	ETM+	No	0.0
23/07/2010	LT51480352010235KHC00*	30	TM	No	0.0
17/10/2010	LT51490352010290KHC00*	30	TM	No	0.0
18/10/2010	LE71480352010291SGS00	15	ETM+	Yes	0.0
12/08/2009	LE71480352009224SGS00	15	ETM+	Yes	0.0
22/08/2010	LE71490352010234EDC00	15	ETM+	Yes	0.1
20/09/2009	LE71490352009263SGS00	15	ETM+	Yes	0.0

Before proceeding to the digitization of the glacier outlines, we first increased the color contrast between the glacier bodies and the surrounding pixels by combining the near infrared and the visible bands of the TM sensor (RGB=543). So doing, we produced false color composite (FCC) images against which we manually digitized each glacier outline separately. The minimum mapped area was 0.01 km^2 as recommended by Paul and others (2009). The debris-free and debris-covered parts of the glaciers were not distinguished in this step. They were split afterwards by identifying the debris pixels within the glacier outlines with a Supervised Classification (see section 3.2).

It is worth to note that the interpretation of the glacier perimeter under debris is not straightforward (Paul and others, 2009), and thus the change analysis may be problematic too. To this end, we cross-checked the position of the actual glacier border under debris with the Landsat images and the high-resolution images from Google Earth. Another crucial aspect in glacier delineation is the location of terminus position. Indeed, it can differ by several hundred meters if glacier outlines were digitized by different analysts (Paul and others, 2013). In this work, the glacier outlines for the two reference

years were drawn by the same analyst, so the change analysis should be reliable. Finally, the definition of the upper glacier boundaries is also a problematic aspect. In general, steep headwalls were excluded from the mapping, similarly to Nuimura and others (2015). The reason is that snow cannot accumulate easily on very steep surfaces (>40°; Nuimura and others, 2015). Moreover, avalanche-fed glaciers prevail in the Karakoram, and many lack an accumulation zone as normally understood (Hewitt, 2011). We used the contour lines derived from the Shuttle Radar Topography Mission 3 DEM (SRTM3, CGIAR-CSI, 2012), to detect the steep slopes in the accumulation areas close to the glacier limits and exclude them from the inventory when there were rock exposed walls covered by thin snow layers or spotty snow patches. However, this criterion might have excluded steep areas in the accumulation zone where snow is present throughout the year, and thus the actual final glacier area might be biased by this exclusion.

Afterwards, we used a Geographic Information System (GIS) to extract topographic parameters based on the glacier outlines and the DEM. The maximum length of each glacier was derived by manually depicting a line from the highest to the lowest altitude within each glacier outline, and passing through the main flow line (according to the contour lines). The mean slope was then calculated for each glacier from elevation range and length data.

Eventually, we identified surging glaciers according to both the magnitude of their termini advance (Cuffey and Paterson, 2010), the presence of looped moraines indicating possible past surge events (Copland and others, 2003), and by comparison against the available literature (Hewitt, 2007; Copland and others, 2011; Quincey and others 2001; Rankl and others, 2014).

3.2 Supraglacial debris mapping

A Supervised Maximum Likelihood (SML) classification on the Landsat FCC image (bands 543) was used to map the supraglacial debris for the years 2001 and 2010. First, the classifier was trained to recognize the supraglacial-debris by choosing appropriate Region of Interests (ROIs). Then, the automatic classification was run against the image of 2001 and then of 2010, on the glaciers only, using the glacier masks of the respective year. So doing we obtained the supraglacial debris maps for both years. Finally, we produced the shadow maps with the same procedure to search for the locations where the glacier area was shaded. This way we were able to identify the areas of possible debris cover excluded by the classification and add them manually to the final map after cross-checking the actual presence of debris with different sources (other Landsat images, Google Earth).

3.3 Glacier outline and error assessment

When dealing with the production of glacier inventories through satellite images, inaccuracies may occur due to classification errors. These depend upon the image resolution and the meteorological and environmental conditions at the time of acquisition, namely cloud- and snow-cover, presence of shadows and debris, hampering ice detection. In the following, the impact of different sources of error are discussed.

Georeferencing error: The geo-referencing accuracy is optimized by the United States Geological Survey (USGS), by means of a correction process based both upon Ground Control Points (GCPs, taken from the 2005 Global Land Survey), and the SRTM DEM (Landsat7 Handbook, 2013). The SRTM DEM is thought to have good accuracy (Falorni and others, 2005). The true geolocation is not too critical for our analysis because our Landsat data are processed in the same way by the USGS.

Linear resolution error (LRE): The image resolution influences the accuracy of glacier mapping. Following Vögtle and Schilling (1999) and Citterio and others (2007), the final planimetric precision value was assessed considering the uncertainty due to the sources (satellite images). The area precision for each glacier was evaluated by buffering the glacier perimeter, considering the area uncertainty. According to O'Gorman (1996), the LRE should be half the resolution of the image pixel, i.e. in our case 7.5 m for the 2001 scenes (because the scenes were PAN-sharpened), and 15 m for the 2010 scenes. This error may be too low for debris pixels, because glacier limits are more difficult to distinguish when ice is covered by debris (Paul and others, 2009). Therefore, we set the error for debris pixels to be three times that of clean ice. The precision of the whole CKNP glacier coverage was estimated as the root squared sum (RSS) of the buffer areas for 2001 and 2010 (Equation 1).

$$AE_{yr} = \sqrt{\sum_{i=1}^{N} \left(p_i * LRE_{yr}\right)^2} \quad , \tag{1}$$

where AE_{yr} is the Areal Error of year 2001 or 2010, pi is the i^{th} glacier perimeter, LRE_{yr} is the LRE of year 2001 or 2010, and N is the total number of glaciers in the inventory. Finally, the total error in area change (AEarea change 2001-2010) was then calculated as the RSS of the areal errors related to each glacier in the 2001 and 2010 (AE2001 and AE2010):

$$AE_{area\,change\,2001-2010} = \sqrt{AE_{2001}{}^2 + AE_{2010}{}^2} \tag{2}$$

Error depending on specific scene conditions: Seasonal snow, cloud cover, presence of shadows and debris can introduce errors in glacier area determination. The scenes were selected to display minimum snow and cloud over the glaciers. In case these features were still present, and to deal with the interpretation of invisible glacier boundaries in cast shadows and the actual perimeter under debris, we used images from different sources (i.e. Landsat and Google Earth) and dates (see Table 1), which enabled us to cross-check the actual glacier limits and to minimize any possible interpretation error.

Error depending on operator's misinterpretation: Because glacier outlines are mapped manually, errors may occur due to the operator's misinterpretation of the image pixels. Nevertheless, although several semiautomated techniques for mapping debris-covered glaciers have been proposed (Paul and others, 2004; Shukla and others, 2010, amongst others), they all require more complex processing, an accurate DEM and final manual editing (Paul and others, 2013). We therefore

preferred the manual approach, trying to reduce any possible misinterpretation error through the choice of an expert eye for the digitization, and a second-round check on the final mapping. Note that this has nothing to do with the automatic classification of the supraglacial-debris, as this was performed after glacier borders were drawn (see previous sections 3.1 and 3.2).

3.4 Snow cover data

We used MODIS MOD10A2-V5 snow product (Hall and others, 2006) to investigate snow-cover variability during 2001–2011 in the CKNP. These data are freely available at the National Snow and Ice Data Center website (NSIDC, 2013). They contain information of maximum snow cover extent over an eight-days period (henceforth the use of a specific "Julian day" refers to the same Julian day and seven days after from here on). Pu and others (2007), reported an average of 90% overall accuracy during 2000–2006 on the Tibetan Plateau using the same product compared with in-situ Chinese snow observations.

We set a threshold for cloud cover to reduce cloud noise in our dataset. We chose 50% cloud cover as the best tradeoff between data reliability and availability, in line with other studies (e.g. Parajka and Blöschl, 2008a).

Because most of the available dataset was not investigated by the NSIDC group for quality check at the time of our analysis, we decided to work only with those images flagged within the NSIDC quality assessment as "INFERRED PASSED". This issue led to the larger loss of data in our time window, especially during winter, when comparatively few images could be retained. We then chose to analyze snow cover dynamics during the ablation season only (from June 18 to September 30), using a total of 37 images. The late summer SCA was used to calculate the late summer Snow Line Altitude (SLA) at the end of the ablation season. We used Julian day 273 as the reference day for late summer SCA, according to the period (i.e. end of the ablation season), and to snow cover minima detected at this day. When this date was not present in the dataset, we used the closest previous date (Table 2). We then inspected the available winter snow coverage to insure the capture of the largest snow cover (SCA_{Max} further on, see section 4.2).

Table 2: Julian days used to calculate late Summer SLA according to data availability.

Year	2001	2002	2003	2004	2005	2006	2007	2008	2009	2010	2011
Julian day	273	241	217	273	201	169	273	273	273	273	273

The results are compared with Thair and others (2011), who studied snow cover in the Hunza basin, North of the CKNP. Because they divided SCA data and trends in three altitude belts (A, B, and C), we divided our dataset much the same way (Table 9 in section 4.2). To provide a meaningful comparison between different years, we compared snow cover at fixed dates. Within the available database of reasonably clear images we chose a number of dates when images were available for

several years. We carried out a linear regression in time of snow cover data for each of these belts to analyze SCA trends over time.

Finally, we validated the MODIS snow product by comparison with several Landsat satellite images of the same period. The comparison and its results are detailed in the Results chapter.

3.5 Climate data analysis

Monthly averaged meteorological variables were provided by the Pakistan Meteorological Department (PMD), derived from measurements at a number of stations in North Eastern Pakistan during 1980–2009. Data from the three closest AWSs to the CKNP area, namely Gilgit, Bunji and Astore (from North to South, Figure 1 and Table 3) are used for this study.

Table 3: Details for the AWSs used in the study, with seasonal averages (1980–2009) of precipitation amounts and air temperature.

AWS	**North [◦]**	**East [◦]**	**Altitude [m a.s.l.]**	**Ave [P_{JFM}] [mm]**	**Ave [T_{JFM}] [°C]**	**Ave [P_{AMJ}] [mm]**	**Ave [T_{AMJ}] [°C]**	**Ave [P_{JAS}] [mm]**	**Ave [T_{JAS}] [°C]**	**Ave [P_{OND}] [mm]**	**Ave [T_{OND}] [°C]**
Astore	35.20	74.54	2168	167	0.5	167	13.8	74	19.3	76	5.8
Bunji	35.40	74.38	1372	26	8.6	66	22.0	51	26.8	18	11.9
Gilgit	35.55	74.20	1460	23	7.4	61	20.6	37	25.0	17	10.1

The AWSs altitudes range from 1460 m a.s.l. (Gilgit) to 2168 m a.s.l. (Astore), which is rather low in comparison with the hypsography of the CKNP. Given the large precipitation lapse rates expected within the upper Karakoram (Winiger and others, 2005; Wulf and others, 2010; Bocchiola and others, 2011), precipitation at these low stations may not be fully representative of precipitation in the CKNP. Data from AWSs at higher altitudes (e.g. Askole, 3015 m a.s.l., and Urdukas, 3926 m a.s.l., installed by Ev-K2-CNR, see Bocchiola and others, 2011) are available, but they cover a very short period (2005–now), and display large lack of data. Therefore, little information is available within the CKNP that we know of, so we could only rely upon data from the three selected AWSs. In spite of the considerable vertical gradients within the area (temperature and precipitation, the latter more uncertain), relative variations observed at the selected stations may be taken as representative of variation also at the highest altitudes, at least in a first approximation.

The main parameters for the climate analysis are the monthly amount of precipitation P_m (mm), the monthly number of wet days D_w, the monthly average of the maximum and minimum day-time air temperature T_{max} (°C), T_{min} (°C). Pm provides the hydrological input on the area, while D_w indirectly indicates the frequency (or average duration) of precipitation events (days with rainfall/snowfall). Unfortunately, no snow gauges are available in the PMD database, so no direct inference can be made about snow amount and Snow Water Equivalent (SWE), neither splitting of precipitation into

either rainfall or snowfall was possible, and Pm is labeled as "monthly amount of precipitation". High altitude snowfall in this area seems still rather unknown. Some estimates from accumulation pits above 4000 m a.s.l. range from 1000 mm to more than 3000 mm, depending on the site (Winiger and others, 2005), and the authors here found ca. 1000 mm per year during 2009-2011 in the Baltoro glacier area at ca. 6000 m a.s.l. (Soncini and others, 2015). However, there is considerable uncertainty about the behavior of precipitation at high altitudes, and lack of snowfall data may lead to underestimation of total precipitation. Here, upon analysis of the average minimum winter temperature T_{min} (below 0°C most of the time at the sites), we may assume that water under snowfall is included and P_m is a measure of total precipitation.

The maximum and minimum day-time temperatures (T_{max} and T_{min}), provide indication about the temperature characteristics in the investigated periods (i.e. arrival and duration of heat waves). Annual (Y) and seasonal (SEA) values of the variables are also derived and used in the analysis, and $P_{m,Y/SEA}$ is the sum of the monthly values during a year/season; $D_{w,Y/SEA}$ represents the mean of monthly values during a year/season; and $T_{max,Y/SEA}$ and $T_{min,Y/SEA}$ are calculated as the mean of monthly values during a year/season.

The data are investigated for trends using linear regression (LR) analysis and the non-parametric Mann-Kendall (MK) test, both traditional and progressive (backward-forward). The significance of LR during the period of observations is given by a p-value (p = 5%, e.g. Jiang and others, 2007). Multiple trends could be identified in the time series analysis, e.g. by assessing slope changes (see Seidou and Ouarda, 2007; Bocchiola, 2014). However, in view of the relative shortness of the series, a single slope regression analysis is carried out. The Mann Kendall test (Mann, 1945; Kendall, 1975) is widely adopted to assess the significance of trends in time series (Zhang and others, 2000; Yue and Wang, 2002; Bocchiola and others, 2008). It is a non-parametric test, less sensitive to extreme values, and independent from the hypothesis about the nature of the trend (e.g. Wang and others, 2005). Here the MK test was applied to raw data, without pre-whitening, according to Yue and Wang (2002). Upon visual inspection of the data, which would not display evident break points or unexpected abrupt changes, and given that no modification of the stations' status was labeled by PMD, we did not carry out any homogenization procedure.

Further on, we tried to verify the hypothesis that the temperature evolution in the Karakoram is related to warming at global or hemispheric scale. To do so, we investigated the correlation between global temperature anomalies, DTG (calculated according to Brohan and others, 2006), and T_{min} and T_{max} at the AWSs. Also, we investigated the correlation of the weather variables against the anomaly (vs long term average) of the Northern Atlantic Oscillation (NAO) index (Hurrell, 1995; Jones and others, 1997; Osborn, 2004; 2006), during 1980–2009. Former studies demonstrated the existence of correlation between the NAO and the Karakoram climate, most notably with precipitation (Archer and Fowler, 2004). We therefore evaluated the (linear) correlation between i) local air temperatures and DT_G, and ii) the investigated weather variables and the NAO index. As a

representative parameter of the region, the averaged values between the three AWSs have been used.

4. Results

4.1 Glacier changes during 2001–2010

According to our inventory, the CKNP hosts 711 glaciers (Table 5). Their total area in 2001 is 4605.9 ± 86.1 km^2, ~35% of the our study site. This area represents ~30% of the glacier surface of the entire Karakoram Range within Pakistan (total area from Bajracharya and Shrestha, 2011). The biggest glacier is 604 km^2 (Baltoro Glacier), while the mean glacier size is 6.5 km^2. We divided the glaciers in size classes following Bhambri and others (2011) (Table 4).

Table 4: Number of glaciers and area distribution within the study region, sorted according to glacier size for 2001.

Size class [km^2]	Number of glaciers	Number of glaciers [%]	2001 glacier area [%]
< 0.5	291	40.9	1.4 ± 0.5
0.5-1.0	140	19.7	2.1 ± 0.5
1.0-2.0	118	16.6	3.7 ± 0.4
2.0-5.0	75	10.3	5.2 ± 1.9
5.0-10.0	36	5.3	5.3 ± 2.3
10.0-20.0	18	2.5	5.4 ± 2.8
20.0-50.0	16	2.3	11.4 ± 2.9
> 50.0	17	2.4	65.4 ± 2.8
Total	711	100	100 ± 1.9

Only 17 glaciers fall within the largest size-class (>50 km^2), but they cover more than half of the glacierized surface of the park. Glacier in the smallest classes (< 1 km^2) account for ca. 61% in number, while covering only 3.5% of the glacier area. Glacier minimum elevation (i.e.: glacier termini elevation) is between 4500 and 5000 m a.s.l. on average, with few larger glaciers reaching farther down (between 3000 and 3500 m a.s.l., Table 5).

Table 5: Glacier number and area distribution with respect to glacier termini elevation based on the 2001 inventory data.

Minimum glacier altitude [m]	Glacier number	Cumulative Area [km^2]	% of total area	% of total number
2000-2500	3	105.8 ± 7.2	2.3 ± 6.8	0.4
2500-3000	12	633.8 ± 29.5	13.8 ± 4.7	1.7
3000-3500	24	2152.5 ± 74.6	46.7 ± 3.5	3.4
3500-4000	83	950.3 ± 29.3	20.6 ± 3.1	11.7
4000-4500	229	449.2 ± 7.1	9.8 ± 1.6	32.2
4500-5000	268	258.6 ± 4.2	5.6 ± 1.6	37.7
5000-5500	77	37.0 ± 0.4	0.8 ± 1.0	10.8
> 5500	15	18.8 ± 0.5	0.4 ± 2.6	2.1
Total	711	4605.9 ± 86.1	100 ± 1.9	100

Smaller glaciers (<1 km^2), tend to have higher termini location, similarly to what is observed in other glaciated regions, including e.g. the Alaska Brooks Range (Manley, 2005), the Swiss glaciers (Kääb and others, 2002), the Cordillera Blanca (Racoviteanu and others, 2008), and the Italian Alps (Diolaiuti and others, 2012).

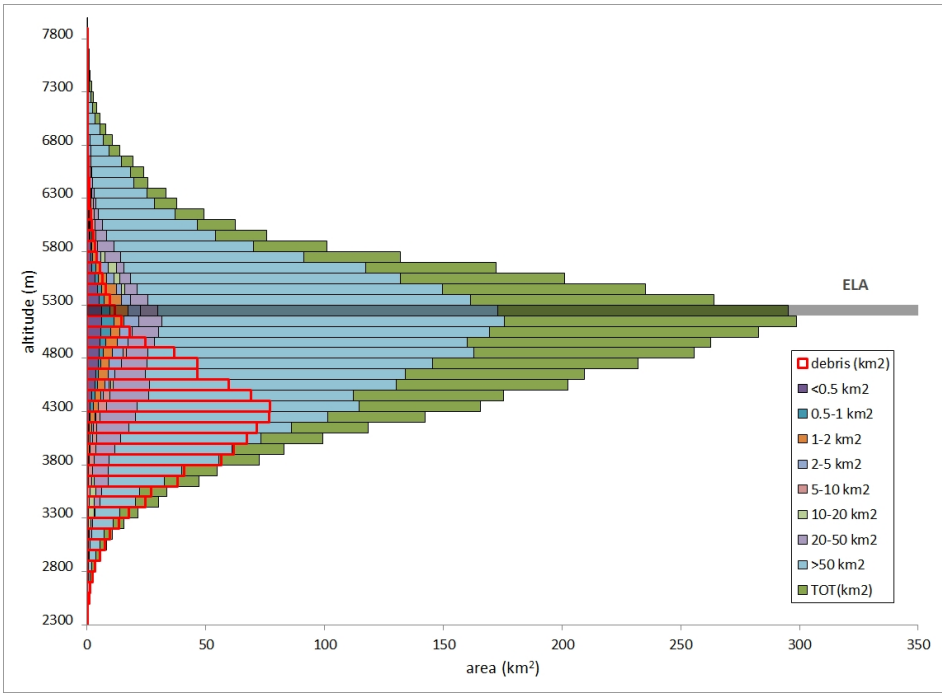

Figure 2: Hypsography of glacier area distribution per size class and debris-cover by 100 m elevation bins (based on 2001 glacier mask). Elevation data are based on the SRTM DEM of 2000. The grey bar represents approximate placement of ELA.

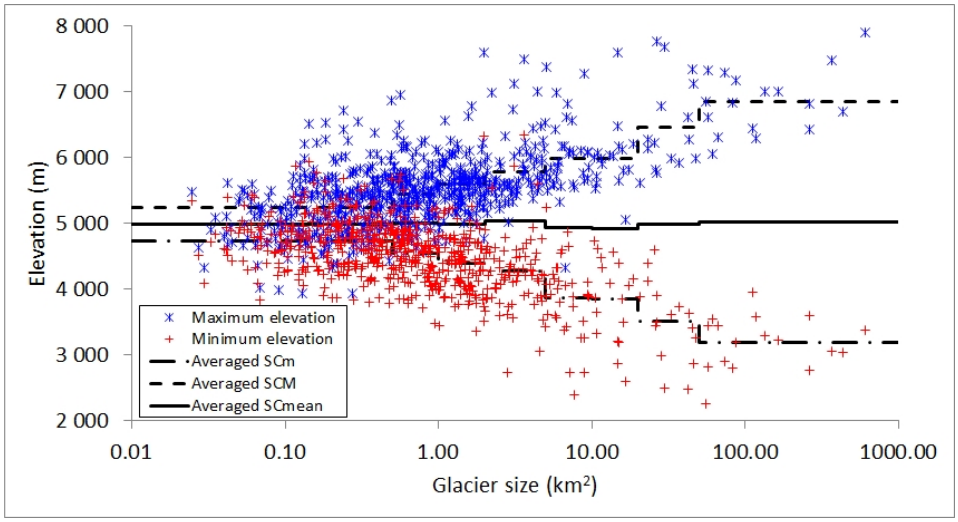

Figure 3: Minimum and maximum elevation versus area size (2001). Values for discrete size classes are also given. Notice the logarithmic scale for glacier size.

From the glacier hypsography, we observe that glaciers range in elevation from 2250 to 7900 m a.s.l. (Figure 2). Small glaciers with areas smaller than 1 km^2 are restricted to elevations above 3500 m a.s.l.. Their elevation range is not very high, but some of them are even found up to 7000 m a.s.l (Figure 3).

Most of the large and prominent glaciers instead originate above 7000 m a.s.l., and have a wide elevation range. Further, the minimum elevation reached by some of these large glaciers is much lower than in the Greater Himalaya of India and Nepal (Hewitt, 2005).

We found a significant correlation (ρ=0.5) of area vs altitudinal range (i.e. maximum minus minimum elevation). Glaciers with smaller vertical extent (i.e. maximum elevation close to the average) feature smaller areas. This is because they have small mass exchanges and therefore they cannot produce long tongues. Also, they can only survive in elevation where accumulation is secured.

In the available literature (Mayer and others, 2006; Mihalcea and others, 2008; Bocchiola and others, 2011; Soncini and others, 2015), the equilibrium line altitude (ELA) for CKNP glaciers is placed between 5200-5300 m a.s.l.. According to Braithwaite and Raper (2009), the ELA can be estimated from the median glacier elevation with an error of ±82 m. The median glacier elevation derived from our inventory is 4985 m a.s.l.. Rather than an indication of negative mass budgets, this discrepancy with the literature value is more likely due to i) the exclusion of the steep headwalls from the upper glacier limits in our inventory (which entails a lower value of median elevation), and ii) the fact that many glaciers are significantly nourished by avalanches and hence have small

accumulation regions. As a best approximation, the actual ELA of the CKNP glaciers could be placed between 5000 and 5200 m a.s.l. (Figure 2).

In 2010 glacier area of CKNP is 4606.3 ± 183.7 km^2, slightly more than 2001. Table 6 shows glacier data from 2001 and 2010, and it highlights some important changes between the two years. Because some glaciers changed their size class during 2001–2010, the analysis of the area changes was performed considering the glaciers to belong to the same size classes of 2001 for both years (Table 6).

Table 6: Area coverage of glaciers within the CKNP according to satellite images (2001 and 2010) (columns 2 and 3). Surface area changes of the CKNP glaciers during 2001–2010 (columns 4 and 5).

Size class [km^2]	**2001 Area [km^2]**	**2010 Area [km^2]**	**ΔA 2001-2010 [km^2]**	**ΔA 2001-2010 [%]**
<0.5	66.2 ± 0.4	66.1 ± 0.7	-0.1 ± 0.8	-0.1 ± 1.2
0.5-1.0	97.4 ± 0.5	97.7 ± 1.0	+0.2 ± 1.2	+0.2 ± 1.2
1.0-2.0	170.4 ± 0.8	170.5 ± 1.6	+0.03 ± 1.8	+0.02 ± 1.0
2.0-5.0	239.9 ± 4.6	231.9 ± 8.7	-8.0 ± 9.9	-3.3 ± 4.2
5.0-10.0	246.3 ± 5.7	257.3 ± 11.9	+11.1 ± 13.1	+4.5 ± 5.2
10.0-20.0	248.1 ± 7.0	251.1 ± 14.8	+3.0 ± 16.3	+1.2 ± 6.5
20.0-50.0	525.6 ± 15.2	525.4 ± 32.0	-0.2 ± 35.4	-0.04 ± 6.7
>50.0	3012.1 ± 84.1	3006.5 ± 179.7	-5.6 ± 198.4	-0.2 ± 6.6
Total	4605.9 ± 86.1	4606.3 ± 183.7	+0.4 ± 202.9	+0.01 ± 4.4

The analysis shows that the total glacier surface is rather stable during 2001–2010. The total area change is 0.4 ± 202.9 km^2; 99 glaciers compared to the entire sample of more than 700 glaciers changed in area (namely the 14% of all the glaciers). Glaciers increasing their areas since 2001 account for an area gain of +9.2 ± 118.5 km^2, while the loss was -8.8 ± 164.7 km^2.

In spite of the overall stable situation some glaciers showed considerable changes. Some of these are surge-type glaciers (Table 7). We found a maximum advance of 2200 m in the study period (Shingchukpi Glacier, Fig. 4a). Examples of important advances are also given by other tributaries of the Panmah Glacier (South Chiring Glacier, Fig. 4b, and Second Feriole Glacier), which have experienced surges in 2001 and 2005 (Hewitt, 2007), now protruding far onto the main trunk of the Panmah Glacier. The overall contribution of the advancing surge-type glaciers to the CKNP area gain is 2.6 km^2, about 28% of the total area gain in 2010 with respect to 2001.

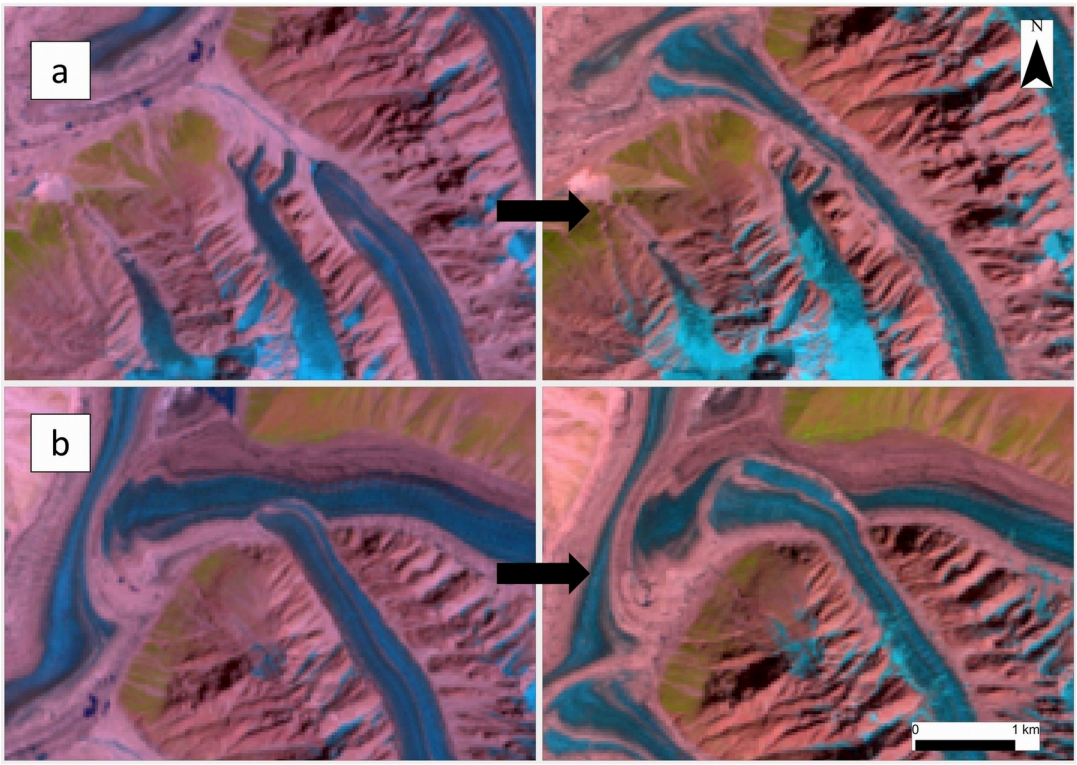

Figure 4: Comparison of Shingchukpi Glacier's (a) and Second Feriole Glacier's (b) positions in 2001 (left) and 2010 (right).

Table 7: List of advancing surging glaciers in the CKNP from 2001 to 2010.

Glacier ID	Name	Latitude(°)	Longitude(°)	Advance (m)	Area_gain (km^2)
276	Second Feriole Glacier	35.86	76.00	1800	0.8
534	Shingchukpi Glacier	35.90	76.02	2220	1.7
601	Skorga Glacier	36.24	75.76	375	0.2
616*	Maedan Glacier	35.93	76.03	900	0.8
616*	Drenmang Glacier	35.97	76.02	800	1.2
642	Unnamed	36.12	75.23	310	0.06
673	Unnamed	36.09	75.88	915	0.8
706	Kunyang Glacier	36.14	75.11	600	2.4

Finally, the total supraglacial-debris coverage was 946.2 ± 57.5 km^2 in 2001, and 1054.6 ± 117.3 km^2 in 2010, i.e. about 20% of the total ice covered area (see also Figure 1). When considering only the ablation area, the relative coverage is up to 31%. The supraglacial-debris covers 20 to 27% of glaciers in the size classes larger than 2 km^2 (size classes 4 to 8, see Tables 4 and 6), with maximum in size class number 7 (20 to 50 km2) (Figure 5).

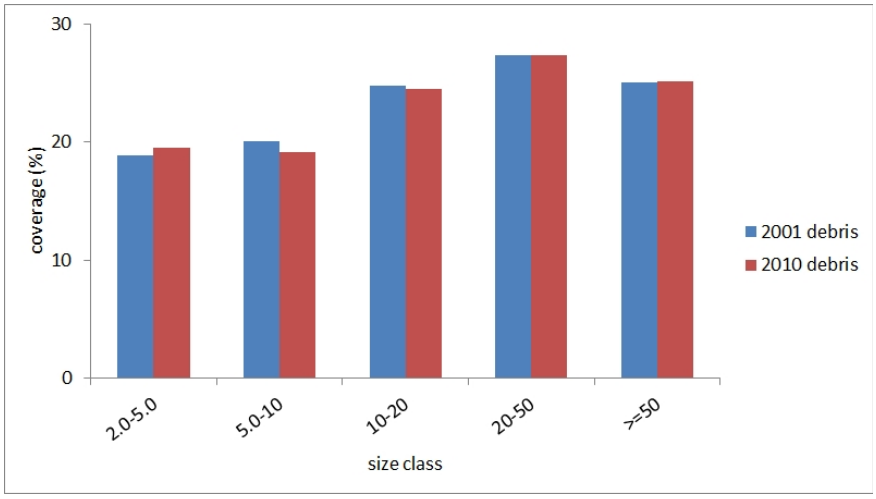

Figure 5: Supraglacial debris coverage for 2001 (upper figures) and for 2010 (lower figures) for a portion of the Chogo Lungma Glacier. FCC images (left), and debris coverage in yellow (right) are shown.

According to our calculation, the debris cover increased by 108.4 ± 130.6 km^2. Despite such error, this increment can be clearly observed on specific glaciers, as for the Chogo Lungma Glacier (Figure 6). The maximum supraglacial-debris cover is found at 4300 m a.s.l (see also Figure 2).

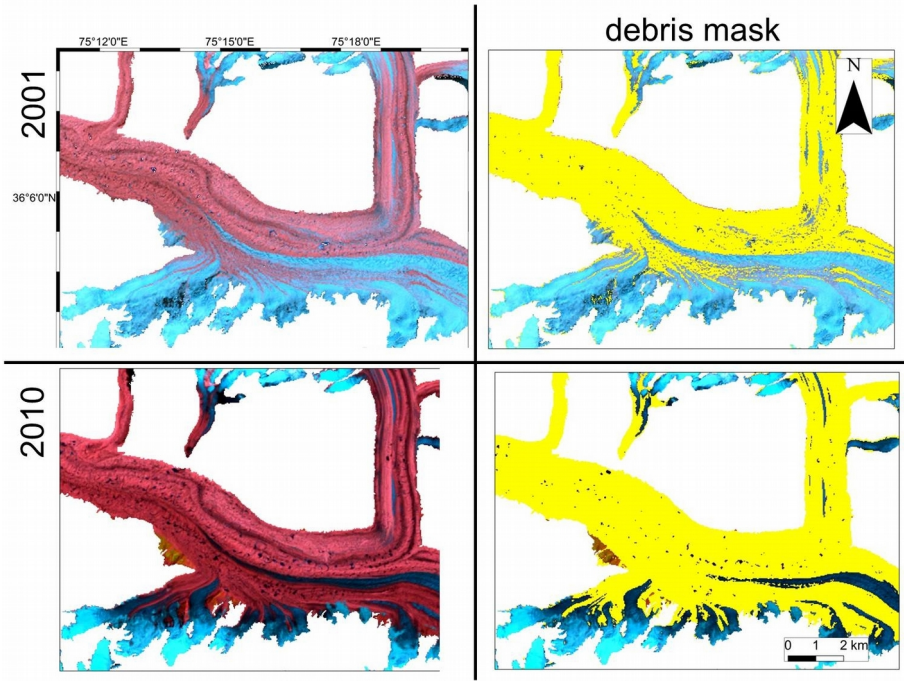

Figure 6: Supraglacial debris coverage for 2001 (upper figures) and for 2010 (lower figures) for a portion of the Chogo Lungma Glacier. FCC images (left), and debris coverage in yellow (right) are shown.

4.2 Snow cover validation and variability

Several Landsat TM and ETM+ scenes were processed to provide high-resolution (30 m) snow maps to be compared with the MOD10A2 product used for the snow cover analysis (Table 8). The snow maps were derived using the Normalized Difference Snow Index (NDSI), which combines the reflectance values of band 2 and 5 (b2, b5) of the Landsat satellite as:

$$NDSI = \frac{b2 - b5}{b2 + b5} \quad . \tag{3}$$

As our snow cover analysis only referred to the ablation season, we selected Landsat scenes from the beginning of July to the first days of October. Moreover, we resampled the Landsat snow maps to match the resolution of the MOD10A2 product (500 m) to evaluate the effect of the spatial resolution on the comparison. The resampling was done using the majority method, which assigns the most common value amongst the original pixels in a specific window to the new larger pixel.

Table 8: Statistics of snow cover area obtained from Landsat NDSI and MOD10A2 snow product for different years. Landsat snow maps are also presented in the 500 m pixel resampled version (majority method).

	path/ row	Date	ETM+ (km^2)	TM (km^2)	MOD-10A2 (km^2)	Relative error (%)	ETM+ 500m (km^2)	TM 500m (km^2)	Relative error (%)
ETM+	148035	July 2001	2798		2904	4	2755		5
	149035	September 2001	3869		4625	20	4646		0
	148035	August 2002	3211		3257	1	3690		-12
	149035	August 2002	2963		3198	8	3722		-14
TM	148035	October 2008		3498	4817	38		4270	13
	149035	September 2008		4410	4853	10		4848	0
	148035	August 2009		3251	3469	7		4033	-14
	149035	August 2009		2812	3353	19		3556	-6
	149035	October 2010		3544	4888	38		3526	39

The relative error ranges from 1 to 38% overall, but a difference is seen if i) Landsat TM and ETM+ scenes are considered separately, and ii) the resampled Landsat snow map is considered instead of the original resolution. In the first case, the relative error is 1–20% when considering the ETM+ sensor, while it is 7–38% for the TM sensor. The comparison is also done with the older Landsat 5 satellite, because of the SCAN-line corrector failure after April 2003 of the Landsat 7 satellite, which caused data loss in the images recorded after this date. The resampled Landsat snow maps might provide a better comparison with the MODIS product due to the identical pixel dimension, which mimics a similar decision strategy as for a MODIS pixel, depending on the used threshold for the MOD10A2 product. The relative error is lower in the resampled snow map than in the original data. In particular, the relative error range (0–14%) is smallest when comparing the resampled snow maps derived from the ETM+ sensor.

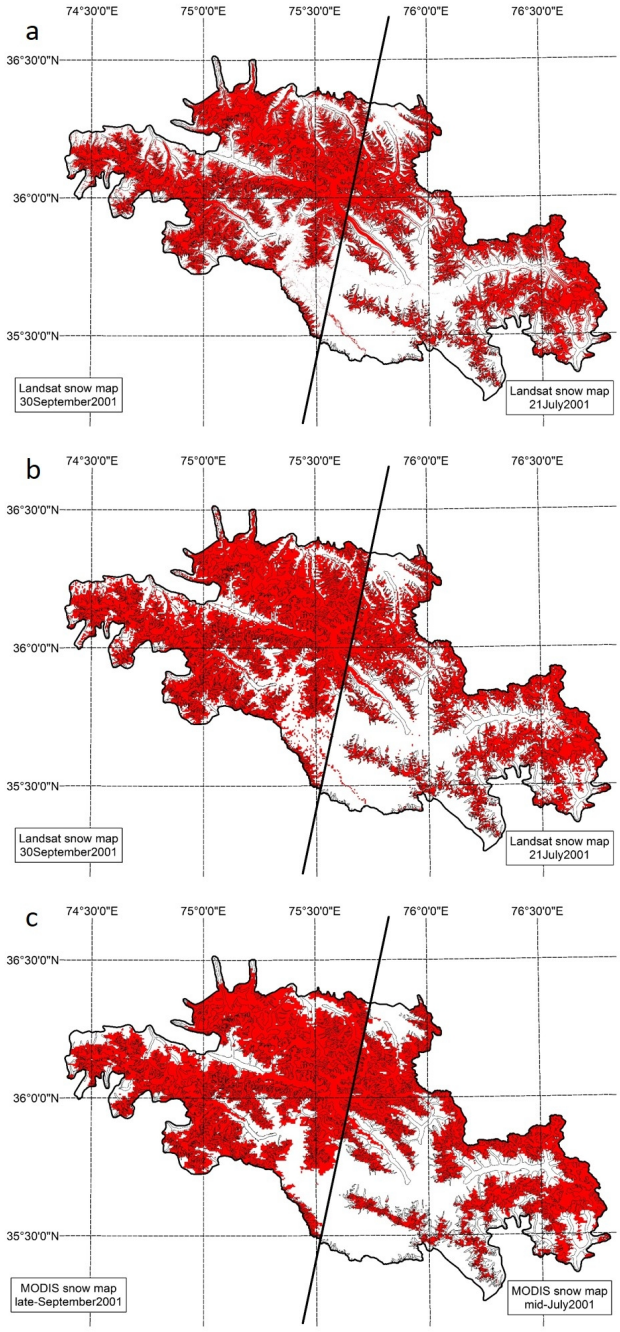

Figure 7: Comparison of snow cover maps a) derived by the ETM+ data with 41% (July) and 61% (September) of snow cover; b) resampled to 500 m with 40% (July) and 73% (September) of snow cover; c) obtained from MOD10A2 with 42% (July) and 72% (September) of snow cover. The solid black line in the center of the image separates the two scenes used for mosaicking (path/row: 149/035, left; 148/035, right). All figures refer to 2001 year.

It is worth to remember that the MOD10A2 product represents an 8-day snow cover bundle, so the

differences can also depend on the different time resolution of the two datasets (1 day for the Landsat satellites, and 8 day for the MOD10A2). In particular, if the Landsat acquisition date coincides with a snowfall event, or is just before, major differences might occur. Moreover, the way the MOD10A2 product is generated by the NSIDC minimizes cloud-cover extent, such that a cell needs to be cloud-obscured for all days in order to be labeled as cloud (nsidc.org). This makes this product preferable to the MOD10A1 daily product (Wang and others, 2007), and does not require additional cloud correction to be used.

The average SCALS, or snow covered area in late summer, during 2001–2011 was investigated with respect to altitude bins of 1000 m, refined into 500 m bins from 3000-6000 m a.s.l., where most of the snow dynamics likely occurs and ELA is expected to dwell (Figure 8). The aspect (8 bins of 45°) is also analyzed to study the variability of snow cover with orientation. A considerable part of the SCA is laid between 4000 and 6000 m a.s.l. as expected, quite rapidly decreasing for lower and higher altitudes. Especially in the lower altitudes the southern slopes show clearly less snow cover than the other orientations.

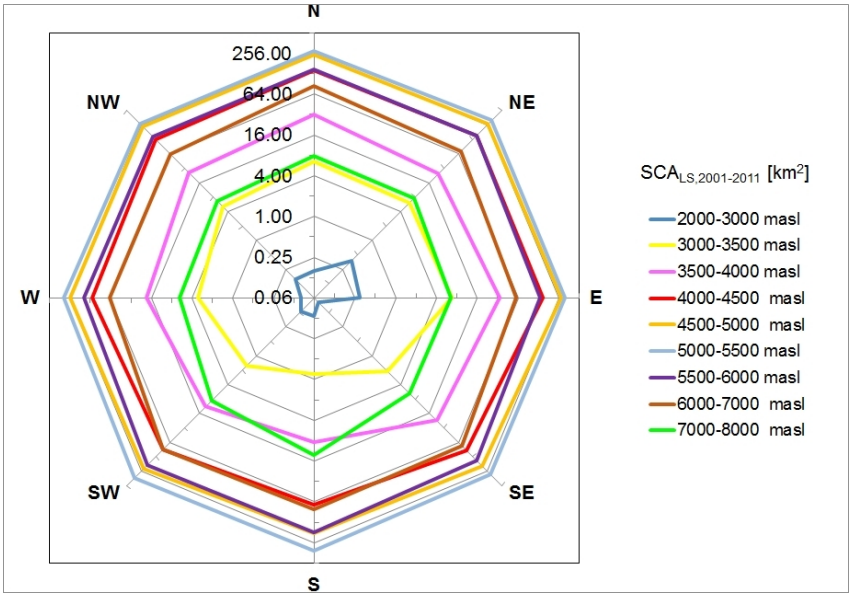

Figure 8: Average snow covered area in late summer, SCA_{LS}, as per altitude bins, and aspect. Logarithmic scale (base 2) is used to enhance small snow covered areas at very low (and very high) altitudes.

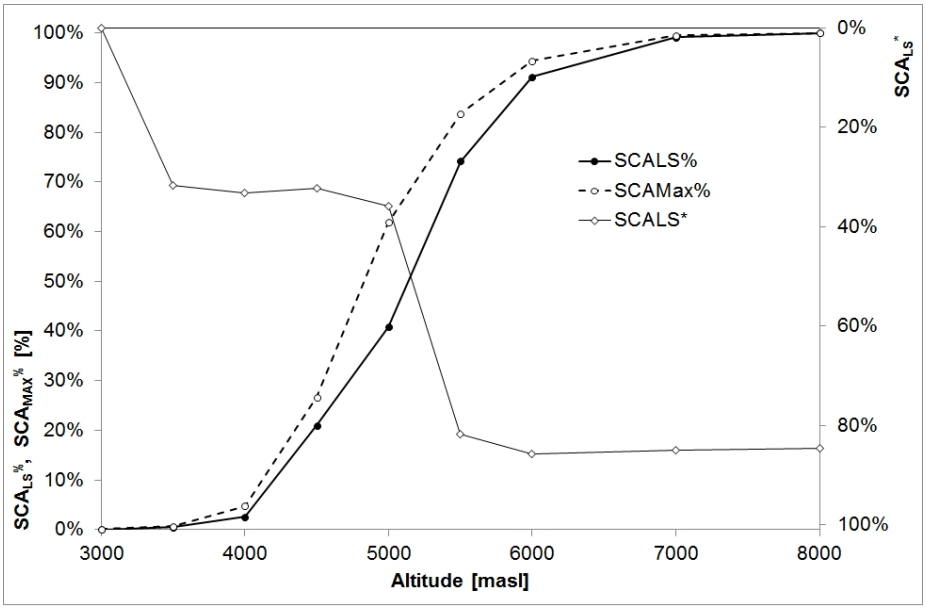

Figure 9: Distribution of 2001–2011 average snow covered area in altitude bins in late summer with respect to the whole area ($SCA_{LS}^{\%}$), of 2001–2011 average snow covered area in late summer (SCA_{LS}^{*}) with respect to greatest (maximum) snow covered area in that bin, and of the 2001–2011 greatest snow covered area in each bin with respect to the sum of 2001–2011 maximum values of snow covered areas in the whole park ($SCA_{Max}^{\%}$). Logarithmic scale (base 2) is used to enhance small snow covered areas at very low (and very high) altitudes.

On average, 88% of SCA in late summer is situated between 4000 and 6000 m a.s.l. ($SCA_{LS}^{\%}$) (Figure 9), thus demonstrating how snow dynamics is most important in this altitude bin, and that such range of altitude is utmost critical, also in view of potential changes of snow cover in response to climate change. From the shape of the SCA_{LS}^{*} curve (2001–2011 average snow cover area in late summer), it is clearly seen how on average, above 5500 m a.s.l. and up to 8000 m a.s.l., snow cover in late summer is stable at about 85% of the maximum seasonal value. Below this altitude, SCA_{LS}^{*} decreases quickly. $SCA_{Max}^{\%}$ indicates the contribution to snow cover of each altitude belt during winter time, i.e. when SCA reaches its largest value. The comparison of $SCA_{LS}^{\%}$ against $SCA_{Max}^{\%}$ quantifies the relative importance of the loss of snow cover at the end of summer in each belt, i.e. as quantified by SCA_{LS}^{*}. Notably the greatest cumulated SCA loss (i.e. the vertical distance between $SCA_{LS}^{\%}$ and $SCA_{Max}^{\%}$) is reached towards an altitude of ca. 5000–5300 m a.s.l. (ca. 20%), with a decrease above. This means that areas above this belt tend to have a continuous snow cover throughout the year. We therefore placed the late summer snow line at an altitude nearby 5300 m a.s.l., which roughly corresponds to the ELA. This is consistent with the pattern of SCA_{LS}^{*}, displaying swift increase above between 5000 and 5500 m as.l..

We finally subdivided our SCA dataset into three elevation bands (A, B, C, Table 9) according to

Tahir and others (2011), for benchmark against their findings (i.e. increased SCA in the Hunza basin in the same period). Table 8 reports the rate of variation in time, or slope, of the snow coverage within each of the three belts. Slope is the value of the rate of variation estimated using linear regression analysis, expressed in km^2 per year. SlopeSCA% is the rate of variation expressed as a percentage of the initial SCA (in 2001) per year. A slight increasing trend of snow cover through time is visible in all the elevation belts (Figure 10). In belt A, a gain of +0.09 km^2 yr^{-1} (or 2% of snow cover area per year), was observed. In belt B, snow cover area increased by +2.35 km^2 yr^{-1}, or +0.6% yr^{-1}. Belt C has increasing snow cover of +14.9 km^2 yr^{-1}, or +0.2% yr^{-1}.

Table 9: Characteristics of three elevation zones for snow cover with slope values from linear regression analysis upon average snow cover.

Zone	**Altitude bin [m]**	**$Surface_{zone}$ [km^2]**	**AveSCA [km^2yr^{-1}]**	**$Slope_{SCA}$ [km^2yr^{-1}]**	**$Slope_{SCA\%}$ [$\%yr^{-1}$]**
A	1900-3300	845	4.6	0.1	2
B	3301-4300	2803	384.4	2.3	0.6
C	4301-8400	9551	6574.6	14.9	0.2
$A_{TOT}/Slope_{\%w}$		13200		17.3	0.25

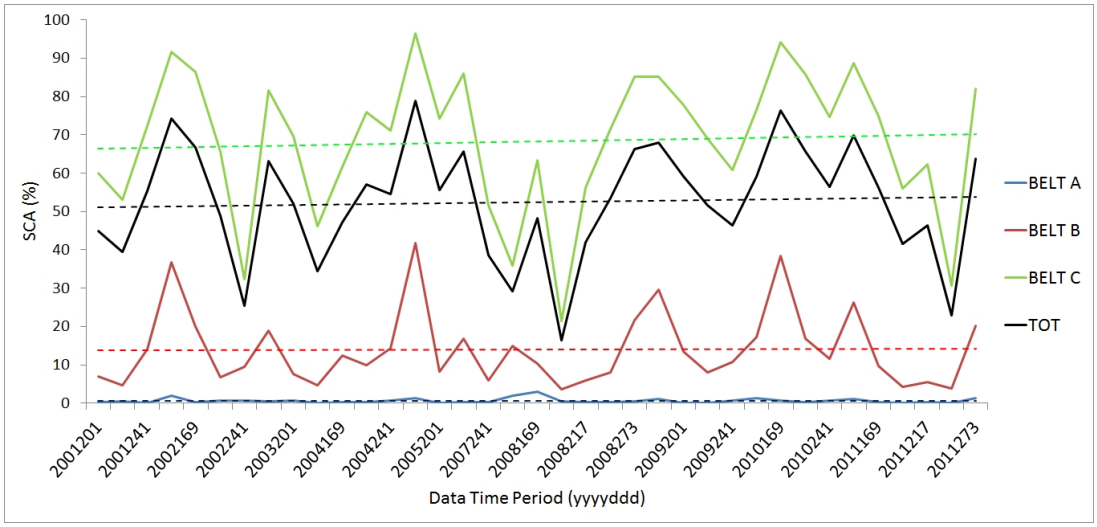

Figure 10: SCA values for three different altitudinal zones (A, B, C see Table 8) of the CKNP for the May-September window in 2000–2011. Data Time Period is given in years and Julian days.

4.3 Climate trends

The results of the trend analysis of climate are shown in Table 10, and Figures 11 to 13, where the

most significant trends are highlighted. The progressive MK test was carried out whenever both MK and LR tests showed non-stationarity, and the results are also shown in Table 10. Precipitation P_m demonstrates a substantial stationary behavior, i.e. no significant change is seen in the area. Concerning the number of wet days (D_w), increasing values are found in Gilgit (yearly, Y, since 2001, JFM, with no clear onset), i.e. there is a significant increase of the number of yearly (and winter) precipitation events (Figure 10). In Astore, significant increase of D_w is found in summer months (JAS) via the LR test. The minimum temperature T_{min} increases significantly in Astore for winter and spring (JFM, AMJ, since 1999–2002) and in Bunji for all periods except in summer (Y, JFM, AMJ, OND, since 1997–2003). In Gilgit, T_{min} decreases significantly during summer (JAS, since 1986). The maximum temperature T_{max} increases significantly yearly, in fall and winter in Astore (Y since 1998, JFM since 2000). Also in Gilgit, significant T_{max} increase is observed for most periods (Y, JFM, since 1995, OND, since 1991), while Bunji shows a significant T_{max} increase only in winter (JFM, since 1997).

In Table 10 we also report the results of the correlation analysis against global drivers of climate. The minimum air temperature T_{min} is significantly positively correlated with respect to DT_G yearly, in winter and spring. The maximum air temperature T_{max} is significantly positively correlated against DT_G yearly, and seasonally, especially in fall and winter. Concerning the NAO index, P_m shows a significant, albeit small correlation (negative vs. Y, and positive vs. JAS and OND). The duration of wet periods D_w is significantly shorter for higher NAO anomalies, unless during Spring. The minimum temperature T_{min} is negatively correlated to NAO during Winter and Spring. T_{max} is negatively correlated to NAO (Y, JFM, AMJ).

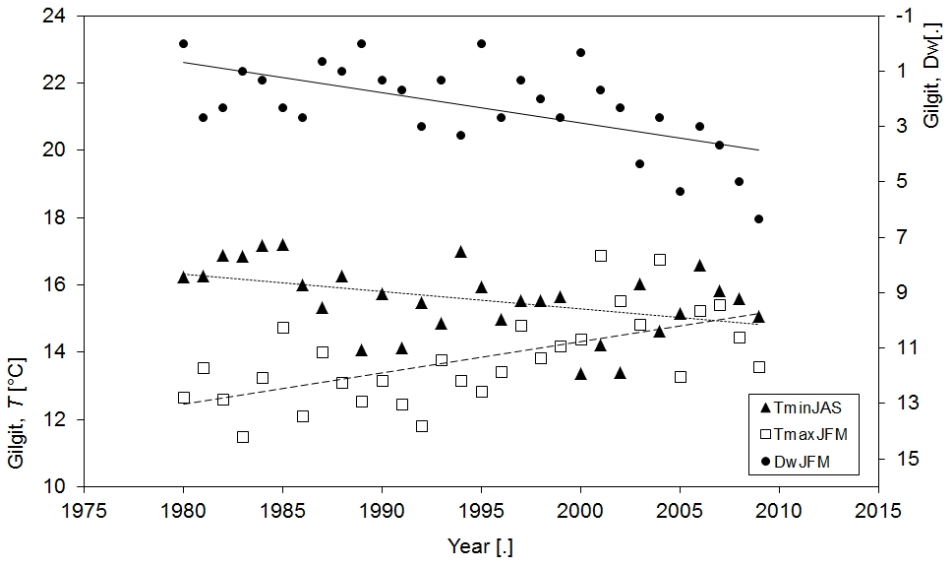

Figure 11: Summer (JAS) minimum air temperatures and winter (JFM) maximum air temperatures for the Gilgit AWS, including their linear trends. In addition also the number of wet days D_w during winter is displayed.

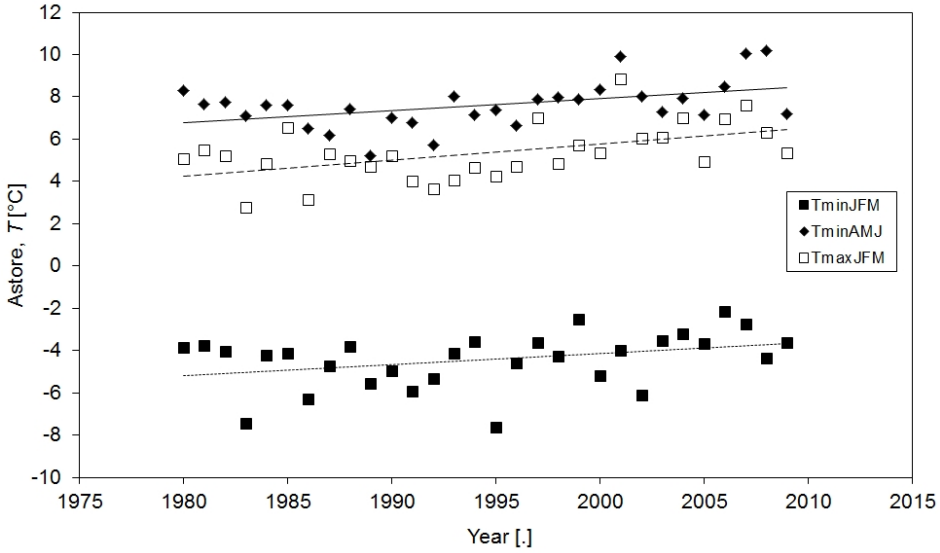

Figure 12: Seasonal minimum air temperatures (winter: JFM, spring: AMJ) and winter maximum air temperatures for the Astore AWS, including their linear trends.

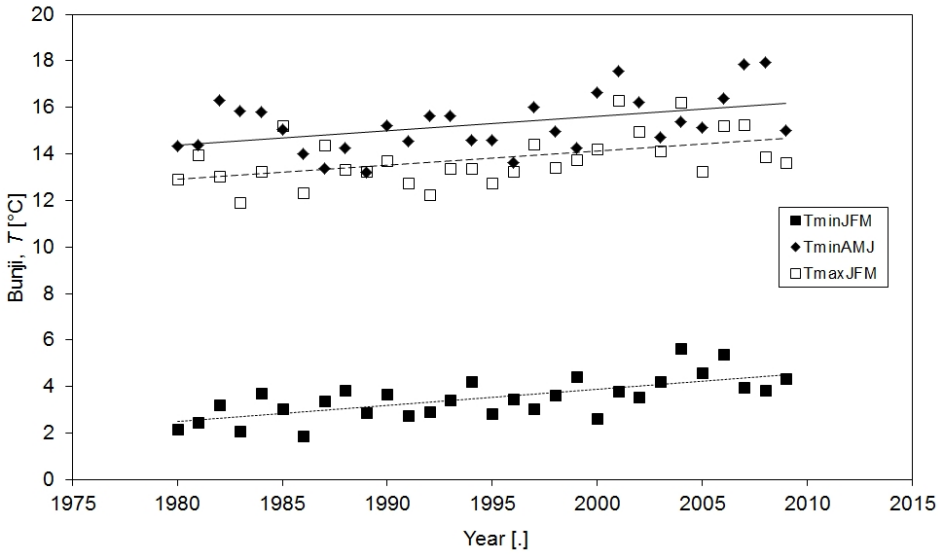

Figure 13: Seasonal minimum air temperatures (winter: JFM, spring: AMJ) and winter maximum air temperatures for the Bunji AWS, including their linear trends.

Table 10: Results of the climate trend analysis: a) results of the LR and MK analysis. For MK, p-val is displayed. The LR values are the linear regression coefficients (i.e. slope of the regression line, unity/year), LRp is corresponding to p-val. In bold significant p-val (α = 5%) are given; b) the beginning year and average values before and after the start for the trends derived from the progressive MK test are given. LT is the long term (1980-2009) average; c) correlation analysis of station mean climatic variables vs global temperature anomalies DT_G and NAO index. The significant correlation (p=5%) results are displayed in bold.

a) AWS	**Pm-Dw**	**P_Y**	**P_{JFM}**	**P_{AMJ}**	**P_{JAS}**	**P_{OND}**	**D_{wY}**	**D_{wJFM}**	**D_{wAMJ}**	**D_{wJAS}**	**D_{wOND}**
Astore	MK	0.38	0.40	0.60	0.90	0.56	0.25	0.96	0.66	0.10	0.71
Astore	LR s	-2.22	-0.94	-0.39	0.00	-0.89	0.34	0.01	-0.01	**0.08**	0.03
Astore	LR p	0.43	0.55	0.84	1.00	0.49	0.22	0.71	0.87	**0.04**	0.27
Bunji	MK	0.90	0.42	0.99	0.99	0.84	0.84	0.38	0.38	0.68	0.79
Bunji	LR s	-0.32	0.29	-0.18	0.03	-0.47	-0.06	-0.01	-0.03	0.00	0.02
Bunji	LR p	0.82	0.49	0.84	0.96	0.39	0.81	0.85	0.44	0.94	0.28
Gilgit	MK	0.42	0.87	0.40	0.79	0.90	**0.00**	**0.00**	0.15	0.21	0.93
Gilgit	LR s	0.59	0.09	0.78	-0.07	-0.20	**0.87**	**0.11**	**0.09**	0.06	0.03
Gilgit	LR p	0.55	0.80	0.34	0.87	0.64	**0.00**	**0.00**	**0.04**	0.12	0.38
AWS	**Tmin-Tmax**	**T_Y**	**T_{JFM}**	**T_{AMJ}**	**T_{JAS}**	**T_{OND}**	**T_Y**	**T_{JFM}**	**T_{AMJ}**	**T_{JAS}**	**T_{OND}**
Astore	MK	0.07	**0.05**	**0.04**	0.71	0.23	**0.01**	**0.01**	0.34	0.99	0.28
Astore	LR s	**0.03**	**0.05**	**0.06**	0.00	0.02	**0.04**	**0.08**	0.05	0.01	0.04
Astore	LR p	**0.02**	**0.05**	**0.01**	0.87	0.23	**0.01**	**0.00**	0.11	0.76	0.09
Bunji	MK	**0.01**	**0.00**	**0.03**	0.82	**0.02**	0.58	**0.01**	0.73	0.07	0.42
Bunji	LR s	**0.04**	**0.07**	**0.06**	-0.01	0.04	0.01	**0.06**	0.01	-0.03	0.02
Bunji	LR p	**0.00**	**0.00**	**0.01**	0.81	**0.04**	0.38	**0.01**	0.73	0.13	0.29
Gilgit	MK	0.16	0.42	0.76	**0.03**	0.49	**0.00**	**0.00**	0.33	0.93	**0.01**
Gilgit	LR s	-0.01	0.02	0.01	**-0.05**	-0.02	**0.05**	**0.09**	0.06	0.00	**0.07**
Gilgit	LR p	0.41	0.39	0.62	**0.02**	0.41	**0.00**	**0.00**	0.07	0.85	**0.00**
b) AWS	**Var.**	**Year st.**	**LT**	**Before**	**After**	**AWS**	**Var.**	**Year st.**	**LT**	**Before**	**After**
Astore	T_{minJFM}	2002	-4.4	-4.8	-3.7	Bunji	T_{minOND}	1997	5.1	4.9	5.5
Astore	T_{minAMJ}	1999	7.6	7.2	8.4	Bunji	T_{maxJFM}	1997	13.8	13.3	14.5
Astore	T_{maxY}	1998	15.7	15.3	16.2	Gilgit	D_{wY}	2001	39.3	33.6	53.4
Astore	T_{maxJFM}	2000	5.4	4.8	6.4	Gilgit	T_{minJAS}	1986	15.6	16.7	15.3
Bunji	T_{minY}	2003	10.9	10.7	11.7	Gilgit	T_{maxY}	1995	24.1	23.7	24.6
Bunji	T_{minJFM}	1997	3.5	3.1	4.1	Gilgit	T_{maxJFM}	1995	13.8	13	14.6
Bunji	T_{minAMJ}	2001	15.3	15	16.2	Gilgit	T_{maxOND}	1991	18.9	18.2	19.3
c)	**Y**	**JFM**	**AMJ**	**JAS**	**OND**	**-**	**Y**	**JFM**	**AMJ**	**JAS**	**OND**
DT_G/T_{min}	0.21	**0.25**	**0.35**	-0.16	0.19	NAO/D_w	**-0.32**	**-0.44**	**0.33**	**-0.33**	-0.10
DT_G/T_{max}	0.55	**0.41**	**0.24**	0.11	**0.33**	NAO/T_{min}	0.00	**-0.36**	**-0.26**	0.05	0.12
NAO/P_m	-0.14	0.10	0.17	**0.18**	**0.17**	NAO/T_{max}	**-0.21**	**-0.23**	**-0.22**	0.06	-0.05

5. Discussion

According to our inventory, the glaciers of the CKNP were rather stable in terms of surface during 2001–2010. This is in contrast to the evolution of most mountain glaciers outside the polar regions, which experienced a general retreat on average (Vaughan and others, 2013). In the present chapter we relate such stability with the results of our climate analysis, the observed abundant supraglacial debris, and the role of the surging glaciers in the region. Then, accuracy and validation of our snow

analysis is discussed, and finally, a comparison between our glacier inventory and the other existing inventories is presented.

5.1 The relation between climate change and glacier stability in the CKNP

The analysis of climate data from 1980 to 2009 measured by three AWSs (Table 3), revealed that the occurrence of precipitation events has increased. Considering that the median elevation of the CKNP glaciers is close to 5000 m, that the average minimum winter air temperature is below 0°C most of the time, and that most of the precipitation occurs in winter, this would translate into more frequent snowfalls. This assumption is confirmed by the analysis of the SCA variation, which revealed slightly increasing snow cover during the 2001–2010 ablation seasons in this area. This finding is in accordance with Hasson and others (2014), who found that summer SCA increased on average during 2001–2012 in the Shigar basin, where most of the CKNP is located. Tahir and others (2011) gave further evidence of increasing SCA in the upper Karakoram for the same period, while Gurung and others (2011) reported rising SCA in the western HKH during 2002–2010.

The role of snow is of great importance for glacier preservation (especially during melt season), as snow reflects a large portion of the incoming solar radiation, protecting the underneath ice from melt. The same increasing trend in SCA is confirmed also between 5000 and 5500 m a.s.l., where i) the greatest cumulated SCA loss (i.e. the vertical distance between $SCA_{LS}^{\%}$ and $SCA_{Max}^{\%}$, see Figure 9) is found; ii) most of the glacier area resides (see Figure 2); and iii) debris cover is sparse and can enhance ice melt.

A decreasing trend in summer mean air temperature was observed at Gilgit AWS during 1980–2009, and this would support snow and ice preservation during the ablation season. Evidences are also given by Shekhar and others (2010), who found a decrease of ~1.6 and 3 °C respectively in maximum and minimum air temperature over the Karakoram range during 1985–2007, while Hasson and others (2015) found a significant cooling in July–October during 1995–2012 in the Upper Indus Basin. Quincey and others (2009) found decreasing mean summer air temperatures modeled over the Baltoro area during 1958–2001. Gardelle and others (2012) who connected the reduced river runoff in the central Karakoram with decreasing ice and snow melt rates (as these would be the major water sources of rivers in this region, according to Immerzeel and others, 2010).

Finally, length and area changes are harder to interpret in climatic terms than mass changes, as they respond slower (and in some cases even not at all) to climate variations. Indeed, there is a delay of the glacier area response to climate change depending on glacier size, with usually longer response times for larger glaciers (Bolch and others, 2012). Glacier area gain may be the result of several decades of positive mass balance for large glaciers (Bhambri and others, 2013), which are frequent in the study area. The observed climate change towards more favorable conditions for glaciers in the Karakoram seems to substantiate the slight glacier mass gain found by Gardelle and others (2012; 2013) for the 1998–2008 period (equal to $+0.10 \pm 0.16$ m w.e. yr^{-1}). Either this mass change

was not large enough to cause an increase of glacier surfaces in the region, or it occurred too recently, and glacier areas might respond in the future only to this changed conditions.

5.2 Difference between debris-free and debris-covered glaciers in the CKNP

If CKNP glaciers are divided into debris-free and debris-covered types, we can immediately recognize two patterns. On the one hand, debris-covered glaciers are mostly larger—Baltoro, Biafo and Hispar glaciers belong to this group—, and they reach the lowest elevations (even below 3000 m a.s.l., see Figure 3). Moreover, they are covered by debris almost entirely up to about 4000 m a.s.l. (see Figure 2). The debris can be brought by landslides from the steep rock-walls surrounding the glaciers, rock falls and debris-laden snow avalanches. On the other hand, debris-free glaciers are in general smaller (the Yazghil Glacier being the largest with 87 km^2), and their termini are found higher up on average (4600 m a.s.l., almost 700 m above the mean termini of debris-covered glaciers) (Figure 14).

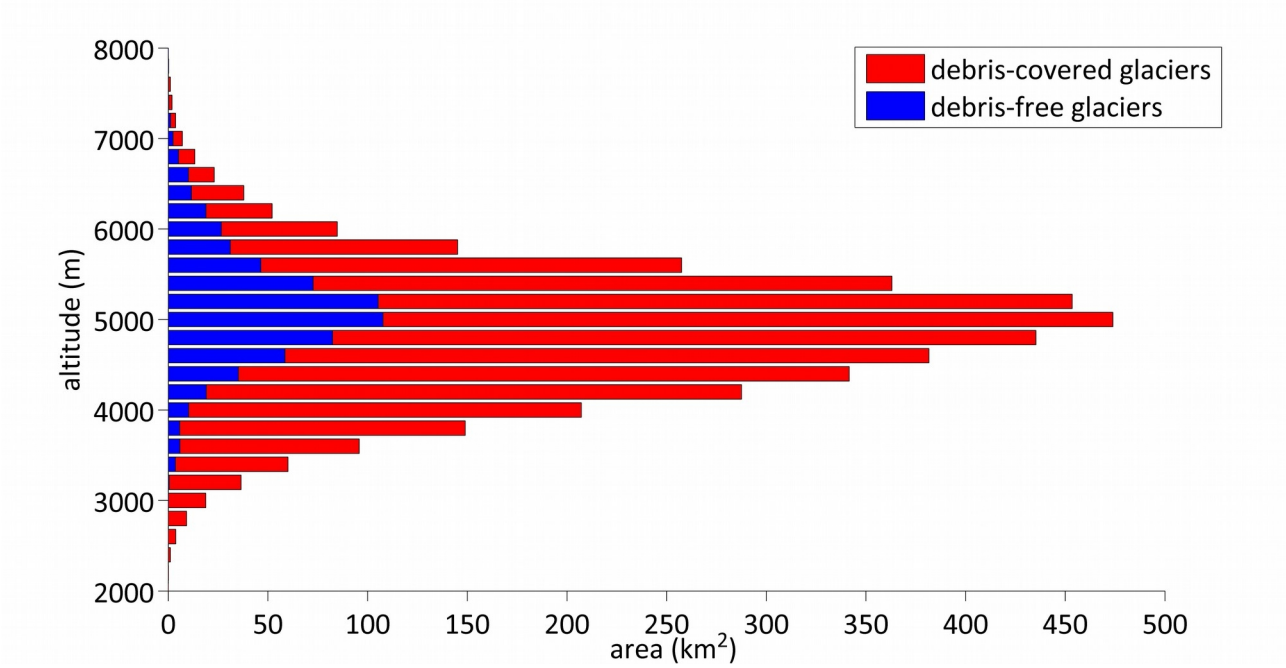

Figure 14: debris-free and debris-covered glacier areas distribution per 200 m altitude bins.

From our analysis, the presence of glaciers below 4000 m a.s.l. seems to be linked with the presence of a supraglacial debris cover. Debris can have two opposite effects on the ice. If it is thick enough (more than a critical thickness, to be derived with field observations, Mattson and others, 1993), it decreases ice melt rates by reducing the heat flux from the top of the debris layer to the debris-ice interface. According to Juen and others (2014) a debris layer thicker than 0.1 m is able to diminish ablation efficiently, while Mihalcea and others (2006) reported a critical debris thickess of around 0.05 m on the Baltoro Glacier. The debris thickness over most of the glacier termini in this region is

very high (often >1 m, Mayer and others, 2006; Copland and others, 2009), and therefore is able to reduce ice melt and preserve glaciers at such low altitudes where temperatures are generally higher.

On the other hand, exposed ice cliffs and meltwater ponds, the presence of which is usually related to debris occurrence (Benn and others, 2012), can enhance ice ablation. Sakai and others (2002) have shown that ice cliffs on glaciers in Nepal could make a large net contribution to total ablation of debris-covered glaciers, although covering a small percentage of the total glacier area. Juen and others (2014) stated, however, that melt on ice cliffs plays a significant role for ice ablation, but not as high as concluded by Sakai and others (1998). Reid and Brock (2014), concluded that ice cliffs (even the smallest ones) account for ~7.4% of the total ablation on the Miage Glacier. The effect of ice cliffs at a local scale can be clearly seen in patterns of glacier elevation change from DEM differencing (Bolch and others, 2011). However, Gardelle and others (2012) found no significant differences in surface elevation change between debris-free and debris-covered glaciers in the Karakoram in the last decade, indicating that the Karakoram Anomaly likely is controlled by other factors than debris cover.

Finally, from Table 11 at section 5.3, we observe that debris-free and debris-covered glaciers contribution are similar but opposite, being the first positive and the second negative. Nevertheless, these area changes represent less than 1% of the glacier area of both categories. In section 5.3 we will see that most of the debris-free gain is due to surge advances.

5.3 The contribution of the surging events to the CKNP glacier area change

The total area of the CKNP glaciers was rather stable during 2001–2010 (+0.4 ± 202.9 km^2 over about 4606 km^2). This value includes also the area gain due to surge activities. As a surge trigger mechanism remains inconclusive in the region and very likely is not directly driven by climate variations (Quincey and Luckman, 2014), we decided to split the analysis between surge- and non-surge-type glaciers. Neglecting the surge-type advances, the remaining glacier surface is still more or less stable. The contribution of the surge-type advances on the total area gain results to 28%. It is also worth to note that four out of eight surge-type glaciers are debris-free, and account for even 77% of the total area change of all the CKNP debris-free glaciers. It means that most of the area change from debris-free glaciers is due to surging. The most prominent surge example is the Shingchukpi Glacier, which is the debris-free glacier with the largest surge advance (2220 m). It is now in touch with the Panmah Glacier. On the other hand, the area change due to surge is negligible for debris-covered glaciers (Table 11).

Table 11: glacier area variation divided into debris-free, debris-covered, and surge and non-surge type glaciers during 2001–2010. $\Delta Acov_{2001\text{-}2010}$[%] is the percentage of area change relative to glacier coverage (debris-free, or -covered), for surge and non-surge area changes. $\Delta Arel_{2001\text{-}2010}$[%] is the percentage of area change relative to the total change (+0.4 ± 202.9 km^2 over about 4606 km^2), for debris-free and debris-covered glaciers. Mean elevation values are also given.

	Debris-free glaciers		**Debris-covered glaciers**		**Total**	
	no surge	**only surge**	**no surge**	**only surge**	**debris-free**	**debris-covered**
Glacier number	528	4	178	1	532	179
Glacier number[%]	74.3	0.6	25.0	0.1	74.8	25.2
2001 Area [km2]	609.7±7.7	50.8±2.6	3940.5±85.7	4.9±0.8	660.5±8.2	3945.4±85.7
2010 Area [km2]	610.7±14.5	54.3±6.4	3936.4±183.0	5.0±1.6	665.0±15.9	3941.4±183.0
ΔA2001-2010[km2]	+1.0±16.5	+3.5±6.9	-4.0±202.1	+0.1±1.8	+4.5±17.8	-4.0±202.1
ΔA2001-2010[%]	+0.2	+0.5	-0.1	+0.002	+0.7	-0.1
ΔAcov2001-2010[%]	+22.6	+77.4	-98.5	+1.5		
ΔArel2001-2010[%]					+52.8	-47.2
Mean altitude[m]	5029	5291	4864	5170	5031	4866

Despite the relatively large length and area changes, and the high flow velocities during the active phase of a surge (up to 5 km yr^{-1} for the Khurdopin Glacier in the 1970s according to Quincey and Luckman, 2014), it is difficult to connect such advances to changes in mass balance. Previous works on surging glaciers in the Karakoram have suggested that climatically induced changes in glacier thermal conditions may be linked to observed exceptional surging (Hewitt, 2005), while others indicate that a change in subglacial drainage is the dominant control (Mayer and others, 2011). Quincey and others (2011) speculated that recent surges in the Karakoram might be controlled by thermal rather than hydrological conditions, coinciding with high-altitude warming from long-term precipitation and accumulation patterns. Nevertheless, there is consensus that surge events are increasing in the Karakoram, and this is likely to reflect somehow recent changes in precipitation and temperature in the region (Hewitt, 2007; Copland and others, 2011). Recently, Herreid and others (2015), found no significant difference in the Hunza basin between surging and non-surging glaciers in terms of total glacier area in a period of 37 years on a sample of 93 glaciers. However, according to the present knowledge, surge-type glaciers might obscure the actual glacier response to climate change in this region — in particular because their return periods are poorly constrained (Quincey and Luckman, 2014) — and should therefore be discussed separately.

5.4 Comparison with the other glacier inventories

We compared our glacier outlines with the ICIMOD inventory (Bajracharya and Shrestha, 2011), and the Randolph Glacier Inventory, version 4.0 (RGI, Arendt and others, 2014), the two other region wide inventories. The source of the data used in the RGI 4.0 for our region is mainly the Global Land Ice Measurements from Space initiative (GLIMS) —which consists mostly of data from the first Chinese Glacier Inventory (Shi and others, 2009)— , but it also includes outlines from a previous ICIMOD inventory (Mool and others, 2007), and some from Bhambri and others (2013)

in the Shyok river basin. To make the comparison consistent, we selected only those glacier polygons which were mapped in all the three inventories at the same time. We chose to compare the outlines from 2001 of our inventory because they are closer in time to both the other inventories. The comparison was made for the entire glacier area and for the accumulation area only, because minor changes over time are expected to occur in the accumulation area. An elevation of 5200 m a.s.l. was used as ELA, for the reasons discussed in the Results chapter.

Table 12 shows the differences in area between the ICIMOD and the RGI inventories, compared to our mapping results. The relative area difference is not large with respect to the total glacier surface, but shows a tendency to higher values above the ELA. Our inventory tends to underestimate the glacier area in the accumulation zone. In particular, the difference in accumulation area amongst our inventory and the ICIMOD one is half the one found by comparing it with the RGI (version 4.0). This might derive from different strategies of mapping the upper glacier limits in the different inventories. In particular, the ICIMOD inventory used a slope criterion to exclude all the headwalls steeper than 60° from the upper glacier limit. This approach can partly explain the lower overall glacier area found in the ICIMOD inventory and the present one, compared to the RGI 4. Indeed, the inclusion of the steep headwalls of the accumulation basins in the glacier outlines, and the presence of seasonal snow cover in the source data, lead to larger glacier areas in the RGI, as also reported by Nuimura and others (2015). These authors present a new glacier inventory (the GAMDAM glacier inventory, GGI) where they report significantly less glacier area compared to RGI 4.0 in the Karakoram region (-13%), and significantly more compared to ICIMOD (+22%). Unfortunately, we are not able to make a direct comparison with the GGI, as this is not available for download, and we cannot extract the glacier areas within the CKNP borders (which correspond to 1/3rd of the whole Karakoram glaciers, according to ICIMOD). We can only observe that our inventory is in-between the RGI and ICIMOD just like the GGI (Table 12).

Table 12: Summary of glaciers in the CKNP glacier inventory (year 2001), ICIMOD inventory, and the RGI 4.0. The areas are compared with respect to the CKNP 2001 inventory (see "Difference" values). Only glacier polygons mapped in all the three inventories at the same time are shown.

	CKNP 2001	**ICIMOD**			**RGI 4.0**		
	Area	**Area**	**Difference**		**Area**	**Difference**	
	[km^2]	**[km^2]**	**[km^2]**	**[%]**	**[km^2]**	**[km^2]**	**[%]**
total area	4256.8 ± 63.9	4185.0	-71.8	-2	4658.5	401.7	9
above ELA	1342.9 ± 2.6	1573.2	230.3	17	1831.6	488.7	36

Very recently, the version 5 of the RGI was released, with a glacier area of 5593.7 km^2 in the study zone.

We overlapped the glacier outlines of all the available inventories by twos, and extracted the regions

which did not match, to study the absolute differences between inventories (Table 13). From this analysis, the RGI resulted the farthest from the other inventories in absolute terms. The greatest difference is found when comparing the accumulation zone, probably for the same reasons just discussed.

Table 13: Glacier areas and absolute differences between inventories. Only glaciers which were mapped in all the three inventories at the same time are considered. Percentages are calculated on the mean of the total area of the two inventories used for comparison.

		total area	**above ELA**
CKNP 2001	[km^2]	4256.8 ± 63.9	1342.9 ± 2.6
ICIMOD	[km^2]	4185.0	1573.2
RGI 4.0	[km^2]	4658.5	1831.6
ICIMOD-CKNP	[km^2]	1297.2	609.9
	[%]	31	42
CKNP-RGI	[km^2]	3014.9	1287.1
	[%]	68	81
ICIMOD-RGI	[km^2]	3056.9	1261.4
	[%]	69	74

6. Conclusions

The present manuscript exploits Landsat images to produce a detailed glacier inventory of the Central Karakoram National Park and to analyze the glacier changes during the first decade in the new millenium. It provides a dataset of glacier boundaries for 711 glaciers for the years 2001 and 2010. A supervised classification on the Landsat images allowed the spatial analysis of the supraglacial debris, which is abundant in the glacier ablation area (~31% coverage). Debris covers most of the glacier area up to 4000 m and its thickness is very high at the terminus (up to >1 m, Mayer and others, 2006; Copland and others, 2009).

The analysis of the area changes during 2001–2010 reveals a general stability (+0.4 ± 202.9 km^2 over 4605.9 ± 86.1 km^2 in 2001), evidence of the anomalous behavior of glaciers in the Karakoram in contrast to a worldwide shrinkage of mountain glaciers. Even when neglecting the surge-type advances, the area change remains stable, but is slightly negative. However, the abundance of surge type glaciers plays an additional role in transporting ice volume towards lower altitudes.

The Karakoram anomaly is analyzed in view of the ongoing climate change. A slight increase in late

summer SCA during 2001–2010 is observed from MODIS snow data. At the same time, the available weather stations reveal an increase of snowfall events and a decrease of mean summer air temperatures since 1980, which would translate into more persistent snow cover during the melt season. These results support an enhanced glaciers preservation in the ablation areas due to a long-lasting snow cover, and stronger accumulation at higher altitudes, pushing towards positive net balances. Nevertheless, linking these observations to the analysis of glacier area changes is not unambiguous, since there is a delay of the glacier area response to climate change depending on glacier size, with usually longer response times (even several decades) for larger glaciers (Bolch and others, 2012).

Eventually, we stress the need to study the contribution of meltwater ponds and steep exposed ice cliffs to the overall ablation of Karakoram glaciers, to improve the understanding of the glacier melting processes in this region, as ice melt in the flat lower part of the glacier tongues represents a major source of water from the Karakoram watersheds to the Indus river.

References

Aggarwal P.K., Joshi P.K., Ingram J.S.I. and Gupta R.K. (2004) Adapting food systems of the Indo-Gangetic plains to global environmental change: key information needs to improve policy formulation. Environ. Sci. Policy 7: 487-498.

Akhtar M., Ahmad N. and Booij M.J. (2008) The impact of climate change on the water resources of Hindukush-Karakoram-Himalaya region under different glacier coverage scenario. J. Hydrol. 355: 148-163.

Archer D.R. and Fowler H.J. (2004) Spatial and temporal variations in precipitation in the Upper Indus Basin, global teleconnections and hydrological implications. Hydrol. Earth Syst. Sci. 8: 47-61, doi:10.5194/hess-8-47-2004.

Archer D.R. (2003) Contrasting hydrological regimes in the upper Indus Basin. J. Hydrol. 274: 198-210.

Arendt A., Bliss A., Bolch T., Cogley J.G., Gardner A.S., Hagen J.O., Hock R., Huss M., Kaser G., Kienholz C., Pfeffer W.T., Moholdt G., Paul F., Radić V., Andreassen L., Bajracharya S., Barrand N., Beedle M., Berthier E., Bhambri R., Brown I., Burgess E., Burgess D., Cawkwell F., Chinn T., Copland L., Davies B., De Angelis H., Dolgova E., Filbert K., Forester R., Fountain A., Frey H., Giffen B., Glasser N., Gurney S., Hagg W., Hall D., Haritashya U.K., Hartmann G., Helm C., Herreid S., Howat I., Kapustin G., Khromova T., König M., Kohler J., Kriegel D., Kutuzov S., Lavrentiev I., LeBris R., Lund J., Manley W., Mayer C., Miles E.S., Li X., Menounos B., Mercer A., Mölg N., Mool P., Nosenko G., Negrete A., Nuth C., Pettersson R., Racoviteanu A., Ranzi R., Rastner P., Rau F., Raup B., Rich J., Rott H., Schneider C., Seliverstov Y., Sharp M., Sigurðsson O., Stokes C., Wheate R., Winsvold S., Wolken G., Wyatt F., Zheltyhina N. (2014) Randolph Glacier Inventory – A Dataset of Global Glacier Outlines: Version 4.0. Global Land Ice

Measurements from Space, Boulder Colorado, USA. Digital Media.

Bajracharya S.R., Shrestha B. (eds) (2011) The status of glaciers in the Hindu Kush-Himalayan region. Kathmandu: ICIMOD

Barrand N. and Murray T. (2006) Multivariate controls on the incidence of glacier surging in the Karakoram Himalaya. Arct. Antarct. Alp. Res. 38: 489-498.

Belò M., Mayer C., Lambrect A., Smiraglia C. and Tamburini A. (2008) The recent evolution of Liligo Glacier Karakoram, Pakistan and its present quiescent phase. Ann. Glaciol. 48: 171-176.

Benn D.I., Bolch T., Hands K., Gulley J., Luckman A., Nicholson L.I., Quincey D., Thompson S., Toumi R. and Wiseman S. (2012) Response of debris-covered glaciers in the Mount Everest region to recent warming, and implications for outburst flood hazards. Earth-Science Reviews, 114, 156-174.

Bhambri R., Bolch T., Chaujar R.K. and Kulshreshtha S.C. (2011) Glacier changes in the Garhwal Himalaya, India, from 1968 to 2006 based on remote sensing. J. Glaciol. 57: 534-556

Bhambri R., Bolch T., Kawishwar P., Dobhal D.P., Srivastava D.P. and Pratap B. (2013) Heterogeneity in glacier response in the upper Shyok valley, northeast Karakoram. The Cryosphere 7:1385-1398.

Bocchiola D. and Diolaiuti G.A. (2013) Recent (1980-2009) evidence of climate change in the upper Karakoram, Pakistan. Theor. Appl. Climatol. doi:10.1007/s00704-012-0803-y.

Bocchiola D., Diolaiuti G.A., Soncini A., Mihalcea C., D'Agata C., Mayer C., Lambrecht A., Rosso R. and Smiraglia C. (2011) Prediction of future hydrological regimes in poorly gauged high altitude basins: the case study of the upper Indus, Pakistan. Hydrol. Earth Syst. Sci. 15: 2059-2075, doi:10.5194/hess-15-2059-2011.

Bocchiola D., Mihalcea C., Diolaiuti G.A., Mosconi B., Smiraglia C. and Rosso R. (2010) Flow prediction in high altitude ungauged catchments: a case study in the Italian Alps (Pantano Basin, Adamello Group). Adv. Water Resources 33(10): 1224-1234.

Bocchiola D. (2014) Long term (1921-2011) changes of Alpine catchments regime in Northern Italy. Adv. Water Resources, 70, 51-64.

Bolch T., Kulkarni A., Kääb A., Huggel C., Paul F., Cogley J.G., Frey H., Kargel J.S., Fujita K., Scheel M., Bajracharya S. and Stoffel M. (2012) The state and fate of Himalayan glaciers. Science 336: 310-314.

Bolch T., Pieczonka T. and Benn D.I. (2011) Multi-decadal mass loss of glaciers in the Everest area (Nepal Himalaya) derived from stereo imagery. The Cryosphere 5: 349-358, doi:10.5194/tc-5-349-2011.

Bolch T., Yao T., Kang S., Buchroithner M.F., Scherer D., Maussion F., Huintjes E. and Schneider C. (2010) A glacier inventory for the Western Nyainqentanglha Range and the Nam Co Basin, Tibet, and glacier changes 1976-2009. The Cryosphere 4: 419-433, doi:10.5194/tc-4-419-2010.

Bookhagen B. and Burbank D.W. (2010) Towards a complete Himalayan hydrologic budget: the spatiotemporal distribution of snow melt and rainfall and their impact on river discharge. J. Geophys. Res. 115: F03019, doi:10.1029/2009jf001426.

Braithwaite R. and Raper S. (2009) Estimating equilibrium-line altitude (ELA) from glacier inventory data. Ann. Glaciol. 50: 127-132.

Brohan P., Kennedy J.J., Harris I., Tett S.F.B. and Jones P.D. (2006) Uncertainty estimates in regional and global observed temperature changes: a new dataset from 1850. Journal of Geophysical Research 111: D12106, doi:10.1029/2005JD006548, 2006.

CGIAR-CSI, Consortium for Spatial Information (2012) http://www.cgiar-csi.org, last access: 20 February 2014.

Citterio M., Diolaiuti G.A., Smiraglia C., D'agata C., Carnielli T., Stella G. and Siletto G.B. (2007) The fluctuations of Italian glaciers during the last century: a contribution to knowledge about Alpine glacier changes. Geogr. Ann. A 89: 164-182.

Cogley J.G. (2009) Geodetic and direct mass-balance measurements: comparison and joint analysis. Ann. Glaciol. 50: 96-100.

Copland L., Sharp M.J. and Dowdeswell J.A. (2003) The distribution and flow characteristics of surge-type glaciers in the Canadian High Arctic. Ann. Glaciol. 36: 73-81.

Copland L., Sylvestre T., Bishop M.P., Shroder J.F., Seoung Y.B., Owen L.A., Bush A. and Kamp U. (2011) Expanded and Recently Increased Glacier Surging in the Karakoram. Institute of Arctic and Alpine Reasearch (INSTAAR), University of Colorado, available at: http://www.bioone.org/doi/full/10.1657/1938-4246-43.4.503.

Cuffey K.M. and Paterson W.S.B. (2010) The Physics of Glaciers. 4th Edn., ISBN: 9780123694614, Pergamon Press, Oxford, UK.

Desio A. (1964) Italian Expeditions to the Karakorum (K2) and Hindu Kush, in: Leader II, vol. 1, edited by: Marussi, A., E. J. Brill, Leiden.

Diolaiuti G.A., D'Agata C., Meazza A., Zanutta A. and Smiraglia C. (2009) Recent (1975-2003) changes in the Miage debris-covered glacier tongue (Mont Blanc, Italy) from analysis of aerial photos and maps. Geogr. Fis. Dinam. Quat. 32: 117-127.

Diolaiuti G.A., Bocchiola D., Vagliasindi M., D'agata C. and Smiraglia C. (2012) The 1975-2005 glacier changes in Aosta Valley (Italy) and the relations with climate evolution. Prog. Phys. Geogr. 36: 764-785, doi:10.1177/0309133312456413.

Diolaiuti G.A., Pecci M. and Smiraglia C. (2003) Liligo Glacier (Karakoram): reconstruction of the recent history of a surge-type glacier. Ann. Glaciol. 36: 168-172.

Fowler H.J. and Archer D.R. (2006) Conflicting signals of climatic change in the Upper Indus basin. J. Climate 19: 4276-4293.

Fujita K. and Nuimura T. (2011) Spatially heterogeneous wastage of Himalayan glaciers. P. Natl. Acad. Sci. USA 108: 14011-14014.

Gardelle J., Berthier E. and Arnaud Y. (2012) Slight mass gain of Karakoram glaciers in the early 10 twenty-first century. Nat. Geosci. Letters 5: 322-325, doi:10.1038/NGEO1450.

Gardelle J., Berthier E., Arnaud Y. and Kääb A. (2013) Region-wide mass balances over the Pamir-Karakoram-Hiimalaya during 1999-2011. The Cryosphere 7: 1263-1286.

Gardner A.S., Moholdt G., Cogley J.G., Wouters B., Arendt A.A., Wahr J., Berthier E., Hock R., Pfeffer W.T., Kaser G., Ligtenberg S.R.M., Bolch T., Sharp M.J., Hagen J.O., Van Den Broeke M.R. and Paul F. (2013) A Reconciled Estimate of Glacier Contributions to Sea Level Rise: 2003 to 2009. Science 852-857.

Gurung D.R., Amarnath G., Khun S.A., Shrestha B., Kulkarni A.V. (2011) Snow-cover mapping and monitoring in the HinduKush-Himalayas. Kathmandu: ICIMOD, (eds) 2011.

Hagg W., Mayer C., Lambrecht A. and Helm A. (2008) Sub-debris melt rates on Southern Inylchek glacier, Central Tian Shan. Geogr. Ann. 90A (1): 55-63.

Hall D.K., Salomonson V.V. and Riggs G.A.(2006) MODIS/Terra Snow Cover 8-Day L3 Global 500m Grid. Version 5. [Jan-Dec, 2001-2010]. Boulder, Colorado USA: National Snow and Ice Data Center.

Hasson S., Lucarini V., Khan M., Pettita M., Bolch T., and Gioli G. (2014), Early 21st century snow cover state over the western river basins of the Indus River system, Hydrol. Earth Syst. Sci. 18, 4077–4100.

Hasson S., Böhner J., and Lucarini V. (2015) Prevailing climatic trends and runoff response from Hindukush-Karakoram-Himalaya, upper Indus basin. Earth Syst. Dynam. Discuss., 6, 579-653, 2015

Herreid S., Pellicciotti F., Ayala A., Chesnokova A., Kienholz C., Shea J .and Shrestha A. (2015) Satellite observations show no net change in the percentage of supraglacial debris-covered area in northern Pakistan from 1977 to 2014, J. Glaciol., Vol. 61, No. 227, doi: 10.3189/2015JoG14J227.

Hewitt K. (2005) The Karakoram Anomaly? Glacier expansion and the "elevation effect", Karakoram Himalaya. Mt. Res. Dev. 25: 332-340.

Hewitt K. (2007) Tributary glacier surges: an exceptional concentration at Panmah Glacier, Karakoram, Himalaya. J. Glaciol. 53: 181-188. doi:10.3189/172756507782202829.

Hewitt K. (2011) Glacier Change, Concentration, and Elevation Effects in the Karakoram Himalaya, Upper Indus Basin. Mt. Res. Dev. 31(3): 188-200, doi: http://dx.doi.org/10.1659/MRD-JOURNAL-D-11-00020.1.

Huang X., Zhang X., Li X., and Liang T. (2007) Accuracy analysis for MODIS Snow Products of MOD10A1 and MOD10A2 in Northern Xinjiang Area. Journal of Glaciology and Geocryology.

Hurrell J.W. (1995) Decadal trends in the North Atlantic Oscillation regional temperatures and precipitation. Science 269: 676-679.

Immerzeel W.W., Van Beek L.P.H. and Bierkens M.F.P. (2010) Climate change will affect the Asian water towers. Science 328: 1382-1385.

Jiang T., Su B., Hartmann H. (2007) Temporal and spatial trends of precipitation and river flow in the Yangtze River Basin, 1961-2000. Geomorphology 85: 143-154.

Juen M., Mayer C., Lambrecht A., Han H. and Liu S. (2014) Impact of varying debris cover thickness on ablation: a case study for Koxkar Glacier in the Tien Shan. The Cryosphere, 8, 377-386.

Kääb A., Berthier E., Nuth C., Gardelle J. and Arnaud Y. (2012) Contrasting patterns of early twenty-first-century glacier mass change in the Himalayas. Nature Letter 488: 495-498, doi:10.1038/nature11324.

Kääb A., Paul F., Maisch M., Hoelzle M. and Haeberli W. (2002) The new remote sensing derived Swiss glacier inventory: II. First results. Ann. Glaciol. 34: 362-366.

Kahlown M.A., Raoof A., Zubair M. and Kemper W.D. (2007) Water use efficiency and economic feasibility of growing rice and wheat with sprinkler irrigation in the Indus Basin of Pakistan. Agr. Water Manage. 8: 292-298.

Kaser G., Fountain A. and Jansson P. (2003) A Manual for Monitoring the Mass Balance of Mountain Glaciers. International Hydrological Programme Technical Documents in Hydrology No. 59, UNESCO, Paris.

Kendall M.G. (1975) Rank Correlation Methods. Oxford Univ. Press, New York.

Kirkbride M.P. and Dugmore A.J. (2003) Glaciological response to distal tephra fallout from the 1947 eruption of Helka, south Iceland. J. Glaciol. 49: 166.

Landsat7 Handbook: http://landsathandbook.gsfc.nasa.gov/, http://lpdaac.usgs.gov, last access: 13 April 2014.

Manley W.F. (2005) Geospatial inventory and analysis of glaciers: a case study for the Eastern

Alaska Range, in: Satellite Image Atlas of Glaciers of the World. Edited by: Williams Jr, R. S. and Ferrigno, J. G., Professional Paper 1386-K, K424-K439, US Geological Survey.

Mann H.B. (1945) Nonparametric tests against trend. Econometrica 13: 245- 259.

Mattson L.E., Gardner J.S. and Young G.J. (1993) Ablation on debris covered glaciers: an example from the Rakhiot Glacier, Punjab, Himalaya. Snow and Glacier Hydrology, Proc. Kathmandu Symp. November 1992, edited by: Young, G. J., IAHS Publ. no. 218, IAHS Publishing, Wallingford, 289-296.

Mayer C., Fowler A.C., Lambrecht A. and Scharrer K. (2011) A surge of North Gasherbrum Glacier, Karakoram, China. J. Glaciol. 57: 904-916.

Mayer C., Lambrecht A., Belò M., Smiraglia C. and Diolaiuti G.A. (2006) Glaciological characteristics of the ablation zone of Baltoro Glacier, Karakoram. Ann. Glaciol. 43: 123-131.

Mayer C., Lambrecht A., Mihalcea C., Belò M., Diolaiuti G.A., Smiraglia C., Bashir F. (2010) Analysis of Glacial Meltwater in Bagrot Valley, Karakoram. Mountain Research and Development 30(2): 169-177.

Mayer C., Fowler A.C., Lambrecht A., and Sharrer K. (2011) A surge of North Gasherbrum Glacier, Karakoram, China. Journal of Glaciology, Vol. 57, No. 204, 2011

Mihalcea C., Mayer C., Diolaiuti G.A., D'agata C., Smiraglia C., Lambrecht A., Vuillermoz E. and Tartari G. (2008) Spatial distribution of debris thickness and melting from remote-sensing and meteorological data, at debris-covered Baltoro glacier, Karakoram, Pakistan. Ann. Glaciol. 48: 49-57.

Mihalcea C., Mayer C., Diolaiuti G.A., Lambrecht A., Smiraglia C. and Tartari G. (2006) Ice ablation and meteorological conditions on the debris covered area of Baltoro Glacier (Karakoram, Pakistan). Ann. Glaciol. 43: 292-300.

Mool P.K., Bajracharya S.R., Shrestha B., Joshi S.P., Shakya K., Baidya A .and Dangol G.S. (2007) Inventory of Glaciers, Glacial Lakes and the Identification of Potential Glacial Lake Outburst Floods (GLOFs) Affected by Global Warming in the Mountains of Himalayan Region. International Centre for Integrated Mountain Development, Kathmandu. DVD, report, data.

Nicholson L. and Benn D.I. (2006) Calculating ice melt beneath a debris layer using meteorological data. Journal of Glaciology 52: 178.

NSIDC, National Snow and Ice Data Center: http://nsidc.org, last access: 13 March 2014.

O'Gorman L. (1996) Subpixel precision of straight-edged shapes for registration and measurement. IEEE Transactions on Pattern Analysis and Machine Intelligence 18: 746-751, doi:10.1109/34.506796.

Osborn T.J. (2004) Simulating the Winter North Atlantic Oscillation: the roles of internal variability and greenhouse gas forcing. Climate Dynamics 22: 605-623.

Osborn T.J. (2006) Recent variations in the Winter North Atlantic Oscillation. Weather 61: 353-355.

Østrem G. (1959) Ice melting under a thin layer of moraine, and the existence of ice cores in moraine ridges. Geogr. Ann. 41(4): 228-230.

Parajka J. and Blöschl G. (2008a) The value of MODIS snow cover data in validating and calibrating conceptual hydrologic models. Journal of Hydrology 358: 240-258.

Parajka J. and Blöschl G. (2008b) Spatio-temporal combination of MODIS images-potential for snow cover mapping. Water Resources Research 44.

Paul F., Huggel C. and Kääb A. (2004) Combining satellite multispectral data and a digital elevation model for mapping debris-covered-glaciers. Remote Sens. Environ., 89 (4), 510-518 (doi: 10.1016/j.rse.2003.11.007).

Paul F., Barry R.G., Cogley J.G., Frey H., Haeberli W., Ohmura A., Ommanney C.S.L., Raup B., Rivera A. and Zemp M. (2009) Recommendations for the compilation of glacier inventory data from digital sources. Ann. Glaciol. 50 (53).

Paul F., Barrand N.E., Baumann S., Berthier E., Bolch T., Casey K., Frey H., Joshi S.P., Konovalov V., Le Bris R., Mölg N., Nosenko G., Nuth C., Pope A., Racoviteanu A., Rastner P., Raup B., Scharrer K., Steffen S. and Windswold S. (2013) On the accuracy of glacier outlines derived from remote-sensing data. Ann. Glaciol. 54 (63).

Peel M.C., Finlayson B. Land McMahon T.A. (2007) Updated world map of the K¨oppen-Geiger climate classification. Hydrol. Earth Syst. Sci. 11: 1633-1644, doi:10.5194/hess-11-1633-2007.

Pu Z., Xu L., Salomonson V.V. (2007) MODIS/Terra observed seasonal variations of snow cover over the Tibetan Plateau. Geophysical Research Letters. 34.

Quincey D.J. and Luckman A. (2014) Brief communication: On the magnitude and frequency of Khurdopin glacier surge events. The Cryosphere, 8, 571-874.

Quincey D.J., Copland L., Mayer C., Bishop M., Luckman A. and Belò M. (2009) Ice velocities and climate variations for Baltoro Glacier, Pakistan. J. Glaciol. Vol 55, No. 194.

Quincey D.J., Braun M., Glasser N.F., Bishop M.P., Hewitt K. and Luckman A. (2011) Karakoram glacier surge dynamics. Geophys. Res. Lett., 38, L18504, doi: 10.1029/2011GL049004.

Racoviteanu A.E., Arnaud Y., Williams M.W. and Ordonez J. (2008) Decadal changes in glacier parameters in the Cordillera Blanca, Peru, derived from remote sensing. J. Glaciol. 54: 499-510.

Rankl M., Kienholz C., and Braun M. (2014) Glacier changes in the Karakoram region mapped by multimission satellite imagery. The Cryosphere, 8, 977-989.

Reid T.D. and Brock B.W. (2010) An energy balance model for debris-covered glaciers including heat conduction through the debris layer. Journal of Glaciology 56: 199.

Reid T.D. and Brock B.W. (2014) Assessing ice-cliff backwasting and its contribution to total ablation of debris-covered Miage glacier, Mont Blanc massif, Italy. J. Glaciol., Vol 60, No. 219.

Reznichenko N., Davies T., Shulmeister J. and McSaveney M. (2010) Effects of debris on ice-surface melting rates: an experimental study. Journal of Glaciology 56: 197.

Sakai A., Nakawo M. and Fujita K. (2002) Distribution characteristics and energy balance of ice cliffs on debris-covered glaciers Nepal Himalaya. Arct. Antarct. Alp. Res., 34, 12-19.

Sakai A., Nakawo M. and Fujita K. (1998) Melt rate of ice cliffs on the Lirung Glacier, Nepal Himalayas, 1996 (1998). Bullettinn of Glacier Reasearch, 16, 57-66.

Salerno F., Buraschi E., Bruccoleri D., Tartari G. and Smiraglia C. (2008) Glacier surface-area changes in Sagarmartha national park, Nepal, in the second half of the 20th century, by comparison of historical maps. J. Glaciol. 54: 738-752.

Seidou O., Ouarda T.B.M.J (2007) Recursion-based multiple changepoint detection in multiple linear regression and application to river stream flows. Wat. Resour. Res. 43: W07404.

Shekhar M.S., Chand H., Kumar S., Srinivasan K., and Ganju A. (2010) Climate-change studies in the western Himalaya. Annals of Glaciology, 51(54) 2010

Scherler D., Bookhagen B. and Srecker Manfred R. (2011) Spatially variable response of Himalayan glaciers to climate change affected by debris cover. Nature Geoscience 4, doi: 10.1038/NGEO1068.

Shi Y.F., Liu C.H. and Kang E.S. (2009) The Glacier Inventory of China, Annals of Glaciology, 50(53), 1–4. doi: 10.3189/172756410790595831.

Shukla A., Arora M.K. and Gupta R.P. (2010) Synergistic approach for mapping debris-covered glaciers using optical–thermal remote sensing data with inputs from geomorphometric parameters. Remote Sens. Environ., 114 (7), 1378-1387

Soncini A., Bocchiola D., Confortola G., Bianchi A., Rosso R., Mayer C., Lambrecht A., Palazzi E., Smiraglia C., Diolaiuti G. (2015). Future hydrological regimes in the upper Indus basin: a case study from a high altitude glacierized catchment, J. Hydrometeorology, 16(1):306-326.

Tartari G., Salerno F., Buraschi E. and Smiraglia C. (2008) Lake surface area variations in the North-Eastern sector of Sagarmatha National Park (Nepal) at the end of the 20th Century by comparison of historical maps, J. of Limnology, Vol 76, No. 2.

Tahir A.A., Chevallier P., Arnaud Y. and Ahmad B. (2011) Snow cover dynamics and hydrological regime of the Hunza River basin, Karakoram Range, Northern Pakistan. Hydrol. Earth Syst. Sci.

15: 2275-2290, doi:10.5194/hess-15-2275-2011.

Vaughan D.G., Comiso J.C., Allison I., Carrasco J., Kaser G., Kwok R., Mote P., Murray T., Paul F., Ren J., Rignot E., Solomina O., Steffen K. and Zhang T. (2013) Observations: Cryosphere. In: Climate Change 2013: The Physical Science Basis. Contribution of Working Group I to the Fifth Assessment Report of the Intergovernmental Panel on Climate Change [Stocker T F, Qin D, Plattner G K, Tignor M, Allen S K, Boschung J, Nauels A, Xia Y, Bex V and Midgley P M (eds.)]. Cambridge University Press, Cambridge, United Kingdom and New York, NY, USA.

Vögtle T. and Schilling K.J. (1999) Digitizing maps, in: GIS for Environmental Monitoring, edited by: Bähr, H.-P. and Vögtle, T., Schweizerbart, Stuttgart, Germany, 201-216.

Wake C.P., Mayewski P.A. and Spencer M.J. (1990) A review of central Asian glaciochemical data. Ann. Glaciol., 14.

Wang X., Xie H., and Liang T. (2008) Evaluation of MODIS snow cover and cloud mask and its application in Northern Xinjiang, China. Remote Sensing of Environment 112 (2008) 1497–1513

Weiers S. (1995) Zur Klimatologie des NW-Karakoram und angrenzender Gebiete. Statistische Analysen unter Einbeziehung von Wettersatellitenbildern und eines Geographischen Information systems (GIS). Bonner Geographische Abhandlungen 92. Bonn, Germany: Geographisches Institut, Universitat Bonn.

Winiger M., Gumpert M. and Yamout H. (2005) Karakoram-Hindukush-Western Himalaya: assessing high-altitude water resources. Hydrol. Process. 19: 2329-2338.

WGMS: Fluctuations of Glaciers Database. World Glacier Monitoring Service, Zurich, Switzerland. DOI:10.5904/wgms-fog-2013-11. Online access: http://dx.doi.org/10.5904/wgms-fog-2014-09, 2013. Last access on the 14th April 2014.

Wulf H., Bookhagen B., Scherler D. (2010) Seasonal precipitation gradients and their impact on fluvial sediment flux in the Northwest Himalaya. Geomorphology 118(1-2): 13-21.

Yao T., Thompson L.G., Yang W., Yu W., Gao Y., Guol X., Yang X., Duan K., Zhao H., Xu B., Pu J., Lu A., Xian Y., Kattel D.B. and Joswiak D. (2012) Different glacier status with atmospheric circulations in Tibetan Plateau and surroundings. Nature Clim. Change 2: 663-667.

Yue S. and Wang C.Y. (2002) Applicability of pre-whitening to eliminate the influence of serial correlation on the Mann-Kendall test. Wat. Resour. Res. 38 (6): 1068, 10.1029/2001WR000861.

Zhang X., Vincent L.A., Hogg W.D. and Niitsoo A. (2000) Temperature and precipitation trends in Canada during the 20th century. Atmos. Ocean 38(3): 395- 429.

Chapter 3

A simple model to evaluate ice melt over the ablation area of glaciers in the Central Karakoram National Park, Pakistan

Published in Annals of Glaciology (2015) by: **Minora U.**, Senese A., Bocchiola D., Soncini A., D'Agata C., Ambrosini R., Mayer C., Lambrecht A., Vuillermoz E., Smiraglia C., Diolaiuti G.

Abstract

This study provides an estimate of fresh water derived from ice melt for the ablation areas of glaciers in the Central Karakoram National Park (CKNP), Pakistan. In the CKNP there are ~700 glaciers, covering ~4600 km^2 , with widespread debris cover (518 km^2). To assess meltwater volume we applied a distributed model able to describe both debris-covered and debris-free ice ablation. The model was calibrated using data collected in the field in the CNKP area and validated by comparison with ablation data collected in the field, independent of the data used in building the model. During 23 July–9 August 2011, the mean model-estimated ablation in the CKNP was 0.024 m d^{-1} in debris-covered areas and 0.037 m d^{-1} in debris-free areas. We found a mean error of –0.01 m w.e. (corresponding to 2%) and a root-mean-square error equal to 0.09 m w.e. (17%). According to our model, the ablation areas of all the glaciers in the CKNP produced a water volume of 1.963 km^3 during the study period. Finally, we performed several sensitivity tests for assessing the impact of the input data variations.

1. Introduction

The largest glacierized region outside the Arctic and the Antarctic is High Mountain Asia (HMA), which covers an area of 118 200 km^2 (Gardner and others, 2013). Changes in glacier extent and volume in this region are spatially heterogeneous and poorly known (Bolch and others, 2012). Indeed, recent studies revealed that most of the northwestern Himalaya have experienced less glacier shrinkage than the eastern parts of the same mountain range (Bhambri and Bolch, 2009; Bolch and others, 2012; Kääb and others, 2012). In the western and central Karakoram region, glaciers showed long-term irregular behavior with frequent advances, and possible slight mass gain in the last decade (Copland and others, 2011; Hewitt, 2011; Bolch and others, 2012; Gardelle and others, 2012, 2013; Kääb and others, 2012; Minora and others, 2013; Soncini and others, 2015). Gardelle and others' (2012, 2013) recent studies demonstrate how, in contrast to widespread global glacier retreat, glaciers in the Karakoram region as a whole have exhibited a general mass-balance stability (the so called 'Karakoram anomaly'; Hewitt, 2005, 2011). Advances of individual glaciers have also been reported in the Shyok valley (eastern Karakoram) during the last decade (Raina and Srivastva, 2008). These individual advances and mass gain episodes could be attributed to surging (Barrand and Murray, 2006; Hewitt, 2007; Copland and others, 2011; Quincey and others, 2011), temperature drops (Shekhar and others, 2010) and increased solid precipitation in the accumulation areas (Fowler and Archer, 2006; Bocchiola and Diolaiuti, 2013). The Karakoram glaciers are a strategic resource for Pakistan, because they provide fresh water for civil use, hydropower production and farming. The glacierized Karakoram is therefore a key area for studying the effects of ongoing climate change on present and future meltwater discharge.

This study focuses on the glacier ablation areas within the Central Karakoram National Park (CKNP), with the aim of assessing the magnitude and rate of ice ablation and evaluating the derived meltwater amount. For this purpose, we applied a distributed model able to describe ablation in debris-covered and debris-free conditions (Pellicciotti and others, 2005; Mihalcea and others, 2008a). Indeed, a significant proportion of the glaciers in the CKNP are covered by a supraglacial debris layer, modulating the magnitude and rate of ice ablation (Nakawo and Young, 1981; Nakawo and Takahashi, 1982; Nicholson and Benn, 2006; Mihalcea and others, 2008a,b; Reid and Brock, 2010). This debris layer must therefore be accurately considered in distributed modeling of ice melt.

While quite a few energy- and mass-balance studies have been performed on debris-free glaciers, studies including debris-covered ice are not numerous. In the recent past, some authors have focused their attention on debris-covered ice only, and at single-point sites. For example, Nicholson and Benn (2006) presented a modified surface energy- balance model to calculate melt beneath a debris layer from daily mean meteorological data on two European debris- covered glaciers (Ghiacciaio del Belvedere, Italy, and Larsbreen, Norway). Han and others (2006) proposed a simple model to estimate ice ablation under a thick debris layer by using surface temperature and debris thermal properties on Koxkar glacier, Tien Shan, China. During the last two decades, a few papers

have focused on debris- covered glaciers in the Himalaya and Karakoram (e.g. Hewitt and others, 1989; Mattson and Gardner, 1989; Mattson and others, 1993; Young and Hewitt, 1993; Nakawo and Rana, 1999; Kayastha and others, 2000; Nakawo and others, 2000; Takeuchi and others, 2000; Lejeune and others, 2013). Some studies have used remote- sensing data to analyze the spatial distribution of surface temperatures and calculate the energy available for melting (Nakawo and others, 1993; Rana and others, 1997; Nakawo and Rana, 1999). Unfortunately, these studies only provided melt data over small areas and short time spans. Mihalcea and others (2008a) modeled debris-covered ice ablation over the whole Baltoro glacier ablation area by applying a distributed approach, based on computation of the conductive heat flux through the debris layer and requiring information on debris thickness distribution derived from ASTER (Advanced Spaceborne Thermal Emission and Reflection Radiometer) thermal data. This approach has also been used by Zhang and others (2011) who applied it on Hailuogou glacier, southeastern Tibetan Plateau, and more recently by Fujita and Sakai (2014) on the Tsho Rolpa glacial lake–Trambau glacier basin in the Nepal Himalaya. Fyffe and others (2014) developed a melt model, which calculates sub-debris melt rates using an existing debris energy- balance model (DEB-Model introduced by Reid and Brock, 2010) and melt rates for clean ice, snow and partially debris- covered ice using standard energy-balance equations. This approach is more exhaustive (but also more complex) than that of Mihalcea and others (2008b), though its application to a whole glacierized watershed or an entire glacier region is not simple, and requires input data featuring high spatial and temporal resolution, not always available in remote high-elevation glacier zones. Therefore, the results we present in this study were obtained for the entire CKNP debris-covered ice zone by applying the model developed by Mihalcea and others (2008b). Furthermore, we assessed the contribution of debris-free ice melt to fresh water from the whole CKNP melting area. Modeling of debris-free ice melt has been extensively analyzed in the recent past, and several attempts have been made to apply the degree-day approach or simplified energy budget computations to large and representative glacierized catchments worldwide. Nevertheless, on large and remote glacierized catchments, only a few attempts to model debris-free ice melt coupled with approaches estimating debris-covered ice ablation are available (e.g. Soncini and others, 2015). In our study, we evaluate ice melt in debris-free conditions by applying an enhanced T-index model (following Pellicciotti and others, 2005), which also considers solar energy inputs in driving ice melt. This melt model was coupled with the debris- covered ice melt model, thus obtaining a suitable tool to be applied on large and remote glacierized areas featuring both debris-covered and debris-free ice conditions.

2. Study site

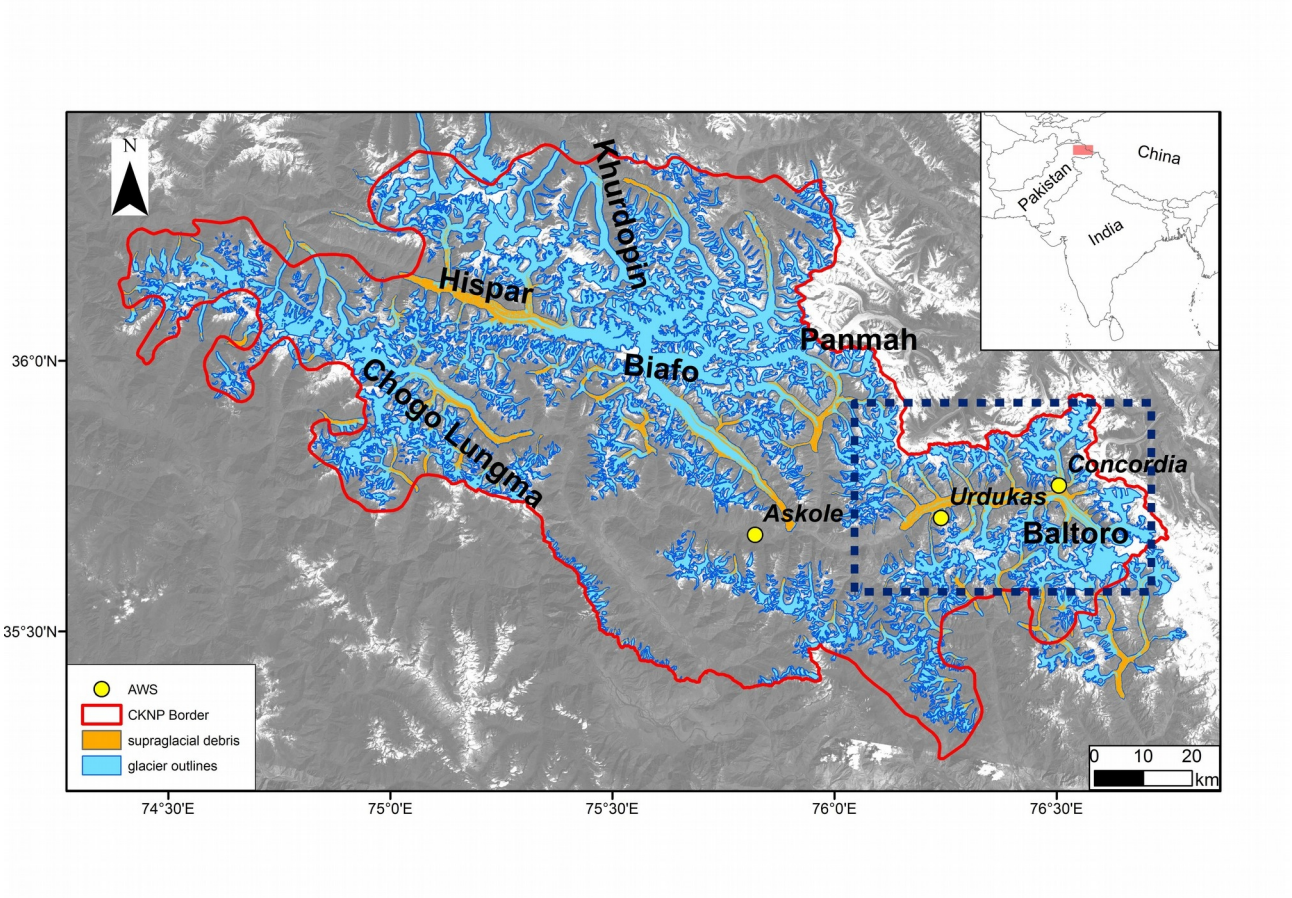

Figure 1: Study area. The map shows the border of the Central Karakoram National Park (CKNP) in northern Pakistan (red line), the automatic weather stations at Askole, Urdukas and Concordia (yellow dots), the glacier boundaries (blue lines), and the glacier areas covered by supraglacial debris (orange). Names of the widest glaciers are shown, with the area of Baltoro glacier highlighted by a box with blue dashed line.

The CKNP is a protected area established in 2009 covering 12 162 km^2 in northeastern Pakistan, at the border with India and China (Fig. 1). The park protects major natural resources for the country, including >700 glaciers, with a total area of 4632 km^2 , corresponding to ~30% of the overall glacier area of the Pakistani Karakoram (ICIMOD, 2013). Glaciers in the CKNP span a broad range of sizes, types (mountain glaciers, glacierets, hanging glaciers, compound-basin valley glaciers), and surface conditions (debris-free and debris-covered ice). In addition, the Karakoram is known to host several surge-type glaciers (Diolaiuti and others, 2003; Barrand and Murray, 2006; Hewitt, 2007, 2011; Kotlyakov and others, 2008; Gardelle and others, 2012), displaying cyclically short active phases involving rapid mass transfer from high to low elevations, and long quiescent phases of low mass fluxes. Copland and others (2011) reported 90 surge-type glaciers in the Karakoram mountains. In particular, in the 14 years after 1990, they found double the number of new surges

(26) compared with those counted in the 14 years before (13 surges).

The ablation areas of many glaciers in the CKNP are heavily debris-covered, because of abundant rockfalls from steep walls, and intense avalanche activity (e.g. Bolch and others, 2012). Supraglacial debris covers ~10% of the total glacier area in the Karakoram (Bolch and others, 2012).

Baltoro glacier is one of the largest debris-covered glaciers in the Karakoram Range, with a maximum length of ~62 km and an area of ~524 km^2 , including all connected tributaries (Mayer and others, 2006). The total drainage basin of Baltoro glacier is ~1500 km^2 . It extends in the east–west direction on the south side of the Karakoram Range, lying in the region 35°35 0 –35°56 0 N, 76°04 0 –76° 46 0 E. The Baltoro glacier elevation ranges between 3370 m a.s.l. and the K2 summit (8611 m a.s.l.). Supraglacial debris of diverse lithology (Desio and others, 1961) occurs below 5000 m a.s.l., and covers ~38% of the glacier area. The grain size shows a large variability on the glacier, from sub-millimeter dust to boulders of a few meters diameter (Mayer and others, 2006), and this is typical of the whole Karakoram debris-covered area (Mihalcea and others, 2008b; Zhang and others, 2013). In the highest parts of Baltoro glacier, the debris occurs over medial moraines, then gradually spreads to a uniform cover across the entire surface, mantling most of the ablation zone. Near the terminus, the debris thickness may exceed 1 m (Mayer and others, 2006). Debris cover has been present on this glacier for at least the last century (historical data reported by Conway, 1894; De Filippi, 1912).

Because of its size and the proportion of area covered by supraglacial debris (38% debris-covered and 62% debris- free), and its elevation (the equilibrium-line altitude (ELA) was reported to be at 5200 m a.s.l. by Mayer and others, 2006, and Bocchiola and others, 2011), Baltoro glacier can be considered paradigmatic of glacierized areas in the CKNP. It will therefore be our focus here for calibrating and validating the melt models.

In addition, permanent automatic weather stations (AWSs) operate on the glacier (at Urdukas, on a lateral moraine at 3926 m a.s.l., and Concordia, on the glacier melting surface at 4700 m a.s.l.), as well as in Askole (3029 m a.s.l.), the first village down-valley from Baltoro glacier (Fig. 1). These AWSs are part of the SHARE (Stations at High Altitude for Research on the Environment) network (an international project launched by the Ev-K2-CNR Chartered Association). These stations, managed with the support and agreement of the Pakistan Meteorological Department, provided input data for developing the melt models.

According to the Köppen–Geiger classification, this area falls in a cold desert region with a dry climate, little precipitation, a mean annual temperature lower than 18°C, and a wide daily temperature range (this type of arid, desert and cold climate is identified with the symbol BWk; Peel and others, 2007). The Nanga Parbat massif forms a barrier to the northward movement of monsoon storms, which intrudes little in Karakoram. The hydrometeorological regime is barely influenced by monsoons, while a major contribution results from snow and ice melt. Precipitation is

gathered in two main periods, summer (July–September) and winter (January–March), i.e. the seasons of the monsoons and the westerlies, the latter providing the dominant nourishment for glaciers. Some studies indicate that the total annual rainfall is 200–500 mm, as generally derived from valley-based stations, less representative for the highest zones (Archer, 2003). Estimates from snow pits above 4000 m a.s.l. range from 1000 to >3000 mm w.e. (Winiger and others, 2005). However, there is considerable uncertainty about the behavior of precipitation at high altitudes. Recent studies (e.g. Bocchiola and Diolaiuti, 2013; Minora and others, 2013) have highlighted climate and snow-cover trends within this area in the period 1980–2009. Even if no significant changes of precipitation amounts have been detected, the number of rainy days appears to have increased. Regarding air temperature, the maxima have generally increased, while the minima appear to have decreased only during summer.

3. Methods

Since snow depth data in the CKNP area are scant and spotty, our study focused on modeling ice melt only, neglecting snowmelt. Following previous studies (Mayer and others, 2006; Mihalcea and others, 2008b; Bocchiola and others, 2011; Soncini and others, 2015), we set the ELA at 5200 m a.s.l., and we then applied the model only to glacier areas below that level, i.e. in the ablation zone. According to this criterion, the ablation zones of glaciers cover 3138 km^2 , or 67.75% of the total glacierized area, in the CKNP. In addition, our analyses covered the period 23 July–9 August 2011, corresponding to the season when the largest glacier melt occurs during the year. The choice of limiting the application of the models to areas <5200 m a.s.l. may lead to underestimation of the actual glacier melt, as melt can occur above this elevation threshold, however limited in this season. Indeed, Soncini and others (2015) analyzed the hydrological regimes of the Shigar river, covering ~7000 km^2 in the upper Karakoram, and nesting ~2000 km^2 of glaciers (including Baltoro, Biafo, Chogo Lungma), and found that snowmelt contribution was limited during our time frame (i.e. <20% considering the entire basin and not only glacier areas).

We applied two distributed melt models, one for debris- covered and one for debris-free areas. Both models were calibrated using field data gathered during an expedition on Baltoro glacier performed during 2011 (see Table 2 further below).

To model the ice melting amount in the whole CKNP glacier ablation area, we considered the following input data:

1. *The glacier boundaries*: the CKNP glacier inventory was derived by Minora and others (2013), who applied remote-sensing investigations. More precisely, Landsat Thematic Mapper (TM) and Enhanced TM Plus (ETM+) scenes of 2010 were processed and analyzed (Table 1).
2. *A digital elevation model* (DEM) describing the CKNP area (derived from the Shuttle Radar Topography Mission, SRTM3).

3. *A supraglacial debris cover map*: a map describing the occurrence of supraglacial debris was obtained by applying a supervised maximum likelihood (SML) classification to a 2011 Landsat false-color composite image (i.e. 543 bands) (Table 1). This map allowed the separation of the debris-free and debris-covered zones of each glacier.

4. *Meteorological input data*: the daily mean air temperature ($T_{a\text{-}Askole}$; °C) and the daily mean incoming solar radiation ($SW_{in\text{-}Askole}$; W m^{-2}) were obtained from hourly data measured during summer 2011 by the permanent AWS installed at Askole (Fig. 1). We used $T_{a\text{-}Askole}$ and $SW_{in\text{-}Askole}$ to evaluate ice melt over debris-free areas, by applying an enhanced T-index approach (Pellicciotti and others, 2005). $SW_{in\text{-}Askole}$ was also considered in the debris-covered ice melt model in order to estimate the surface debris temperature ($T_{S\text{-}point}$; °C) driving the energy available at the debris–ice interface for ice melt.

5. *Debris data*: (a) a map describing the supraglacial debris thicknesses (DT_{point}; m) was derived from Landsat TM thermal band imagery from August 2011 ($T_{S\text{-}Landsat}$; K); (b) daily surface debris temperatures ($T_{S\text{-}point}$; °C) in each pixel of the DT point map and for each day in our period were computed by considering both daily incoming solar radiation data ($SW_{in\text{-}point}$; W m^{-2}) and debris thickness values (DT_{point}; m); and (c) the debris effective thermal resistance (DR_{point}; m^2 °C W^{-1}) was evaluated from debris thickness values by applying an empirical relation developed by Mihalcea and others (2008b). The data in (a), (b) and (c) are the main inputs in the debris- covered ice melt model because they allowed estimation of the conductive heat flux through the debris layer and, consequently, of the ablation rate.

The total melting (M_{TOT}; m w.e.) in both debris-covered and debris-free ice zones was estimated as

$$M_{TOT}=\sum_{i=1}^{k}\left[\sum_{point=1}^{n}\left(M_{DC-point}\right)+\sum_{point=1}^{m}\left(M_{DF-point}\right)\right], \quad (1)$$

where *n* and *m* are the total number of pixels (each pixel is 30 m x 30 m in size) of the digital image corresponding, respectively, to debris-covered and debris-free glacier areas, *k* is the length of the study period (days) and $M_{DC\text{-}point}$ and $M_{DF\text{-}point}$ are the melting rates over debris-covered and debris-free areas, respectively. $M_{DC\text{-}point}$ and $M_{DF\text{-}point}$ are fully described in Sections 3.3 and 3.4 respectively. The distribution of the meteorological parameters is reported in Section 3.1 and the evaluation of debris features is discussed in Section 3.2.

3.1 Distribution of the meteorological parameters

The meteorological data obtained from the AWS at Askole were corrected applying an altitudinal gradient to obtain estimated meteorological data on the whole glacier ablation areas of the CKNP. In particular, the daily mean air temperature ($T_{a\text{-}point}$; °C) was modeled by applying a constant lapse rate of –0.0075°C m^{-1} (Mihalcea and others, 2006). For the whole CKNP glacierized area, $T_{a\text{-}point}$ was calculated as

$$T_{a-point} = T_{a-Askole} + (-0.0075\,^{\circ}C m^{-1}) * \Delta z \quad , \tag{2}$$

where Δz is the difference in altitude (m) between the glacier pixel and Askole.

The daily mean incoming solar radiation ($SW_{in\text{-}point}$; W m^{-2}) was estimated at each pixel based on the data gathered at Askole ($SW_{in\text{-}Askole}$) (Mihalcea and others, 2008b):

$$SW_{in-point} = SW_{in-Askole}[1 + (2.4 * 10^{-5} \Delta z)] \quad . \tag{3}$$

3.2 Distribution of the debris thickness

There is no fully updated map of the glaciers in the CKNP. The first Park Glacier Inventory was only recently developed from Landsat imagery dating from 2010 (Minora and others, 2013). The debris coverage within glacierized areas below 5200 m a.s.l. (i.e. the ablation zone) was assessed by the SML classification applied to Landsat TM images from 2011. This approach involved training the classification algorithm with a number of sites where the classification output (i.e. presence or absence of debris on the glacier surface) was known (Brown and others, 1998). The SML algorithm assumes that values in each spectral band from Landsat TM are normally distributed and calculates the probability that a given image pixel is debris-covered or debris-free based on the values of all spectral bands. Each pixel is finally classified as debris-covered or debris-free according to the class that has the highest probability (Richards, 1999). The details of the satellite images used are shown in Table 1. In particular, we used band combination 543 (as red, green, blue) of Landsat TM scenes to draw 20 regions of interest (ROIs) and train the classifier. ROIs are sample areas that we know were covered by supraglacial debris in 2011. After training, the classifier was run on all the glacierized areas of the CKNP, assuming a probability threshold of 90% to separate debris-covered from debris-free pixels (i.e. a pixel was classified as 'supraglacial debris-covered' when the probability of a pixel belonging to this class was >0.9). The remaining pixels within glacierized areas and below the ELA were considered debris-free areas.

Table 1: Source, acquisition date and code scene of each satellite image used for the assessment of debris thickness distribution. Site displayed by each image is also reported

Source	Acquisition date	Code scene	Site
Landsat	10th August 2011	LT51480352011222KHC00	East part of the CKNP mosaic
Landsat	17th August 2011	LT51490352011229KHC00	West part of the CKNP mosaic
Landsat	14th August 2004	LE71480352004227PFS01	Baltoro Glacier, used in this study for comparison with Mihalcea and others (2008b)
Aster	14th August 2004	AST_08_00308142004054614	Baltoro Glacier, analyzed by Mihalcea and others (2008b)

To map the thickness of supraglacial debris over the whole glacierized area of the CKNP, we used the method developed by Mihalcea and others (2008b) for Miage glacier, Mont Blanc massif, Italy,

and already applied to Baltoro glacier by Mihalcea and others (2008a). This method is based on the relationship between surface temperature and supraglacial debris thickness (Taschner and Ranzi, 2002). The input data are (1) debris thickness measured in the field on a wide and representative debris-covered glacier area and (2) satellite-derived surface temperatures. The empirical relationship between these data is a valuable tool for estimating debris thickness over unmeasured glacier zones (Mihalcea and others, 2008a,b). This approach was initially developed on ASTER temperature data acquired on 14 August 2004 and applied to Baltoro glacier by Mihalcea and others (2008a) (Table 1). Unfortunately, the ASTER images were not available for the whole CKNP area on the same date. We therefore modified the approach of Mihalcea and others (2008a,b) to use Landsat TM images covering the entire CKNP area. To evaluate the suitability for debris assessment of Landsat TM images instead of ASTER ones, firstly we processed the Landsat image of the debris-covered portion of Baltoro glacier acquired on 14 August 2004, 05:18 GMT (10:18 local time), only 28 min before the acquisition of the ASTER image analyzed by Mihalcea and others (2008a), and then we compared the results.

To assess surface temperature from Landsat images ($T_{S\text{-}Landsat}$; K), Landsat TM band 6 (i.e. thermal wavelength) digital numbers were first converted to radiance values (R Landsat ; W m^{-2} sr^{-1} μm^{-1}) (Coll and others, 2010), and then $T_{S\text{-}Landsat}$ was calculated applying the inverted Planck function:

$$T_{S-Landsat} = \frac{K_2}{\ln\left(K_1 \frac{\varepsilon}{R_{Landsat}} + 1\right)} \quad (4)$$

where K_1 and K_2 are constant values (607.76 W m^{-2} sr^{-1} μm^{-1} and 1260.56 K, respectively; NASA, 2011), and " is the sky emissivity including atmospheric scatter (set to 0.95; Barsi and others, 2003, 2005). The temperatures estimated using the two different images showed a good correlation (R^2 = 0.91; mean, maximum and minimum temperature differences 2.1 K, 14.5 K and 0.0 K, respectively), thus supporting the use of Landsat data to describe supraglacial thermal conditions. Secondly, we used the same field data of debris thickness gathered in 2004 and used by Mihalcea and others (2008a) to assess the best empirical function linking Landsat 2004 thermal data and debris thickness. The best-fitting function (R^2 = 0.99) is

$$DT = \exp\left(0.17\, T_{S-Landsat} - 51.18\right) \quad , \quad (5)$$

where DT is debris thickness (m) and $T_{S\text{-}Landsat}$ is the Landsat-derived surface temperature. This equation is similar to that found by Mihalcea and others (2008a) and describes the nonlinear relation between debris thickness and surface temperature. Moreover, we compared DT values obtained applying the equation reported in Mihalcea and others (2008a) to 2004 ASTER data against the values derived from Eqn (5) on 2004 Landsat data on the Baltoro glacier area. The results (Fig. 2) show a good correlation between the two datasets (R^2 = 0.85) and suggest a similar performance of the two models.

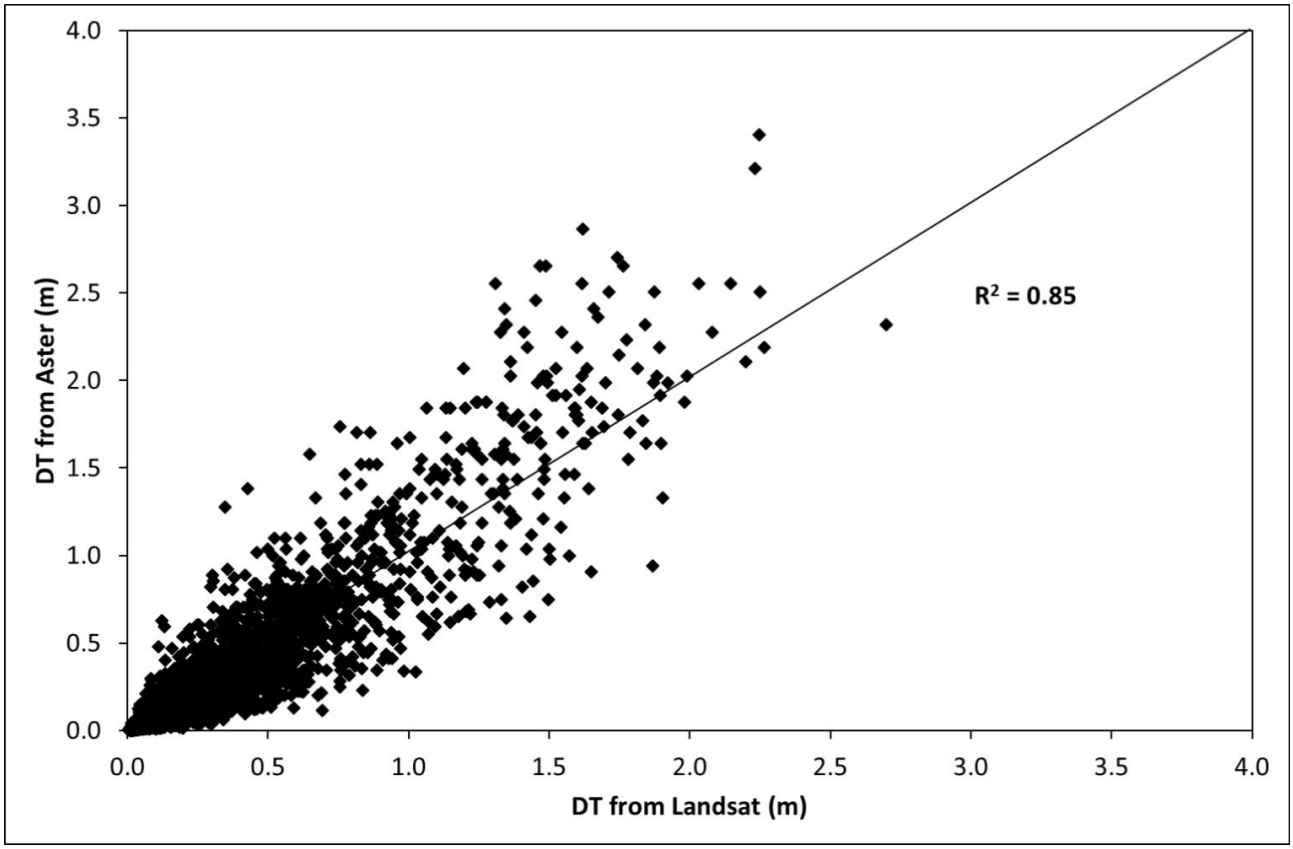

Figure 2: Scatter plot showing DT values derived from 2004 ASTER (using equation reported in Mihalcea and others, 2008a), and the ones from 2004 Landsat (applying Eqn (5)); 8700 pixels were considered.

Hence, these preliminary tests support the suitability of Landsat-derived surface temperatures to describe supraglacial debris thickness. We therefore used the debris thickness dataset collected in the field on the surface of Baltoro glacier during an expedition in July–August 2011 (a total of 57 samples ranging from a few centimeters to 2 m at the tongue). Regarding the Landsat surface temperatures, a single image covering the whole CKNP was not available; therefore, we used two images acquired on 10 August 2011 05:18 GMT and on 17 August 2011 5:24 GMT (Table 1). The images selected were particularly useful for our analyses because they were taken during the same period as the field measurements, and they partly overlap; they both cover part of the Baltoro glacier tongue (where field DT data were sampled). These data allowed us to assess two empirical equations linking debris thickness measured in the field to surface temperatures derived from Landsat images. The best- fitting equation ($R^2 = 0.75$) obtained from the image taken on 10 August 2011 (which covers the whole Baltoro glacier area) was

$$DT = \exp\left(0.16\, T_{S-Landsat} - 49.22\right) \quad , \tag{6}$$

while the one ($R^2 = 0.91$) from the image acquired on 17 August 2011 (covering part of the Baltoro

glacier tongue) was

$$DT = \exp(0.20\, T_{S-\,Landsat} - 59.97) \quad . \tag{7}$$

We then applied Eqn (6) to thermal data derived from the Landsat image acquired on 10 August 2011, and Eqn (7) to thermal data derived from the Landsat image acquired on 17August 2011. For the area covered by both overlapping images, results from Eqn (6) applied to the 10 August image were preferred because Baltoro glacier was only partially covered by the 17 August image, while it was completely covered by the 10 August image. Thus, the use of results from the 10 August image provided consistent estimates of the supraglacial debris thicknesses over the whole ablation area of Baltoro glacier.

3.3 Melt over debris-covered areas

The amount of ice melt under a debris cover ($M_{DC\text{-}point}$; m w. e.) depends on the energy available at the debris–ice interface and can be estimated as

$$M_{DC-\,point} = \frac{G_{point}\,\Delta t}{\rho_i\, L_m} \quad , \tag{8}$$

where G point corresponds to the conductive heat flux (W m^{-2}), Δt is the time step, ρ_i is the ice density (917 kg m^{-3}) and L_m is the latent heat of melting (3.34 x 10^5 J kg^{-1}). According to Mihalcea and others (2008a), G_{point} can be estimated assuming a linear temperature gradient from the top of the debris layer to the ice surface for mean daily conditions (Nakawo and Young, 1981; Nakawo and Takahashi, 1982; Mihalcea and others, 2008a):

$$G_{point} = \frac{(T_{S-\,point} - T_i)}{DR_{point}} \quad , \tag{9}$$

where T_i is the ice temperature (set to the melting point, 0°C; i.e. we neglected refreezing phenomena, which generally do not occur during the main ablation season; Mihalcea and others, 2006, 2008a) and DR_{point} is the effective thermal resistance of the debris layer (m^2 °C W^{-1}).

To derive DR_{point} over the whole debris-covered glacier area, an empirical relationship was applied (Mihalcea and others, 2008a):

$$DR_{point} = 19.841\, DT_{point} + 1.0262 \tag{10}$$

DR_{point} can be assumed constant over an ablation season as it mainly depends on debris thickness, which is generally considered stable over short periods (1–2 months; Fyffe and others, 2014).To model the daily mean debris surface temperature at each pixel ($T_{S\text{-}point}$), we considered both daily incoming solar radiation ($SW_{in\text{-}point}$) and debris thickness (DT_{point}), because higher radiation and thicker debris lead to higher surface temperatures (Mihalcea and others, 2006, 2008a,b; Mayer and others, 2010). $T_{S\text{-}point}$ was estimated according to the empirical function

$$T_{S-point} = 13.1667\, DT_{point} + 0.0352\, SW_{in-point} \quad (11)$$

with a root-mean-square error (RMSE) of 2.1°C. This relation was based on field data of debris thickness and surface temperature sampled on Baltoro glacier during summer 2011 and incoming solar radiation estimated in the same gridpoints. Finally, the daily ablation ($M_{DC\text{-}point}$; m w.e.) at each pixel of the CKNP debris-covered glacier area was modeled as

$$M_{DC-point} = \frac{T_{s-point}}{DR_{point}} \frac{1}{L_m \rho_w} \Delta t \quad , \quad (12)$$

where Δt is the number of seconds in a day (8.64×10^4).

3.4 Melt over debris-free areas

The daily ice melt at each pixel with debris-free ice ($M_{DF-\ point}$) was estimated by applying an enhanced T-index model (Pellicciotti and others, 2005):

$$M_{DF-point} = \begin{cases} TMF * T_{a-point} + RMF\,(1-\alpha)\, SW_{in-point} & T_a \le 0\,^\circ C \\ 0 & T_a > 0\,^\circ C \end{cases} \quad (13)$$

where $T_{a\text{-point}}$ is the daily mean air temperature (°C), α is the surface albedo, $SW_{in\text{-point}}$ is the daily mean incoming solar radiation (W m^{-2}), and TMF (32.43×10^{-4} m d^{-1} $°C^{-1}$) and RMF (0.79×10^{-4} m d^{-1} W^{-1} m^2) are the temperature and radiative melting factors, respectively. These melting factors are assessed from ablation measured at some selected sites on Baltoro glacier (from 3939 to 5200 m a.s.l.) from 23 July to 7 August 2011 (Table 2). Melting factors estimated from field data are taken as constant in time and space (Hock, 1999). Albedo was estimated by analyzing incoming and outgoing solar radiation data recorded during 2012 by a net radiometer (CNR1, Kipp and Zonen) installed at the Concordia supraglacial AWS. The spectral range considered was 0.3– 3 μm. Data show a high debris-free ice reflectivity, with a mean value of 0.30. Since distributed outgoing solar radiation data are not available for Baltoro glacier, we used the mean albedo value observed at Concordia. A lower ice reflectivity may be due to the presence of water, dust, debris and organic matter increasing the absorbed solar radiation and therefore the melting rate. Consequently, our assumption of a constant albedo equal to 0.30 may have led to a slight underestimation of the amount of meltwater, i.e. if the glacier ice is not completely clean in some parts of its debris-free area.

In any case, it is worth noting that other authors applying enhanced T-index approaches have also used constant albedo values (e.g. Pellicciotti and others, 2005).

4. Results

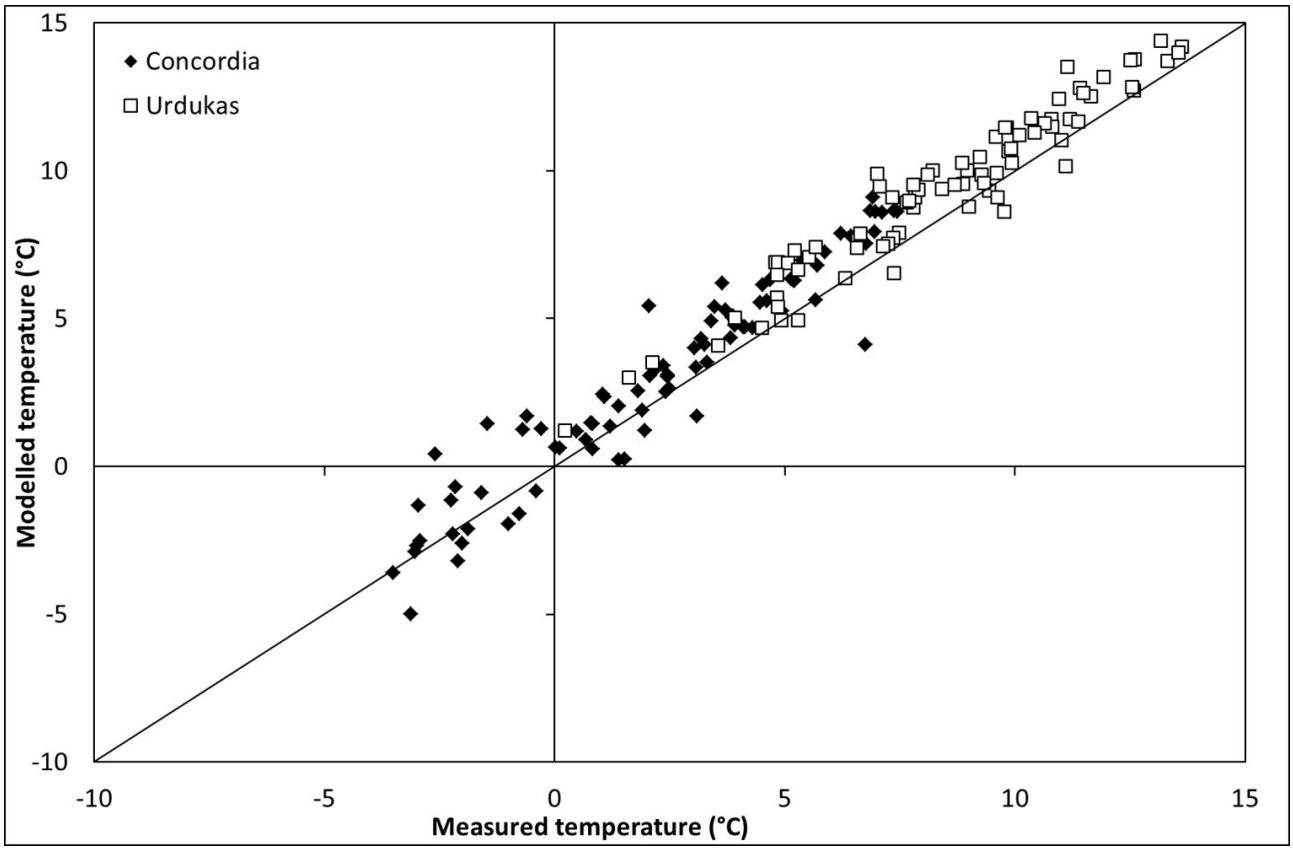

Figure 3: Daily mean temperatures recorded by the AWS installed at Urdukas during 2011 (x-axis) vs modeled daily mean temperatures (y-axis) obtained by applying a constant local lapse rate of –0.0075°C m^{-1} to Askole temperatures (open box). The same analysis was performed for the Concordia dataset during 2012 (solid diamond).

Modeled meteorological variables (Eqns (2) and (3)) agree well with those measured at Urdukas in 2011 and at Concordia in 2012. RMSEs regarding air temperature datasets are found equal to 1.2°C (for Urdukas) and 1.3°C (for Concordia), indicating that the local gradient by Mihalcea and others (2006) can be considered accurate (Fig. 3). Modeled incoming solar radiation values resulted in a good match with the measured ones (Fig. 4), with RMSE values of 39 and 125 W m^{-2} for Urdukas and Concordia, respectively.

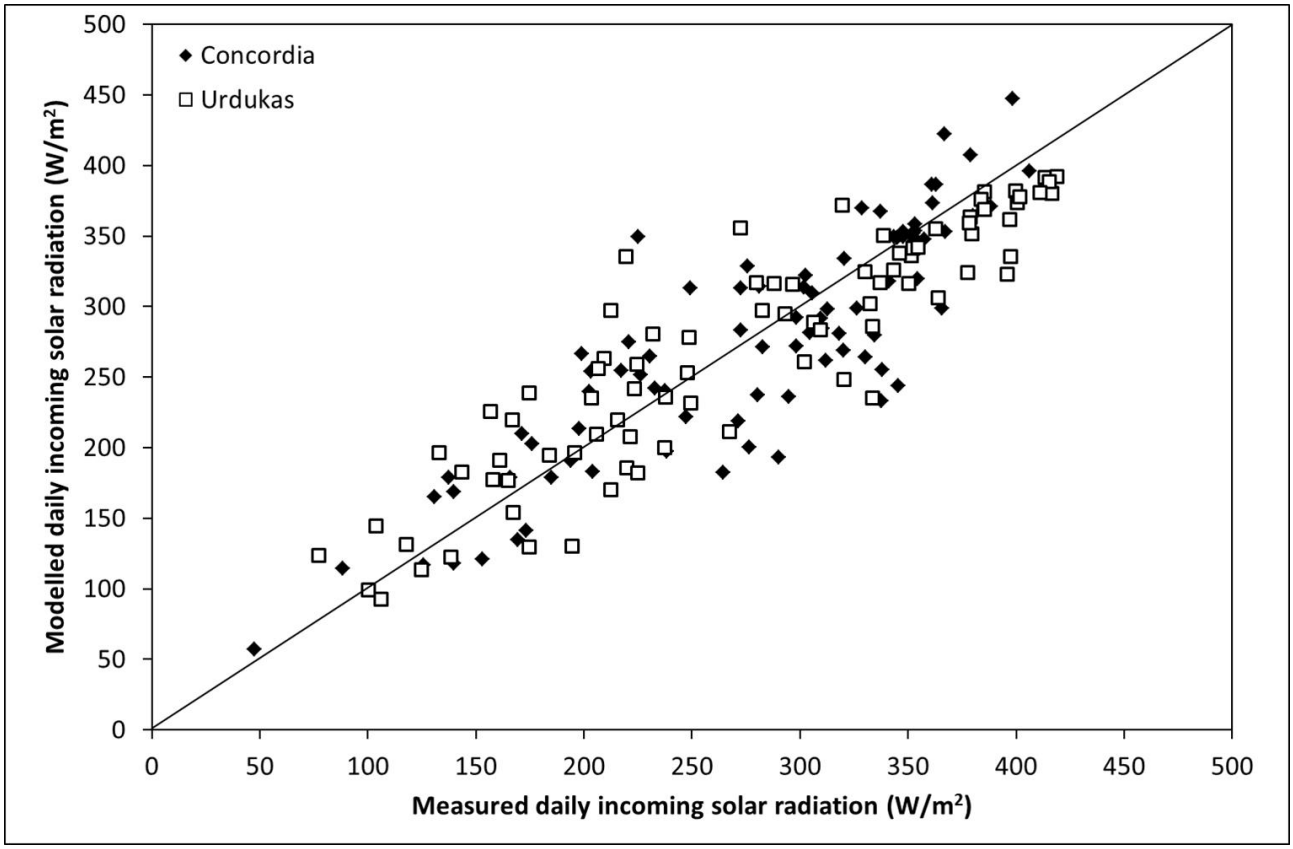

Figure 4: Daily mean incoming solar radiation recorded by the AWSs installed at Urdukas during 2011 and at Concordia during 2012 (x-axis) vs the modeled values (y-axis) derived from Askole data.

Supraglacial debris covers 518.47 km^2 (16.5%, 576 072 pixels) of the ablation zone of all the CKNP glaciers, while the extent of the debris-free area was 2619.61 km^2 (2 910 672 pixels). An example of debris occurrence is shown in Figure 5, where Panmah glacier (located in the central part of the CKNP, northwest of Baltoro glacier) is displayed. As regards the supraglacial debris thickness (Fig. 6), a mean value of 0.23 m was found, with maxima of ~3 m.

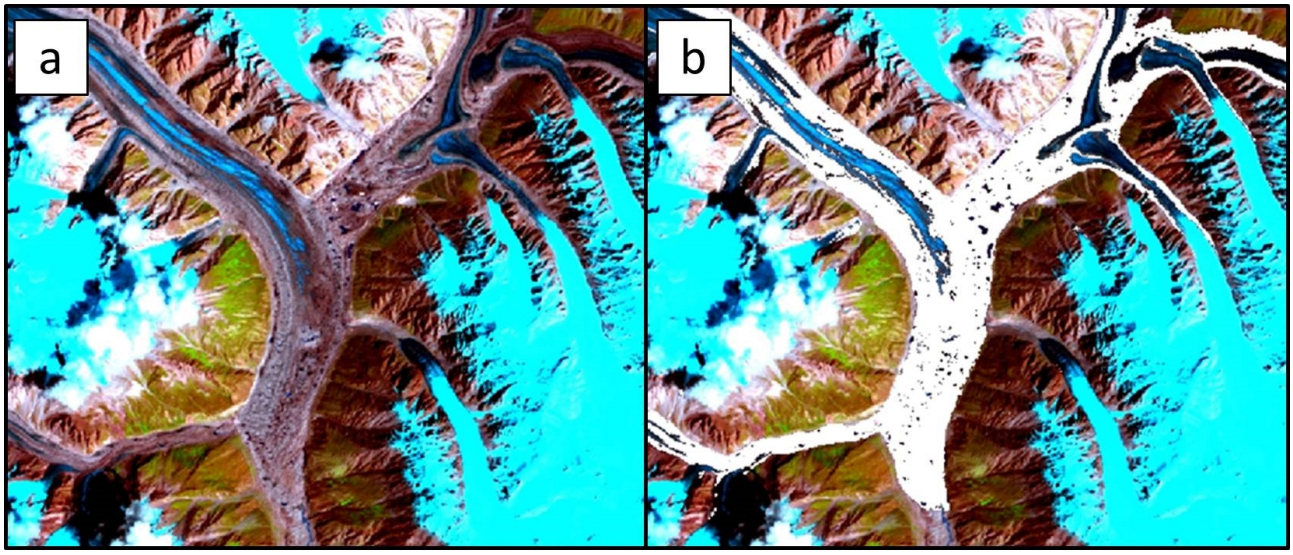

Figure 5: a) Landsat TM image with RGB=543 of portion of the Panmah Glacier. b) The same image with pixels classified as covered by supraglacial debris highlighted in white.

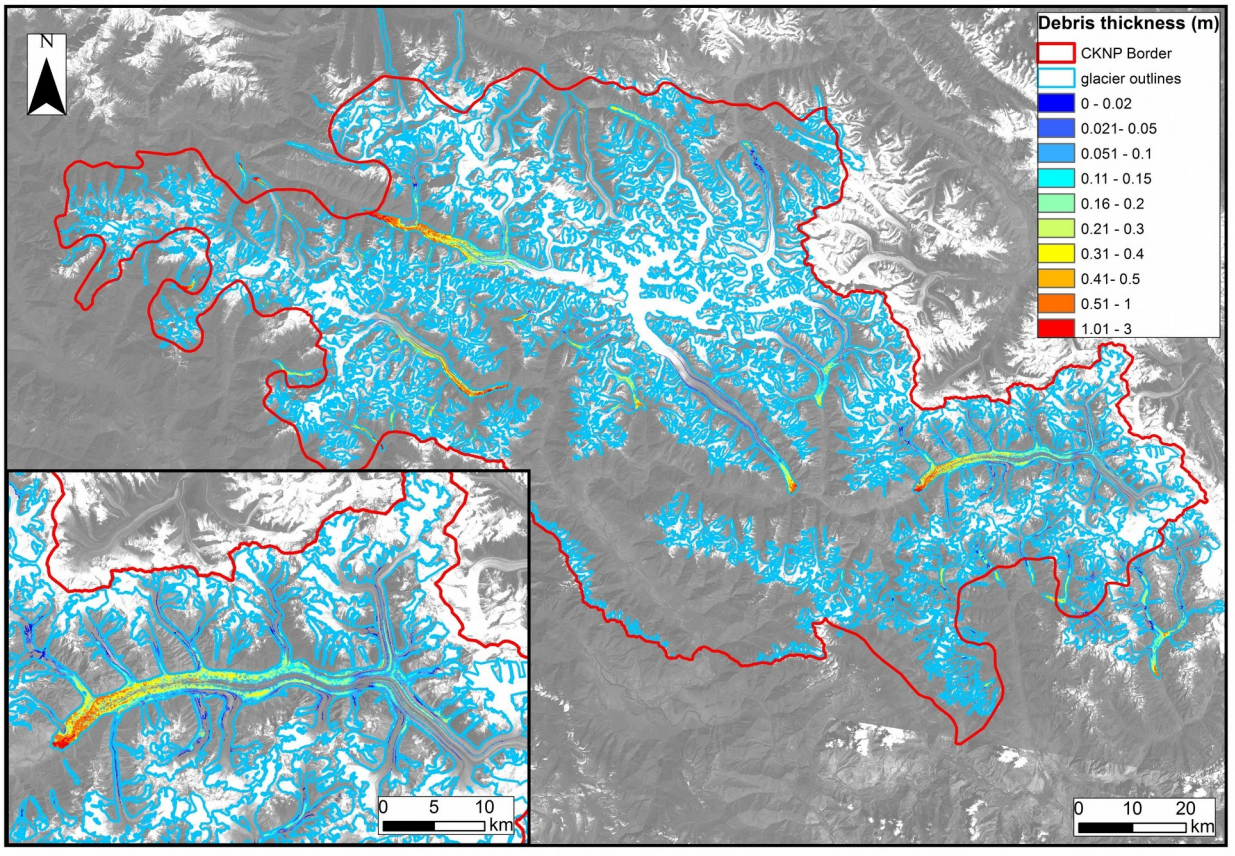

Figure 6: Map showing the supraglacial debris thicknesses over CKNP area, and a zoom on Baltoro glacier (lower left box).

During the 2011 ablation season, we collected 29 measurements on Baltoro glacier (both debris-covered and debris-free conditions). We divided this dataset into two subgroups: one for calibrating our melt models and the other for validating them. Table 2 reports the two sub-datasets used to calibrate and validate the models.

Table 2: Dataset used to calibrate and validate melt models. Dataset indicates whether ablation recorded at that site was used to calibrate (C) or to validate (V) the models; the site was debris-covered (DC) or debris-free (DF); Elev: elevation (m a.s.l.); X and Y: projected coordinates (WGS84UTM zone 43N); DR: debris effective thermal resistance (m^2 °C W^{-1}); DT-res and M-res: debris-thickness and melt residuals (modeled minus observed values); err: melt residual (%).The period considered is from the end of July to mid-August

Dataset-Debris	**Elev**	**X**	**Y**	**DT-observed**	**DT-modeled**	**DT-res**	**DR**	**M-observed**	**M-modeled**	**M-res**	**err**
C-DC1	3699	606400	3952497	0.38	0.55	+0.17	8.47	0.12	0.15	+0.04	+30%
C-DC2	3822	610488	3953487	0.32	0.43	+0.11	7.28	0.14	0.18	+0.04	+26%
C-DC3	3923	613550	3954650	0.13	0.17	+0.04	3.61	0.40	0.29	-0.11	-28%
C-DC4	3980	615221	3955685	0.26	0.14	-0.06	6.18	0.25	0.21	-0.04	-16%
C-DF1	3939	612778	3954341	0.00	-	-	-	0.85	0.85	0.00	0%
C-DF2	4554	636142	3956930	0.00	-	-	-	0.62	0.61	-0.01	-1%
C-DF3	5200	639556	3968575	0.00	-	-	-	0.00	0.34	+0.34	-
C-AVE						**+0.07**				**+0.04**	**+2%**
C-RMSE						**+0.11**				**+0.14**	**+25%**
V-DC1	3985	616248	3955171	0.03	0.10	+0.07	1.52	0.64	0.48	-0.16	-25%
V-DC2	3997	616148	3955855	0.15	0.41	+0.26	4.00	0.24	0.21	-0.03	-11%
V-DC3	4008	616056	3956353	0.02	0.20	+0.18	1.42	0.59	0.51	-0.08	-13%
V-DC4	4188	623369	3956355	0.41	0.11	-0.30	9.16	0.11	0.12	+0.01	+11%
V-DC5	4077	618774	3955909	0.03	0.25	+0.22	1.62	0.49	0.46	-0.03	-7%
V-DC6	4163	621318	3955889	0.11	0.00	-0.11	3.21	0.27	0.26	-0.01	-5%
V-DC7	4178	623804	3955827	0.02	0.08	+0.06	1.42	0.46	0.52	+0.06	+12%
V-DC8	4178	623801	3955858	0.02	0.05	+0.03	1.42	0.49	0.52	+0.03	+5%
V-DC9	4178	623798	3955889	0.01	0.05	+0.04	1.23	0.48	0.59	+0.11	+23%
V-DC10	4178	623808	3955914	0.04	0.05	+0.01	1.82	0.40	0.41	+0.02	+5%
V-DC11	4178	623813	3955942	0.02	0.05	+0.03	1.42	0.49	0.52	+0.03	+5%
V-DC12	4178	623833	3955939	0.05	0.05	0.00	2.02	0.38	0.38	0.00	-1%
V-DC13	4178	623851	3955914	0.06	0.05	-0.01	2.22	0.30	0.35	+0.05	+16%
V-DC14	4178	623807	3955982	0.01	0.05	+0.04	1.23	0.58	0.59	+0.01	+2%
V-DC15	4178	623818	3955951	0.01	0.05	+0.04	1.23	0.48	0.59	+0.12	+24%
V-DC16	4178	623878	3956476	0.10	0.17	+0.07	3.01	0.35	0.27	-0.08	-23%
V-DF1	4181	623382	3955368	0.00	-	-	-	0.47	0.49	+0.02	+4%
V-DF2	4178	623848	3955914	0.00	-	-	-	0.37	0.49	+0.12	+32%
V-DF3	4178	623830	3955979	0.00	-	-	-	0.56	0.49	-0.07	-13%
V-DF4	4178	623832	3955985	0.00	-	-	-	0.54	0.49	-0.05	-9%
V-DF5	4178	623827	3956013	0.00	-	-	-	0.64	0.49	-0.15	-23%
V-DF6	4178	623894	3956430	0.00	-	-	-	0.39	0.49	+0.10	+26%
V-AVE				**0.07**	**0.11**	**+0.04**				**0.00**	**+2%**
V-RMSE						**+0.13**				**+0.08**	**+16%**
AVE						**+0.04**				**+0.01**	**+2%**
RMSE						**+0.13**				**+0.09**	**+17%**

The validation indexes display the performance of our models for estimating debris-free and debris-covered ice melt. In particular, we found a mean error of –0.01 m w.e. (corresponding to 2%) and a RMSE equal to 0.09 m w.e. (17%). In addition, we assessed any error due to the methodology applied for distributing the meteorological variables. For this purpose, we calculated the melt amount at selected debris-free (C-DF1, C-DF2, C-DF3) and debris-covered (C-DC1, C-DC2, C-DC3, C-DC4) ice field points varying the meteorological model inputs (T_a , T_S and Sw_{in}) by their maximum RMSE (i.e. ±1.3°C, ±2.1°C and ±125 W m^{-2}, respectively). Changing T_a and SW_{in} , the debris-free ice melt variations range from ±10% to ±25% (at higher altitudes); debris-covered ice melt instead shows differences around ±30% when changing SW_{in} , while variations in T_S drive a lower alteration around ±15%, not particularly influenced by elevation. Thus, the debris-covered ice melt model is more sensitive to the errors in the meteorological input data. However, debris-covered ice melt accounts for only 11% of the total melt. Moreover, these error tests were made considering the worst cases (maximum RMSE).

The debris-covered and debris-free ice melt models were therefore applied to the whole glacierized area of the CKNP below the ELA. The results are shown in Figure 7.

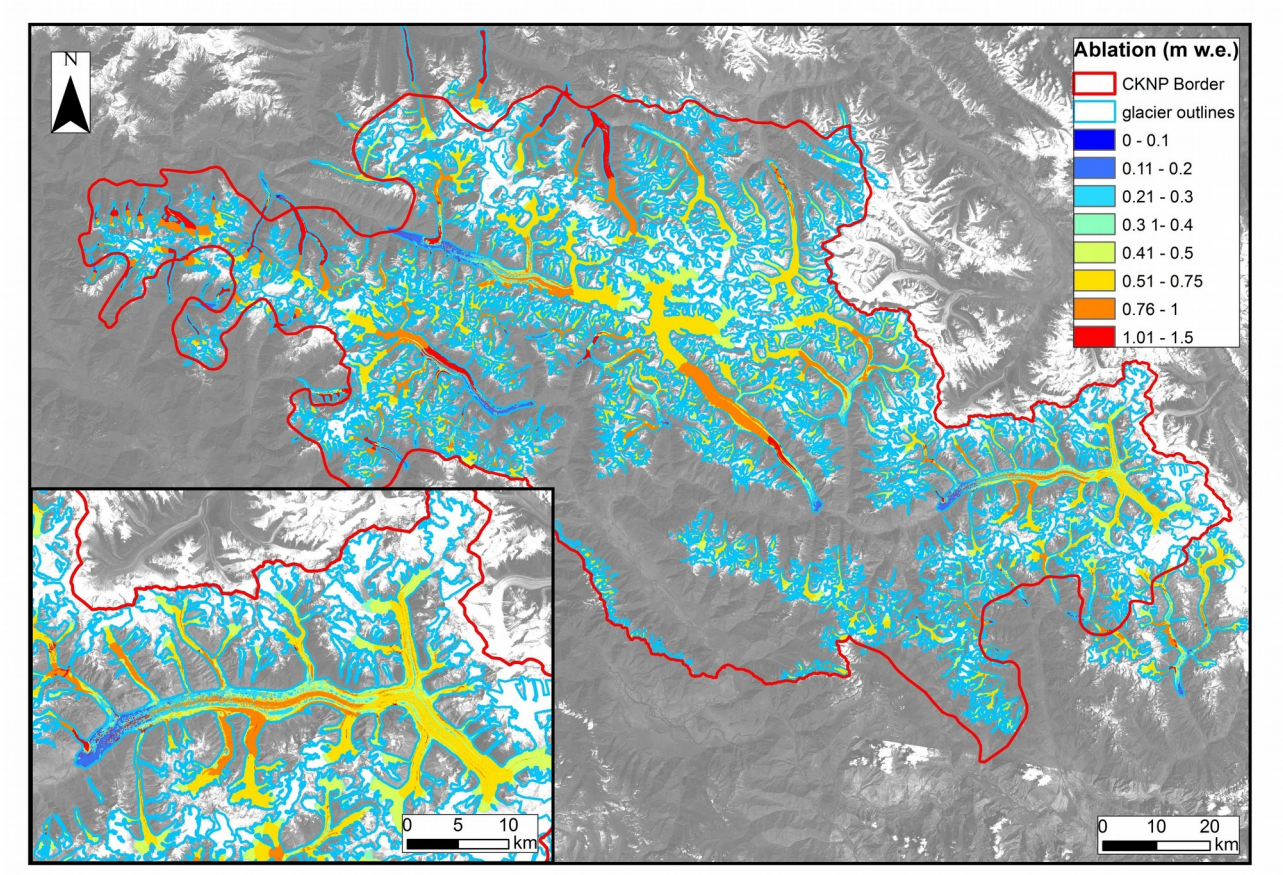

Figure 7: Ablation map of CKNP glaciers below the ELA in the period 23 July–9 August 2011, and a zoom on Baltoro glacier (lower left box).

Given that the solar radiation was used to estimate debris surface temperatures, affecting in turn conductive heat fluxes, melt in debris-covered areas (M_{DC}) was largely linked to incoming solar radiation (SW_{in}). Indeed, the minimum and maximum daily melt (0.005 and 0.089 m w. e., respectively) occurred during days with the lowest and highest incoming solar radiation (respectively, 112 and 371 W m^{-2}, in Askole; Fig. 8a). Conversely, melting in debris-free areas showed extreme daily values (0.009 and 0.110 m w.e.) in days with extreme air temperatures (respectively +14.1°C and +22.7°C recorded at Askole; Fig. 8b). Overall, the greatest ablation occurred on 5 August, when incoming solar radiation was high, but not the highest, while the minima occurred on days (28–31 July) with minimum radiative input.

Table 3: Modeled melt rates over debris-covered (DC) and debris-free (DF) areas, and the total ablation in the period 23 July–9 August 2011

	DC	**DF**	**Total**
area (km^2)	518	2620	3138
min daily M (m w.e. day^{-1})	0.011	0.016	0.011
max daily M (m w.e. day^{-1})	0.031	0.053	0.031
mean daily M (m w.e. day^{-1})	0.024	0.037	0.035
M (m w.e.)	0.432	0.666	0.630
min daily M (km^3 day^{-1})	0.006	0.041	0.006
max daily M (km^3 day^{-1})	0.016	0.139	0.139
mean daily M (km^3 day^{-1})	0.012	0.097	0.109
M (km^3)	0.223	1.740	1.963

These findings indicate that (1) melt from the debris-covered parts of the glaciers (M_{DC}) is mostly influenced by the incoming solar radiation, since it depends on the conductive heat flux, and (2) melt of debris-free parts of the glaciers (M_{DF}) is more sensitive to air temperature.

On debris-covered areas of the whole CKNP, the daily average ablation was 0.024 m w.e. d^{-1}, while on debris-free areas it was 0.037 m w.e. d^{-1}. Considering both debris-free and debris-covered areas in the whole CKNP and the entire analyzed period, we estimated a total melt of 0.63 m w.e., corresponding to an average ablation of 0.035 m w.e. d^{-1}. Hence, over the period we considered, melting of the debris-covered parts of all the glaciers in the CKNP produced 0.223 km^3 of meltwater (total M_{DC}), with a daily average of 0.012 km^3 w.e. d^{-1}. The total meltwater from the debris-free parts (total M_{DF}) was 1.740 km^3, with an average of 0.097 km^3 d^{-1}. The total ice melt from the CKNP was thus equal to 1.963 km^3, with a daily average of 0.109 km^3 d^{-1}. This water volume equals ~14% of the reservoir capacity of the Tarbela Dam, a very large dam on the Indus River that plays a key role for irrigation, flood control and the generation of hydroelectric power for Pakistan (Thompson, 1974). Table 3 shows a summary of the model results.

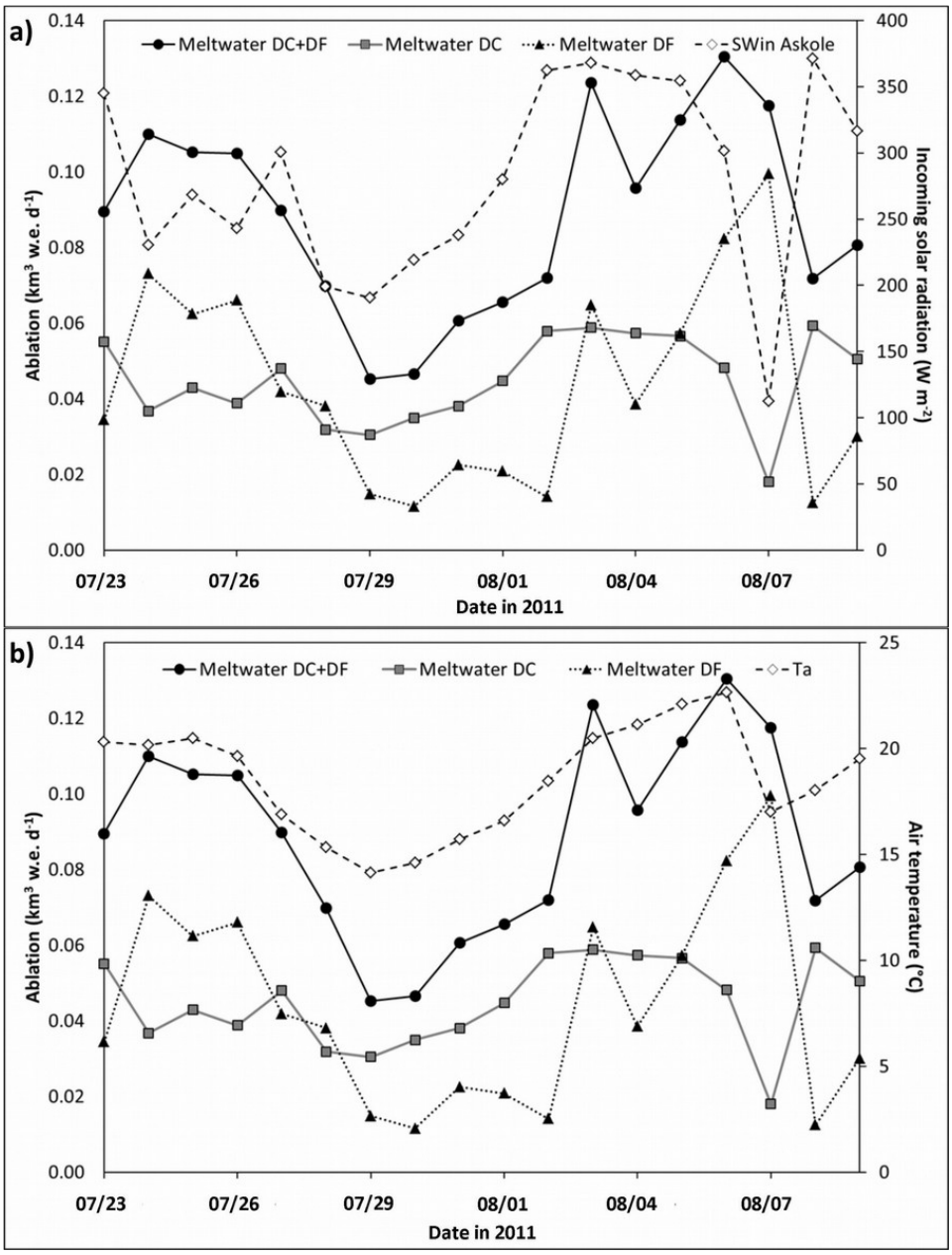

Figure 8: Daily meltwater production from 23 July to 9 August 2011 from all the CKNP glaciers over the debris-free (DF) and debris-covered (DC) areas and the total (DC+DF). Same data are presented with (a) daily incoming solar radiation (SW) and (b) daily mean air temperature (Ta) recorded at Askole. Date format is mm/dd.

5. Discussion

Supraglacial debris thickness was derived from Landsat thermal data (60 m x 60 m pixel size), limiting the spatial resolution of debris-covered ice melt calculations. The results could, however, be acceptable given the extent of the analyzed debris-covered area (518 km^2). The obtained DT values were cross-checked against a selection of field data, and a good fit was found (see Table 2). The main limitation comes from the fact that the supraglacial debris thicknesses derived from Landsat thermal data are average values at the pixel scale. The approach does not consider meltwater ponds, supraglacial lakes and sectors with crevasses and ice seals covering glacier areas smaller than the pixel size. Consequently, the model performs better in estimating debris layers thicker than 0.1 m (i.e. debris coverage is relatively continuous), while slight overestimation occurs for thin and sparse debris areas (<0.1 m; Table 2). The same limitation in DT modeling by means of remote sensing was found by Mihalcea and others (2008a).

Mapping of debris thickness is fundamental for estimating debris resistivity, and therefore debris-covered ice melt. Other approaches have been proposed to produce debris thickness maps at higher resolution than ours (Foster and others, 2012), but they require meteorological data (including, among others, wind speed and direction and turbulent heat fluxes) on the glacier surface, as well as high-resolution DEMs (e.g. from lidar surveys), which were not available for glaciers in the CKNP area. Hence, our simple approach is suitable for investigating a wide and remote glacier area where high-resolution information is not available.

In the debris-covered ice melt model we assumed a linear vertical temperature profile within the debris layer (with 0°C at the melting ice surface), which is usually considered a good approximation for calculating daily melt rates (Mattson and others, 1993; Mayer and others, 2010). In the period under study, refreezing during the night can be considered negligible in the debris-covered areas, because hourly air temperatures at Urdukas were always positive. This is also in agreement with data collected on the tongue of Hinarche glacier, Bagrot valley, CKNP, at 2757 m a.s.l. from 26 July to 5 August 2008 (Mayer and others, 2010), where air temperature (2 m above the debris surface) ranged between +14°C and +24°C, and never dropped below +9.9°C. When our model is applied to the onset and the end of the ablation season, it may overestimate meltwater discharge, and therefore may require further calibration.

We performed several sensitivity tests and evaluated model responses to varying input data at field survey sites (Tables 4 and 5) as well as over the whole CKNP ablation area (Table 6). First, we considered the debris-covered areas. We varied the daily incoming solar radiation by ±10% and ±20%. Then we studied the effect of varying the debris thickness upon melt results (±10%, ±1 cm, ±5 cm and ±10 cm with respect to the actual debris thickness values). The model response at field survey points (C-DC1 to C-DC4) is shown in Table 4.

Table 4: Sensitivity tests performed by applying different input data to the debris-covered ice melt model. We applied the model to four points where actual ablation data were collected in the field (the calibration points in Table 2) and calculated melt anomalies (ΔM) with respect to M_{DC} by modifying the incoming shortwave radiation and debris thickness. The reference modeled melt is given by M_{DC} mod

	C-DC1	**C-DC2**	**C-DC3**	**C-DC4**
Elevation (m a.s.l.)	3699	3822	3923	3980
Debris thickness (cm)	37.5	31.5	13.0	26.0
Time frame (days)	11	12	12	13
M meas (m w.e.)	0.12	0.14	0.4	0.25
R (°C m^2 W^{-1})	8.47	7.28	3.61	6.18
M_{DC} mod (m w.e.)	0.15	0.18	0.29	0.21
$\Delta M_{+10\% SWin}$ (m w.e.)	0.01	0.013	0.025	0.016
$\Delta M_{-10\% SWin}$ (m w.e.)	0.01	0.013	0.025	0.016
ΔM ave $\%_{\pm 10\% SWin}$	±6.7	±8.7	±16.7	±10.7
$\Delta M_{+20\% SWin}$ (m w.e.)	0.021	0.025	0.05	0.031
$\Delta M_{-20\% SWin}$ (m w.e.)	0.021	0.025	0.012	0.031
ΔM ave $\%_{\pm 20\% SWin}$	±14	±16.7	±20.7	±20.7
$\Delta M_{+10\% DT}$ (m w.e.)	0.008	0.009	0.015	0.011
$\Delta M_{-10\% DT}$ (m w.e.)	0.009	0.011	0.018	0.013
ΔM ave $\%_{\pm 10\% DT}$	±5.7	±6.7	±11.0	±8.0
$\Delta M_{+1cm DT}$ (m w.e.)	0.002	0.003	0.012	0.005
$\Delta M_{-1cm DT}$ (m w.e.)	0.002	0.003	0.013	0.005
ΔM ave $\%_{\pm 1 cm DT}$	±1.3	±2.0	±8.3	±3.3
$\Delta M_{+5cm DT}$ (m w.e.)	0.01	0.014	0.05	0.02
$\Delta M_{-5cm DT}$ (m w.e.)	0.013	0.019	0.088	0.028
ΔM ave $\%_{\pm 5 cm DT}$	±7.7	±11.0	±46.0	±16.0
$\Delta M_{+10cm DT}$ (m w.e.)	0.018	0.025	0.082	0.035
$\Delta M_{-10cm DT}$ (m w.e.)	0.029	0.044	0.283	0.069
ΔM ave $\%_{\pm 10 cm DT}$	±15.7	±23.0	±121.7	±34.7

These tests suggest that changing the debris thickness or radiative input noticeably affects the debris-covered ice melt. In particular, this appears more evident in the presence of a thin debris thickness. Indeed, whenever shallow debris layers occur (see C-DC3 compared to C-DC1 in Table 4), even slight input variations entail evident changes in the underlying ice ablation, as the debris insulating effect is weaker.

Next, we considered the debris-free areas. We varied the daily incoming solar radiation by ±10%. Then we shifted the daily air temperature by ±0.1, ±1.0 and ±2.5°C with respect to the measured values. Finally, we investigated the effect of changing the albedo values by ±10%. Table 5 shows the model responses at field survey points (C-DF1 to C-DF3).

Table 5: Sensitivity tests performed by applying different input data to the debris-free ice melt model. We applied the model to three points where actual ablation data were collected in the field (the calibration points in Table 2) and calculated melt anomalies (ΔM) with respect to M_{DF} by varying the air temperature, the incoming shortwave radiation and the albedo. The reference modeled melt is given by M_{DF} mod

	C-DF1	**C-DF2**	**C-DF3**
Elevation (m a.s.l.)	3939	4554	5200
Time frame (days)	18	18	18
M meas (m w.e.)	0.850	0.615	0.000
M_{DF} mod (m w.e.)	0.850	0.615	0.335
$\Delta M_{-0.1°C}$ (m w.e.)	-0.005	-0.005	-0.004
$\Delta M_{+0.1°C}$ (m w.e.)	0.005	0.005	0.004
ΔM ave $\%_{\pm 0.1°C}$ (m w.e.)	±0.6%	±0.8%	±1.2%
$\Delta M_{-1.0°C}$ (m w.e.)	-0.052	-0.052	-0.075
$\Delta M_{+1.0°C}$ (m w.e.)	0.052	0.052	0.066
ΔM ave $\%_{\pm 1.0°C}$ (m w.e.)	±6.1%	±8.4%	±20.9%
$\Delta M_{-2.5°C}$ (m w.e.)	-0.130	-0.130	-0.138
$\Delta M_{+2.5°C}$ (m w.e.)	0.130	0.130	0.161
ΔM ave $\%_{\pm 2.5 °C}$ (m w.e.)	±15.3%	±21.1%	±44.7%
$\Delta M_{+10\% SWin}$ (m w.e.)	0.025	0.025	0.020
$\Delta M_{-10\% SWin}$ (m w.e.)	-0.025	-0.025	-0.020
ΔM ave $\%_{\pm 10\% SWin}$ (m w.e.)	±2.9%	±4.1%	±6.1%
$\Delta M_{+10\% albedo}$ (m w.e.)	-0.035	-0.036	-0.029
$\Delta M_{-10\% albedo}$ (m w.e.)	0.035	0.036	0.029
ΔM ave $\%_{\pm 10\% albedo}$ (m w.e.)	±4.1%	±5.8%	±8.7%

The debris-free ice model is very sensitive to variations in air temperature, and the ablation varied by ±45% with changes of ±2.5°C. Minor impacts derived from changing SW_{in} inputs, showing a maximum variation of only 6%. This is a consequence of applying an enhanced T-index model, which indeed gives a primary role to temperature in driving ice melt, and a complementary role to incoming solar radiation (see, e.g., Pellicciotti and others, 2005). Concerning ice albedo, our model assumes a constant value of 0.30 for the whole area, thus probably entailing an over- or underestimation of the actual ice melt. Common albedo values for snow and ice surfaces range from 0.20 to 0.85; the albedo therefore has a very large and important influence on the total shortwave radiation absorbed by the surface, SW_{in} (1 - α), and hence on ablation. In the absence of direct measurements, albedo is often estimated from 'typical' published values for snow or ice (Cutler and Munro, 1996): a clean ice surface generally features an albedo of 0.30–0.46, while a debris-rich ice surface is characterized by an albedo of 0.06–0.30 (Cuffey and Paterson, 2010). Thus, the choice of albedo is a very critical issue in accurately estimating the ice melt. In this study, we adopted the mean value (i.e. 0.30) obtained by incoming and outgoing solar radiation data gathered by the supraglacial AWS placed at Concordia (in a debris-free area of Baltoro glacier). In previous studies, some authors applied similar approaches using an albedo of 0.30 (e.g. Pellicciotti and others, 2005). Oerlemans (2001) reported a mean albedo value for debris-free ice of ~0.30. So we followed these previous studies supporting the use of a constant albedo of 0.30. The sensitivity test at field survey sites showed that changing the albedo by ±10% may lead to melt change of up to ±9% on debris-

free areas (Table 5).

In addition to these model sensitivity tests, we considered the whole CKNP area totally debris-free, obtaining a total melt of 2.22 km^3, with an increase of 0.48 km^3 (more than twice as much) with respect to that obtained on actual debris-free areas (Table 6). This suggests that the debris layer is thick enough (more than the local critical value; Mattson and others, 1993) to constrain the ice melt rates on average. To assess the effects of albedo, we changed the albedo of debris-free areas by a factor of ±10%, finding only a moderate impact on total melt (±5%). Similar results were obtained by changing SW_{in} by ±10%. Moreover, stronger impacts (±7%) are caused by changing air temperature by ±1.0°C. Finally, we investigated the impact of DT by changing its values by ±10%, ±50% and ±100%. In spite of the small impact on the total melt amount (+3.9% with –50% of DT and –3.2% with +100% of DT), the applied changes largely affected debris-covered ice melt. As the overall mean DT we derived from Landsat imagery (0.23 m) is surely higher than the local critical value (~0.05 m on Baltoro glacier according to Mihalcea and others, 2006), the model is more sensitive to reduction than to increases of the actual DT value. This agrees with the well-known nonlinear relation between debris-covered ice melt and DT (see also fig. 7 in Mihalcea and others, 2006). Indeed, when DT was decreased by 50%, melt in debris-covered areas increased by up to +34%, while when it was doubled, melt decreased by –28% (see Table 6).

Table 6: Sensitivity test performed by applying different input data to both the debris-free and debris-covered ice melt models. The model results without input variation are shown in line 2 (M). We considered the whole CKNP ablation area

	DC (km^3)	**DF (km^3)**	**DC+DF (km^3)**	**%ΔDC**	**%ΔDF**	**%Δtotal**
M	0.22	1.74	1.96	-	-	-
$M_{\text{all debris-free}}$	0.00	2.22	2.22	-	-	+13.0%
$M_{\text{+10\% albedo}}$	0.22	1.64	1.86	-	-6.0%	-5.3%
$M_{\text{-10\% albedo}}$	0.22	1.85	2.07	-	+6.0%	+5.3%
$M_{\text{+10\% SWin}}$	0.24	1.81	2.06	+8.7%	+4.2%	+4.7%
$M_{\text{-10\% SWin}}$	0.20	1.67	1.87	-8.7%	-4.2%	-4.7%
$M_{\text{+1.0°C}}$	0.22	1.89	2.11	-	+8.4%	+7.4%
$M_{\text{-1.0°C}}$	0.22	1.59	1.82	-	-8.4%	-7.4%
$M_{\text{+10\% DT}}$	0.21	1.74	1.95	-4.3%	-	-0.5%
$M_{\text{-10\% DT}}$	0.23	1.74	1.97	+4.9%	-	+0.6%
$M_{\text{+50\% DT}}$	0.18	1.74	1.92	-17.3%	-	-2.0%
$M_{\text{-50\% DT}}$	0.30	1.74	2.04	+34.2%	-	+3.9%
$M_{\text{+100\% DT}}$	0.16	1.74	1.90	-28.1%	-	-3.2%

6. Conclusions

We applied a simple model to evaluate the meltwater from debris-free and debris-covered ice ablation in the CKNP area, a wide glacierized zone of Pakistan. Our model estimates melt below 5200 m a.s.l. by applying an enhanced T-index model over the debris-free areas, and computing the conductive heat flux through the debris layer on the debris- covered zones. We neglected snowmelt, since snow data in the study area are not systematically available. We then focused on the peak ablation season, from 23 July to 9 August 2011, when meltwater is largely derived from ice melt, with snow thaw playing a minor role (Soncini and others, 2015). Glacier features (i.e. surface area, supraglacial debris occurrence and thickness) were estimated from remote-sensing analysis of recent satellite imagery (2010– 11). Meteorological input data were distributed starting from data acquired at Askole. The data distribution procedure was validated by comparing the results with data recorded by two AWSs within the SHARE network (Urdukas and Concordia). The modeled ablation data were in strong agreement with measurements collected in the field during 2011 on Baltoro glacier, which can be considered representative of CKNP glaciers.

Our model estimated 0.223 km^3 (on average, 0.012 km^3 d^{-1}; min–max 0.006–0.016 km^3 d^{-1}) of meltwater from the debris-covered parts, and 1.740 km^3 (on average, 0.097 km^3 d^{-1}; min–max 0.041–0.139 km^3 d^{-1}) from debris- free sectors of the CKNP glacier ablation zone from 23 July to 9 August 2011. The total fresh water from the ablation areas of CKNP glaciers during the same period was therefore 1.963 km^3 (on average, 0.109 km^3 d^{-1}), corresponding, for example, to 14% of the water contained in a large strategic dam along the Indus River, of which all CKNP glaciers are tributaries.

The present model requires only a small number of input data, such as air temperature and SW_{in} (recorded by most of the standard AWSs), a DEM, and debris thickness measurements collected in the field. The relatively simple model we developed should provide portability to other regions, even if adjustments of the parameters against field measurements are necessary. In particular, (1) the lapse rate to distribute the air temperature (see Eqn (2)) should be locally evaluated; (2) the use of a constant albedo of 0.30 might be invalid for areas with debris-free ice affected by dust and black carbon deposition (see Azzoni and others, 2014), thus requiring dedicated analyses; (3) the debris effective thermal resistance (DR) estimation requires debris-covered ice ablation and debris surface temperature data collected in the field.

The sensitivity tests suggest that melting will increase largely if summer air temperature increases. Also, any increase in the extent of debris coverage (which will likely occur due to augmented macrogelivation processes and rockfall events) will affect melt depending on new debris thickness. Thus, it will be important to monitor debris cover variations in time to update these crucial input data. Finally, albedo variations have to be properly considered, because surface darkening is reported as a result of increasing amounts of fine debris (Oerlemans and others, 2009; Azzoni and others, 2014). A further improvement of our approach will be the spatial distribution of debris-free

ice albedo by applying methods based on remote-sensing investigations (see Klok and others, 2003).

References

Archer D.R. (2003) Contrasting hydrological regimes in the Indus Basin. J. Hydrol., 274, 198–210 (doi: 10.1016/S0022-1694(02) 00414-6)

Azzoni R.S., Senese A., Zerboni A., Maugeri M., Smiraglia C. and Diolaiuti G. (2014) A novel integrated method to describe dust and fine supraglacial debris and their effects on ice albedo: the case study of Forni Glacier, Italian Alps. Cryosphere Discuss., 8, 3171–3206 (doi: 10.5194/tcd-8-3171-2014)

Barrand N. and Murray T. (2006) Multivariate controls on the incidence of glacier surging in the Karakoram Himalaya. Arct. Antarct. Alp. Res., 38, 489–498 (doi: 10.1657/1523-0430(2006) 38%5B489:MCOTIO%5D2.0.CO;2)

Barsi J.A., Barker J.L. and Schott J.R. (2003) An atmospheric correction parameter calculator for a single thermal band earth-sensing instrument. In Stein T. ed. IGARSS 2003, International Geoscience and Remote Sensing Symposium, 21–25 July 2003, Toulouse, France. Proceedings. Institute of Electrical and Electronic Engineers, Piscataway, NJ (doi: 10.1109/ IGARSS.2003.1294665)

Barsi J.A., Schott J.R., Palluconi F.D. and Hook S.J. (2005) Validation of a web-based atmospheric correction tool for single thermal band instruments. Proc. SPIE-Int. Soc. Opt. Eng., 5882 (doi: 10.1117/ 12.619990)

Bhambri R. and Bolch T. (2009) Glacier mapping: a review with special reference to the Indian Himalayas. Progr. Phys. Geog., 33, 672–704 (doi: 10.1177/0309133309348112)

Bocchiola D. and Diolaiuti G. (2013) Recent (1980–2009) evidence of climate change in the upper Karakoram, Pakistan. Theor. Appl. Climatol., 111 (doi: 10.1007/s00704-012-0803-y)

Bocchiola D., Diolaiuti G.A., Soncini A., Mihalcea C., D'Agata C., Mayer C., Lambrecht A., Rosso R. and Smiraglia C. (2011) Prediction of future hydrological regimes in poorly gauged high altitude basins: the case study of the upper Indus, Pakistan. Hydrol. Earth Syst. Sci. 15: 2059-2075, doi:10.5194/hess-15-2059-2011.

Bolch T., Kulkarni A., Kääb A., Huggel C., Paul F., Cogley J.G., Frey H., Kargel J.S., Fujita K., Scheel M., Bajracharya S. and Stoffel M. (2012) The state and fate of Himalayan glaciers. Science 336: 310-314.

Brown D.G., Lusch D.P. and Duda K.A. (1998) Supervised classification of types of glaciated landscapes using digital elevation data. Geomorphology, 21, 233–250 (doi: 10.1016/S0169-555X (97)00063-9)

Coll C., Galve J.M., Sánchez J.M. and Caselles V. (2010) Validation of Landsat-7/ETM+ thermal-band calibration and atmospheric correction with ground-based measurements. IEEE Trans. Geosci. Remote Sens., 48(1), 547–555 (doi: 10.1109/ TGRS.2009.2024934)

Conway W.M. (1894) Climbing and exploration in the Himalayas. Fisher Unwin, London

Copland L., Sylvestre T., Bishop M.P., Shroder J.F., Seoung Y.B., Owen L.A., Bush A. and Kamp U. (2011) Expanded and Recently Increased Glacier Surging in the Karakoram. Institute of Arctic and Alpine Reasearch (INSTAAR), University of Colorado, available at: http://www.bioone.org/doi/full/10.1657/1938-4246-43.4.503.

Cuffey K.M. and Paterson W.S.B. (2010) The physics of glaciers. Academic Press, Amsterdam

Cutler P.M. and Munro D.S. (1996) Visible and near-infrared reflectivity during the ablation period on Peyto Glacier, Alberta, Canada. J. Glaciol., 42(141), 333–340

De Filippi F. (1912) La spedizione di S.A.R il Principe Luigi Amedeo di Savoia Duca degli Abruzzi nel Karakorum e nell'Himalaya occidentale (1909). Zanichelli, Bologna

Desio A., Marussi A. and Caputo M. (1961) Glaciological research of the Italian Karakorum Expedition 1953–1955. IAHS Publ. 52 (General Assembly of Helsinki 1960 – Snow and Ice), 224–232

Diolaiuti G., Pecci M. and Smiraglia C. (2003) Liligo Glacier (Karakoram): reconstruction of the recent history of a surge- type glacier. Ann. Glaciol., 36, 168–172 (doi: 10.3189/ 172756403781816103)

Foster L.A., Brock B.W., Cutler M.E.J. and Diotri F. (2012) A physically based method for estimating supraglacial debris thickness from thermal band remote-sensing data. J. Glaciol., 58(210), 677–691 (doi: 10.3189/2012JoG11J194)

Fowler H.J. and Archer D.R. (2006) Conflicting signals of climatic change in the upper Indus basin. J. Climate, 19, 4276–4293 (doi: 10.1175/JCLI3860.1)

Fujita K. and Sakai A. (2014) Modelling runoff from a Himalayan debris-covered glacier. Hydrol. Earth Syst. Sci., 18(7), 2679–2694 (doi: 10.5194/hess-18-2679-2014 014)

Fyffe C.L., Reid T.D., Brock B.W., Kirkbride M.P., Diolaiuti G., Smiraglia C. and Diotri F. (2014) A distributed energy-balance melt model of an alpine debris-covered glacier. J. Glaciol., 60(221), 587–602 (doi: 10.3189/2014JoG13J148)

Gardelle J., Berthier E. and Arnaud Y. (2012) Slight mass gain of Karakoram glaciers in the early 21st century. Nature Geosci., 5, 322–325, (doi: 10.1038/ngeo1450 (doi: 10.1038/ngeo1450)

Gardelle J., Berthier E., Arnaud Y. and Kääb A. (2013) Region-wide glacier mass balances over the Pamir–Karakoram–Himalaya during 1999–2011. Cryosphere, 7, 1263–1286 (doi: 10.5194/tc- 7-

1263-2013)

Gardner A.S., Moholdt G., Cogley J.G., Wouters B., Arendt A.A., Wahr J., Berthier E., Hock R., Pfeffer W.T., Kaser G., Ligtenberg S.R.M., Bolch T., Sharp M.J., Hagen J.O., Van Den Broeke M.R. and Paul F. (2013) A Reconciled Estimate of Glacier Contributions to Sea Level Rise: 2003 to 2009. Science 852-857.

Han H., Ding Y. and Liu S. (2006) A simple model to estimate ice ablation under a thick debris layer. J. Glaciol., 52(179), 528–536

Hewitt K. (2005) The Karakoram Anomaly? Glacier expansion and the 'elevation effect', Karakoram Himalaya. Mt. Res. Dev., 25, 332–340 (doi: 10.1659/0276-741(2005)025%5B0332:TKA- GEA%5D2.0.CO;2)

Hewitt K. (2007) Tributary glacier surges: an exceptional concentration at Panmah Glacier, Karakoram, Himalaya. J. Glaciol., 53, 181–188 (doi: 10.3189/172756507782202829)

Hewitt K. (2011) Glacier change, concentration, and elevation effects in the Karakoram Himalaya, upper Indus basin. Mt. Res. Dev., 31, 188–200 (doi: 10.1659/MRD-JOURNAL-D-11- 00020.1)

Hewitt K., Wake C.P., Young G.J. and David C. (1989) Hydrological investigations at Biafo Glacier, Karakorum Range, Himalaya; an important source of water for the Indus River. Ann. Glaciol., 13, 103–108

Hock R. (1999) A distributed temperature-index ice- and snowmelt model including potential direct solar radiation. J. Glaciol., 45(149), 101–111

International Centre for Integrated Mountain Development (ICIMOD) (2013) State of the knowledge and Workshop on Hindu Kush Himalayan Cryosphere Data Sharing Policy. International Conference on the Cryosphere of the Hindu Kush Himalayas, 14–18 May 2012. (ICIMOD Project Document) ICIMOD, Kathmandu

Kääb A., Berthier E., Nuth C., Gardelle J. and Arnaud Y. (2012) Contrasting patterns of early twenty-first-century glacier mass change in the Himalayas. Nature, 488, 495–498 (doi: 10.1038/ nature11324)

Kayastha R.B., Takeuchi Y., Nakawo M. and Ageta Y. (2000) Practical prediction of ice melting beneath various thickness of debris cover on Khumbu Glacier, Nepal using a positive degree day factor. IAHS Publ. 264 (Symposium at Seattle 2000 – Debris- Covered Glaciers), 71–81

Klok E.J., Greuell W. and Oerlemans J. (2003) Temporal and spatial variation of the surface albedo of Morteratschgletscher, Switzerland, as derived from 12 Landsat images. J. Glaciol., 49(167), 491–502 (doi: 10.3189/172756503781830395)

Kotlyakov V., Osipova G. and Tsvetkov D. (2008) Monitoring surging glaciers of the Pamirs, central Asia, from space. Ann. Glaciol., 48, 125–134 (doi: 10.3189/172756408784700608)

Lejeune Y., Bertrand J.M., Wagnon P. and Morin S. (2013) A physically based model for the year-round surface energy and mass balance of debris-covered glaciers. J. Glaciol., 59(214), 327–344 (doi: 10.3189/2013JoG12J149)

Mattson L.E. and Gardner J.S. (1989) Energy exchange and ablation rates on the debris-covered Rakhiot Glacier, Pakistan. Z. Gletscherkd. Glazialgeol., 25(1), 17–32

Mattson L.E., Gardner J.S. and Young G.J. (1993) Ablation on debris covered glaciers: an example from the Rakhiot Glacier, Punjab, Himalaya. IAHS Publ. 218 (Symposium at Kathmandu 1992 – Snow and Glacier Hydrology), 289–296

Mayer C., Lambrecht A., Beló M., Smiraglia C. and Diolaiuti G. (2006) Glaciological characteristics of the ablation zone of Baltoro glacier, Karakoram, Pakistan. Ann. Glaciol., 43, 123–131 (doi: 10.3189/172756406781812087)

Mayer C., Lambrecht A., Mihalcea C., Belò M., Diolaiuti G.A., Smiraglia C., Bashir F. (2010) Analysis of Glacial Meltwater in Bagrot Valley, Karakoram. Mountain Research and Development 30(2): 169-177.

Mihalcea C., Mayer C., Diolaiuti G., Lambrecht A., Smiraglia C. and Tartari G. (2006) Ice ablation and meteorological conditions on the debris-covered area of Baltoro glacier, Karakoram, Pakistan. Ann. Glaciol., 43, 292–300 (doi: 10.3189/ 172756406781812104)

Mihalcea C., Mayer C., Diolaiuti G.A., D'agata C., Smiraglia C., Lambrecht A., Vuillermoz E. and Tartari G. (2008a) Spatial distribution of debris thickness and melting from remote-sensing and meteorological data, at debris-covered Baltoro glacier, Karakoram, Pakistan. Ann. Glaciol. 48: 49-57.

Mihalcea C., Brock B.W., Diolaiuti G., D'Agata C., Citterio M., Kirkbride M.P., Cutler M.E.J. and Smiraglia C. (2008b) Using ASTER satellite and ground-based surface temperature measurements to derive supraglacial debris cover and thickness patterns on Miage Glacier (Mont Blanc Massif, Italy), Cold Regions Science and Technology, 52, pp. 341-354.

Minora U., Bocchiola D., D'Agata C., Maragno D., Mayer C., Lambrecht A., Mosconi B., Vuillermoz E., Senese A., Compostella C., Smiraglia C. and Diolaiuti G. (2013) 2001-2010 glacier changes in the Central Karakoram National Park: a contribution to evaluate the magnitude and rate of the 'Karakoram anomaly'", The Cryosphere Discussion, 7, pp. 2891-2941.

Nakawo M. and Rana B. (1999) Estimate of ablation rate of glacier ice under a supraglacial debris layer. Geogr. Ann., 81A(4), 695–701

Nakawo M. and Takahashi S. (1982) A simplified model for estimating glacier ablation under a debris layer. IAHS Publ. 138 (Symposium at Exeter 1982 – Hydrological Aspects of Alpine and High Mountain Areas), 137–145 (doi: 10.3189/ 172756481794352432)

Nakawo M. and Young G.J. (1981) Field experiments to determine the effect of a debris layer on ablation of glacier ice. Ann. Glaciol., 2, 85–91

Nakawo M., Moroboshi T. and Uehara S. (1993) Satellite data utilization for estimating ablation of debris covered glaciers. IAHS Publ. 218 (Symposium at Kathmandu 1992 – Snow and Glacier Hydrology), 75–83

Nakawo M., Raymond C.F. and Fountain A. eds (2000). IAHS Publ. 264 (Workshop at Seattle 2000 – Debris-Covered Glaciers)

NASA ed. (2011) Landsat 7 science data users handbook. Landsat Project Science Office, NASA Goddard Space Flight Center, Greenbelt, MD

Nicholson L. and Benn D.I. (2006) Calculating ice melt beneath a debris layer using meteorological data. J. Glaciol., 52(178), 463–470 (doi: 10.3189/172756506781828584)

Oerlemans J. (2001) Glaciers and climate change. Balkema, Lisse

Oerlemans J., Giesen R.H. and Van den Broeke M.R. (2009) Retreating alpine glaciers: increased melt rates due to accumulation of dust (Vadret da Morteratsch, Switzerland). J. Glaciol., 55, 729–736 (doi: 10.3189/002214309789470969)

Peel M.C., Finlayson B.L. and McMahon T.A. (2007) Updated world map of the Köppen–Geiger climate classification. Hydrol. Earth Syst. Sci., 11, 1633–1644 (doi: 10.5194/hess-11-1633-2007)

Pellicciotti F., Brock B.W., Strasser U., Burlando P., Funk M. and Corripio J.G. (2005) An enhanced temperature-index glacier melt model including shortwave radiation balance: development and testing for Haut Glacier d'Arolla, Switzerland. J. Glaciol., 51, 573–587 (doi: 10.3189/172756505781829124)

Quincey D.J., Braun M., Bishop M.P., Hewitt K. and Luckman A. (2011) Karakoram glacier surge dynamics. Geophys. Res. Lett., 38, L18504 (doi: 10.1029/2011GL049004)

Raina V.K. and Srivastava D. (2008) Glacier atlas of India. Geological Society of India, Bangalore

Rana B., Nakawo M., Fukushima Y. and Ageta Y. (1997) Application of a conceptual precipitation–runoff model (HYCYMODEL) in a debris-covered glacierized basin in the Langtang Valley, Nepal Himalaya. Ann. Glaciol., 25, 226–231

Reid T.D. and Brock B.W. (2010) An energy-balance model for debris-covered glaciers including heat conduction through the debris layer. J. Glaciol., 56(199), 903–916 (doi: 10.3189/002214310794457218)

Richards J.A. (1999) Remote sensing digital image analysis. Springer- Verlag, Berlin (doi: 10.1007/978–3-662-03978-6)

Shekhar M.S., Chand H., Kumar S., Srinivasan K. and Ganju A. (2010) Climate-change studies in

the western Himalaya. Ann. Glaciol., 51, 105–112 (doi: 10.3189/172756410791386508)

Soncini A., Bocchiola D., Confortola G., Bianchi A., Rosso R., Mayer C., Lambrecht A., Palazzi E., Smiraglia C., Diolaiuti G. (2015). Future hydrological regimes in the upper Indus basin: a case study from a high altitude glacierized catchment, J. Hydrometeorology, 16(1):306-326.

Takeuchi N., Kohshima S., Yoshimura Y., Seko K. and Fujita K. (2000) Characteristics of cryoconite holes on a Himalayan glacier, Yala Glacier, central Nepal. Bull. Glaciol. Res. 17, 51–59

Taschner S. and Ranzi R. (2002) Comparing the opportunities of LANDSAT-TM and ASTER data for monitoring a debris covered glacier in the Italian Alps within GLIMS Project. In IGARSS 2002, International Geoscience and Remote Sensing Symposium, 24–28 June 2002, Toronto, Canada. Proceedings, Vol. 2. Institute of Electrical and Electronic Engineers, Piscataway, NJ, 1044–1046 (doi: 10.1109/IGARSS.2002.1025770)

Thompson M.H. (1974) Some construction aspects of Tarbela Dam, J. Construc. Div., 100(3), 247–255

Winiger M., Gumpert M. and Yamout H. (2005). Karakorum– Hindukush–Western Himalaya: assessing high-altitude water resources. Hydrol. Process., 19(12), 2329–2338 (doi: 10.1002/ hyp.5887)

Young G.J. and Hewitt K. (1993) Glaciohydrological features of the Karakoram Himalaya: measurement possibilities and constraints. IAHS Publ. 218 (Symposium at Kathmandu 1992 – Snow and Glacier Hydrology), 273–283

Zhang Y., Fujita K., Liu S.Y., Liu Q. and Nuimura T. (2011) Distribution of debris thickness and its effect on ice melt at Hailuogou glacier, southeastern Tibetan Plateau, using in situ surveys and ASTER imagery. J. Glaciol., 57(206), 1147–1157 (doi: 10.3189/ 002214311798843331)

Zhang .Y, Hirabayashi Y., Fujita K., Liu S. and Liu Q. (2013) Spatial debris-cover effect on the maritime glaciers of Mount Gongga, south-eastern Tibetan Plateau. Cryosphere Discuss., 7, 2413–2453 (doi: 10.5194/tcd-7-2413-2013)

Chapter 4

2008–2011 snow covered area (SCA) variability over 18 watersheds of the central Chile through MODIS data

Published on GFDQ (2016) by: **Minora U.**, Godone D., Lorenzini S., D'Agata C., Bocchiola D., Barcaza G.S., Smiraglia C., Diolaiuti G.

Abstract

Snowmelt contributes largely to water budget of several Chilean mountain watersheds. To describe snow covered area (SCA) variability within 18 watersheds in Central Chile during 2008–2011 we used MODIS data (i.e. MOD10A2-V5 maximum snow cover extent in eight-day periods). The study area was divided into three different zones (Northern, Central, and Southern), due to its large extent (~205,000 km^2), and according to former studies performed by the Direccíon General de Aguas (DGA) of the Chilean Government covering the time window 2000–2007. After georeferencing our data to the WGS84 Datum (UTM Projection, zone 19S), the scenes were cropped to fit the study area. We selected and set a threshold for cloud coverage (<30%) in order to discard the images with too cloud cover, so losing only 2% of the sample. Hypsographic and aspect analyses were performed using the SRTM3 elevation model. We found largest values of SCA during 2008–2011 in the Central Zone, while the topographic and climatic features (i.e. lower altitudes in the South, and a drier climate in the North) limit snow deposition elsewhere. Similarly, snow line is higher in the Northern zone (due to the presence of the plateau), and lower moving southwards. In the North the minimum SCA is reached sooner than elsewhere, lasting for a longer period (November to March). West apects showed the maximum of SCA in all zones throughout the study period. The present work extends in time the dataset of SCA in the Central Chile, adding information for statistic assessment, and trend analysis of snow cover in this area.

1. Introduction

In mountainous basins with temperate or mediterranean climate, large volumes of snow can be stored at higher elevations, and subsequently be released during spring and summer snowmelt events (Verbunt and others 2003). This natural process is critical for sustaining agricultural activities, hydropower production, urban water supplies and wildlife habitats. However, in the case of the Chilean Andes there is a lack of both meteorological input and hydrological validation data, which complicates the analysis of those hydrological processes (Sther and others, 2009).

Here we try to fill this gap using the Moderate Resolution Imaging Spectroradiometer (MODIS) sensor to estimate the snow cover variability during 2008–2011 within 18 catchments in Central Chile. This study furthers a previous work performed by the Direccíon General de Aguas of the Chilean Government (DGA, 2008), which analyzed the same watersheds in the previous 2000–2007 time window with daily MODIS snow data. The use of MODIS imagery can provide a reasonable estimate of snow cover extent, especially in those areas where little ground-observed snow cover information is available (Ghanbarpour and others, 2007). Godone and others (2011) have shown that there is good agreement between snow cover extent and duration derived from MODIS, and from in-situ measurements in the northwestern Alps. The snow covered area (SCA) is analyzed for temporal (with monthly and annual resolutions), and spatial variability (snow cover surface, snow hypsography and aspects, in altitude belts of 200, and 1000 m).

2. Study site

The study area stretches from North-to-South from the Copiapó River (in the Atacama Region), to the Petrohué River (Los Lagos Region), covering to 205,000 km^2 (fig. 1), and ca. 15° of latitude in the Southern Hemisphere (26°S–41°S). It includes 18 watersheds (fig. 1). Due to its shape, topography, and location, Chile presents contrasting climatic patterns. Mid-latitude Chile is characterized by a semiarid– mediterranean type climate controlled by the seasonal influence of the Southern Westerlies. Precipitation values at 33°S range between 400 mm/yr at the coast (Valparaiso) and 1000 mm/yr in the high Andes. To the north, precipitation declines, whereas southwards significantly higher values, and lower seasonality, occur in both coastal and mountain areas (Miller, 1976). Snow settles on the Chilean Andes, covering the eastern boundaries of the country.

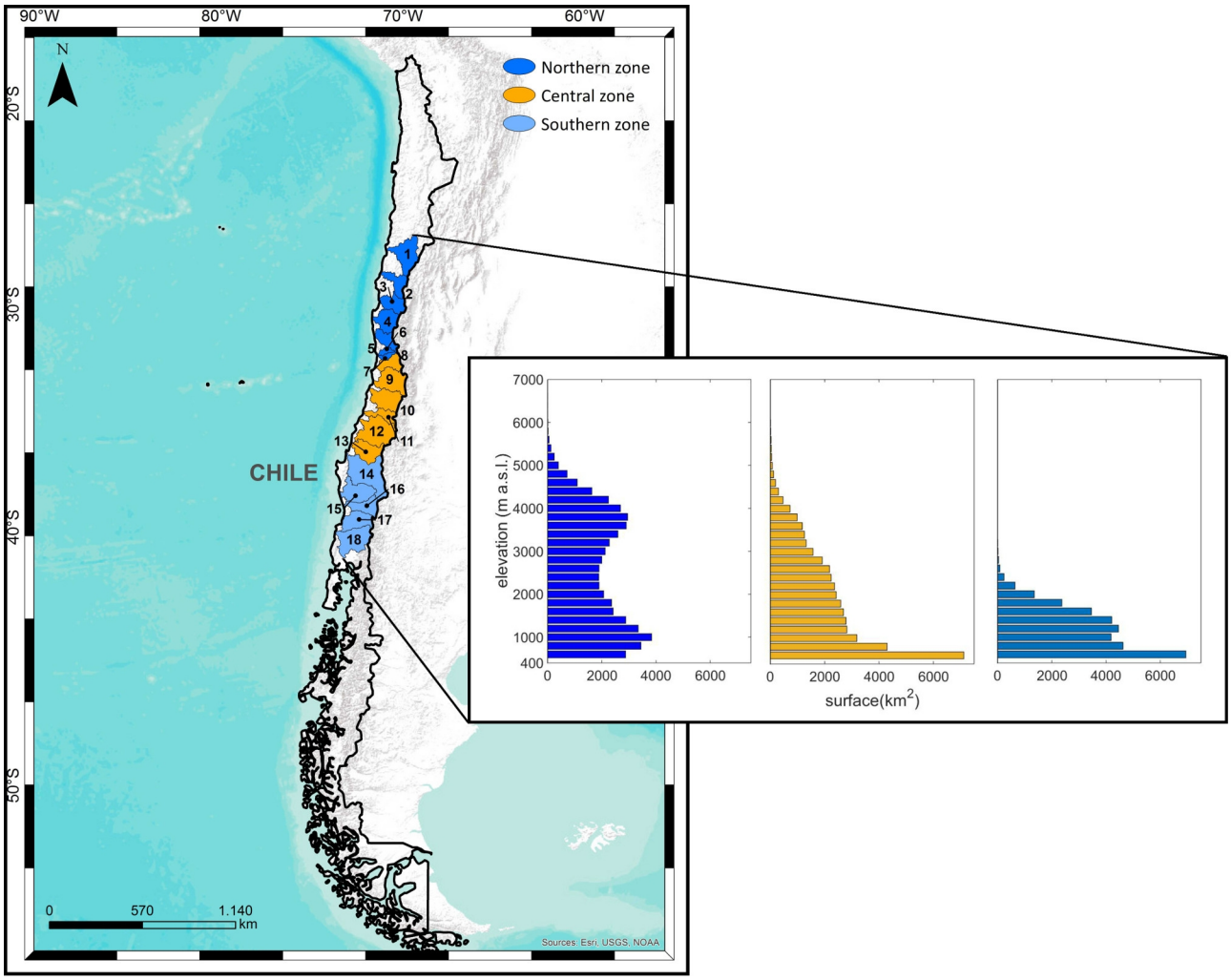

Figure 1: A map of Chile and the study area. The three zones are shown in dark blue (Northern), orange (Central), and light blue (Southern). Numbers represent the various watersheds (as in tab. 1). The hypsograpic curve of the surface of the three zones is also represented in 200 meters altitude bands, above 400 m a.s.l..

3. Materials and methods

Given the study area size and the study period, a massive amount of data needed to be analyzed. Therefore we divided the area into three zones (i.e. Northern, Central, and Southern, see fig. 1 and tab. 1), to better show our findings. This choice is based on the previous DGA report (DGA, 2008), where the same zones were used. We used MODIS data , in particular the MOD10A2-V5 snow product (Hall and others, 2006), already used in other studies concerning SCA in Chile (e.g. Favier and others, 2009; Sther and others, 2009). Data can be downloaded from the National Snow and Ice Data Center website (NSIDC, nsidc.org). The dataset contains information of maximum snow cover extent in an eight-day period (bundle), with 500 meters of resolution. We also used the DEM from

the Shuttle Radar Topography Mission (SRTM90, see www2.jpl.nasa.gov/srtm), which features a resolution of 90 meters, to depict topography. The same MODIS sensor and DEM were used in the previous DGA report (DGA, 2008).

The MODIS scenes were first re-projected from the original sinusoidal format to the WGS84 Datum (Zones 19S and 18S). Then, the DEM was resampled to match the MODIS resolution. The MODIS images and the DEM were subsequently cropped to fit the area of the watersheds studied here. In this phase, we used the catchments' template provided by the Dirección General de Aguas (DGA) in the form of polygonal shapefiles as a basis for clipping.

A pre-processing phase consisted in the selection of the images with low cloud coverage, necessary to attain unbiased SCA analysis. A threshold of 30% was set for cloud cover, to ensure the best tradeoff between image quality and number of scenes available for the analysis. So doing, only 2% of the data was discarded. The choice of this threshold was largely influenced by the high presence of cloud cover over the Bueno basin, where clouds were more frequent than all the other watersheds. Other studies (e.g. Gafurov and Bàrdossy, 2009; Paudel and Andersen, 2011), developed an algorithm to remove cloud noise from the MODIS products. This was not necessary here because, being the MOD10A2 product a bundle of eight-day, the cloud coverage is much lower compared to the daily product, as a pixel needs to be cloud obscured for 8 days to be flagged as cloud. This makes this product preferable to the MOD10A1 daily product (Wang and others, 2007), and does not require additional cloud correction to be used.

Further on, the DEM was reclassified into altitude belts of 200 meters to analyze SCA hypsography. Assignment of snow data to each watershed in the altitude belts was performed combining a script written in Python (python.org), and a Geographic Information System (GIS). Altitudes below 400 meters were excluded from the analysis, because no solid precipitation is expected here (DGA, 2008).

Finally, the study of the SCA divided per aspect and 1000 m altitude bins was performed by means of another reclassification of the DEM, and the aspect map derived from it. The workflow is summarized in fig. 2.

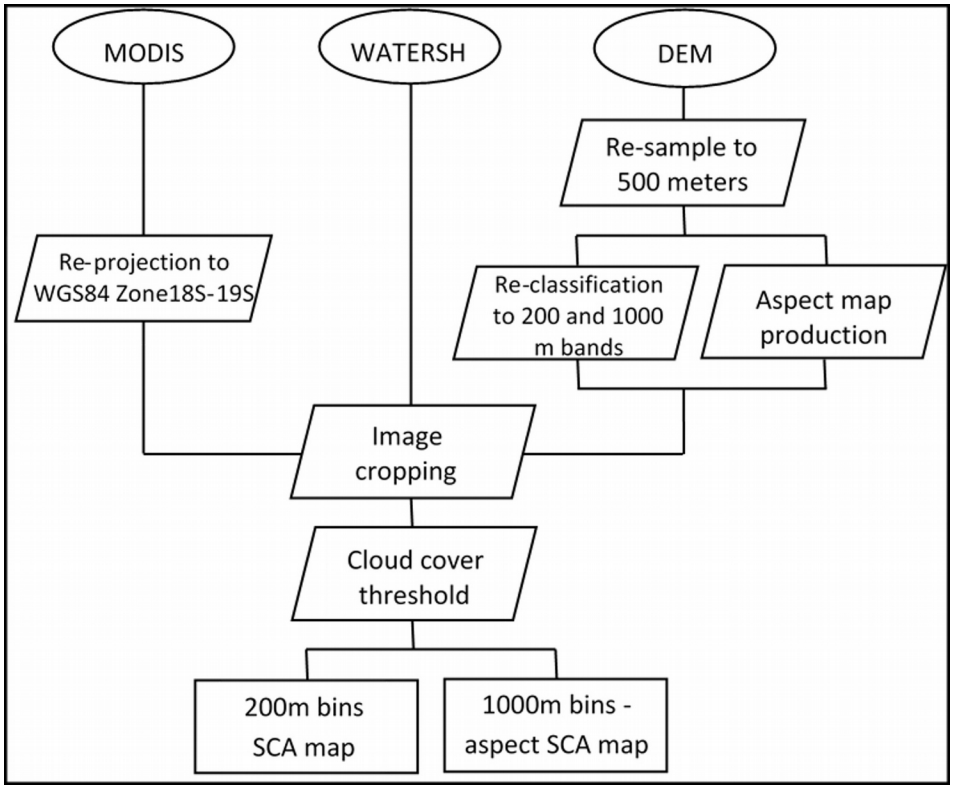

Figure 2: Data processing workflow.

4. Results and discussions

Fig. 3 shows the summary results of the SCA analysis for all the three zones. Snow ablation starts in September, then SCA minima are reached in December in all the zones, while the maximum values are reached in July (i.e. at the end of the austral winter).

The Central zone has much higher values of SCA than the other zones. On the one hand, this is because the Central zone is the largest one (tab. 1). On the other hand, the low topography of the Southern zone and the drier climate towards the north are two major causes of this difference.

Table 1: The three zones we analyzed, and the respective watersheds (name of the rivers are provided, the numbers are referred to the watershed id code we assigned in fig. 1). Latitudes (in degrees) and surfaces (in km2, square brackets) are also provided.

Northern Zone (26°S–33°S)			Central Zone (33°S–38°S)			Southern Zone (38°S–41°S)		
1.	Copiapó	[18704]	8.	Aconcagua	[7334]	14.	Bío Bío	[24371]
2.	Huasco	[9814]	9.	Maipo	[15274]	15.	Imperial	[12669]
3.	Elqui	[9826]	10.	Rapel	[13767]	16.	Toltén	[8449]
4.	Limarí	[11696]	11.	Mataquito	[6332]	17.	Valdivia	[10245]
5.	Choapa	[7654]	12.	Maule	[21054]	18.	Bueno	[15367]
6.	Petorca	[1988]	13.	Itata	[11327]			
7.	Ligua	[1980]						
TOT zone		[61662]			[75088]			[71100]
TOT				[207851]				

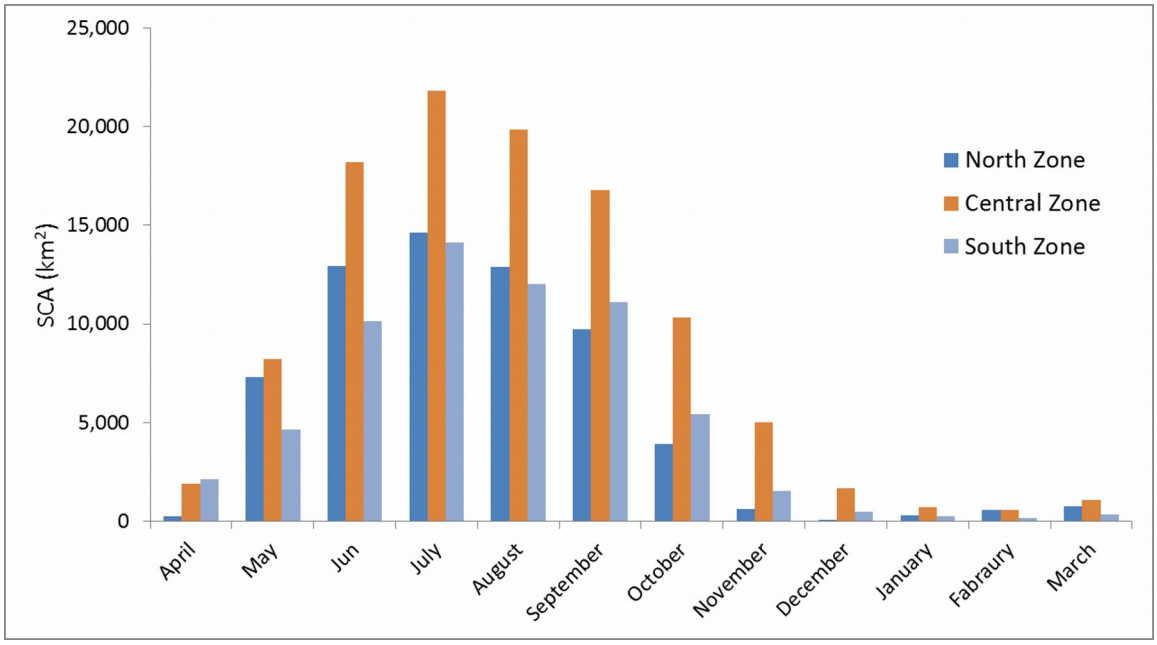

Figure 3: Monthly snow cover variation averaged on 2008–2011.

In fig. 4 we report the SCA distribution per aspect (45° bins) and altitude (1000 m bins). Most of the snow cover shows prevalently westward aspects in all zones, both in winter and summer. The reason of such distribution is not straightforward. On the one hand, the Northern zone shows the most heterogeneous distribution of snow per aspect. Here the presence of glaciers and the plateau makes the recognition of a predominant orientation of snow difficult to be interpreted. In the Elqui and Choapa watersheds snow accumulates and persists more westwards due to the presence of transverse ridges (DGA, 2008). On the other hand, the other zones show much smaller variation of the distribution of snow per aspect, especially during winter. In summer, when snow melts, it tends to persist more on south aspects, due to the minor solar radiation received in the austral hemisphere.

Most of the snow of the Central and Southern zones is found in the 2000–3000 m a.s.l. belt in winter (when SCA is at its maximum). In the same season, in the Northern zone the belt where most of the snow is found is 3000–4000 m a.s.l., higher than in the other zones, due to the presence of the plateau.

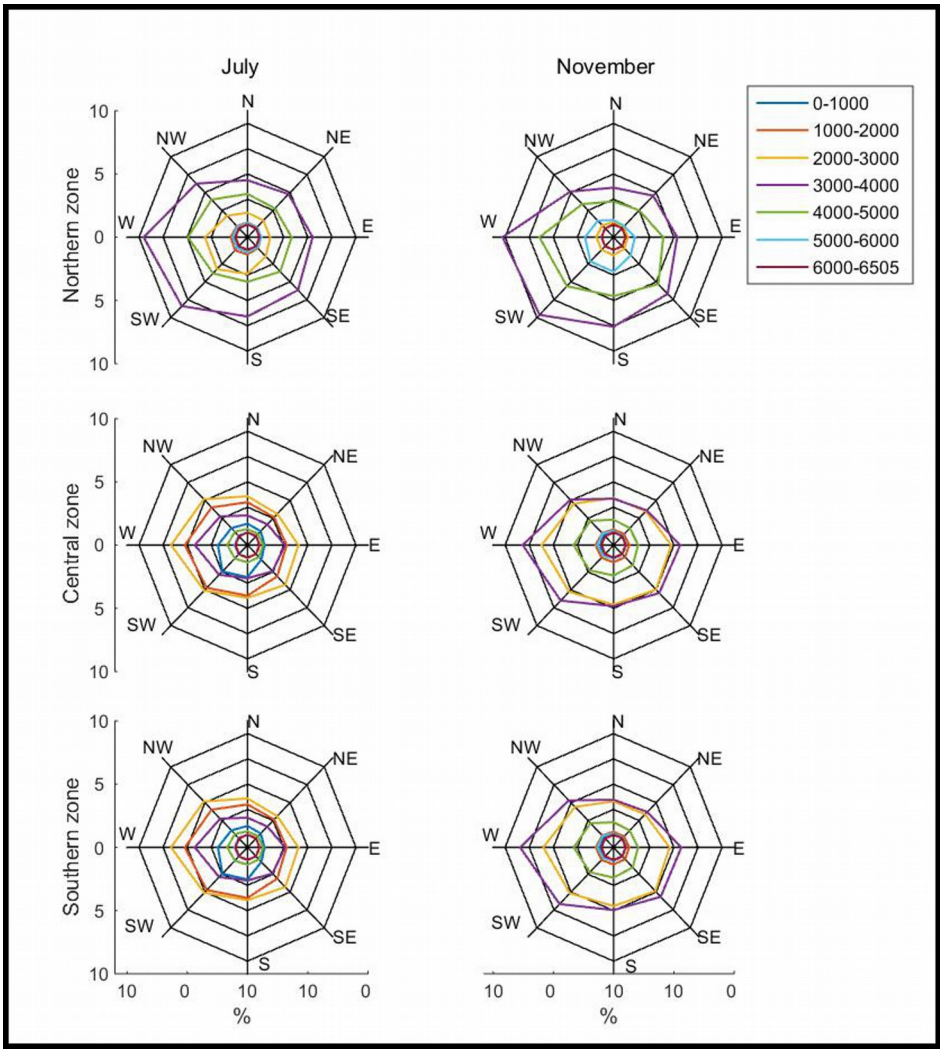

Figure 4: Aspect frequency distribution. It is reported the percentage of SCA as per aspect (45° bins) and 1000 m altitude belts averaged on 2008–2011 in Winter (July, left), and Summer (November, right) in the Northern, Central, and Southern zone.

4.1 Northern zone

The Northern zone shows highest variability of monthly SCA amongst the considered years. Snow cover ranges from the maxima of the winter season, up to 18,244 km^2 (in 2007–2008 hydrological year), to as little as 25 km^2 in summer 2009. The percentage of snow cover over the entire zone at maximum snow extent is the lowest of the three considered zones (<30%). In general, SCA

decreased during the four years here considered, and the maximum is always reached in July.

In the southernmost watersheds of this zone (i.e. Limarí, Choapa, Petorca, and Ligua basins), no snow is found in our analysis since the end of November until the beginning of the next hydrological year (in April). DGA (2008) depicts the same situation during 2000–2007. This is probably due to the less frequent precipitation than the other zones, and because the altitude is lower than the other watersheds of the same zone, thus consisting in the melt of all the snow accumulated during winter.

4.2 Central zone

SCA variability is almost constant in the Central zone during 2008–2011. Maximum values are much higher than the other zones (up to 29,106 km^2 in 2010 July), because i) this is the widest zone (tab. 1), ii) precipitation are higher than the Northern zone, and iii) maximum elevations are on average much higher than the Southern zone, thus facilitating snow accumulation. Glaciers are abundant in this zone. Ablation rates are less evident than the Northern zone, and the accumulation season extends to mid-September. This is in accordance with the previous DGA report (DGA, 2008). In general, SCA decreases through years during the study period, with the hydrological year 2010–2011 showing 10% less SCA than in 2008–2009. A decrease in precipitation (although not significant), was observed during 1970–2004 by Pellicciotti and others (2007) in the Aconcagua region and this might have caused a decrease in the snow cover in the same decades. Nevertheless, SCA values during 2008–2011 are higher than 2000–2007 on average (data from DGA, 2008). In particular, the maximum value found during 2000–2007 is 5,000 km^2, lower than the values found in winter in our study period. Finally, maxima are observed between 2200 and 2600 m a.s.l. in July, while snow is still found even in the warmer season at the highest altitudes (>4000 m a.s.l., with the maximum represented by the Aconcagua peak, the highest peak of the Southern hemisphere with its 6960 m a.s.l.). Note that only the Aconcagua, Maipo, and Rapel watersheds are higher than 4000 m a.s.l..

4.3 Southern zone

The annual variability of SCA during 2008–2011 is very high in the Southern zone. Maximum values are found since June to August, depending on the hydrological year. Also, SCA decreases on average during 2008-2010, only to increase in 2011. Thaw season begins in September as also reported in the previous DGA report (DGA, 2008), for the period 2000–2007, with high rates leading to minimum cover already in November. The observed maximum value is 21,843 km^2 in August 2007. In general, the relatively low elevations limits snow accumulation here (elevation is often lower than 3000 m a.s.l.). However, precipitation is abundant (especially towards the coasts), and snow is found even below 3000 m. Unfortunately, we could not make a comparison with the previous DGA report, because the SCA analysis during 2000–2007 was made impossible by the massive presence of clouds in this zone. The use of the bundled (8-days) MODIS product against the daily product used in the previous report (MOD10A2 versus MOD10A1), allowed us to have a

good dataset for this zone where precipitation (and thus clouds) is frequent throughout the year. As our study period is too short for assessing if SCA variation was significant, we refer to Bown and Rivera (2007), who studied the climate changes during the second half of the 20th century in the Chilean Lake District (38°S–42°S, about the same latitudinal range of the Southern zone). The regional rainfall data they collected from 1961 to 2000 showed an overall decrease with a maximum rate of −15 mm/year at Valdivia station (39°38′S/73°05′W). They speculated that this reduction in precipitation might be related to El Niño–Southern Oscillation (ENSO) phenomena which have been more frequent after 1976.

5. Conclusions

The present contribution aimed at showing SCA variability during 2008–2011 in the Central Chile, over 18 mountainous watersheds (205,000 km^2). MODIS snow products from the NDSIC were used for the analysis. The dataset (consisting of eight-day bundles of maximum snow cover) was processed combining GIS tools and the Python programming language to automate the production of snow cover maps. We showed that SCA decreased during the four considered years. This is true also looking at a longer time window (i.e. since 2000), according to the previous DGA report (DGA, 2008), except for the Central zone, where SCA was higher in 2008–2011. The maximum SCA was found in the Central Zone, while the topographic and climatic features (i.e. lower altitudes in the South, and a drier climate in the North) limited snow deposition elsewhere. The snow line is higher in the Northern zone due to the presence of the plateau, and it decreases southwards. In the Northern Zone the minimum SCA is reached sooner than elsewhere, and lasts for a longer period (November to March), probably because the drier climate. West aspects showed the maximum of SCA in all zones throughout the study period. In the present work we showed how the MOD10A2 product can be used for studying snow covered areas over an extended domain. The spatial (500 m) and temporal (weekly) resolution of the MODIS sensor, its many bands (36 channels), and the availability of the data at no cost, makes it a reliable product to study SCA where few in-situ measurements are available.

References

Bown F. and Rivera A. (2007) Climate changes and recent glacier behaviour in the Chilean lake District. Global and Planetary Change, 59, 79–86.

DGA, Direcciòn General de Aguas (2008) Dinámica de la cobertura nival entre las cuencas de los ríos Copiapó y Petrohue utilizando imágenes satelitales. Dirección General de Aguas, Unidad de Glaciología y Nieves, Santiago de Chile.

Favier V., Falvey M., Rabatel A., Praderio E. and Lòpez D. (2009) Interpreting discrepancies between discharge and precipitation in high-altitude area of Chile’s Norte Chico region (26–32°S). Water Resources Research, Vol. 45, W0242, doi: 10.1029/2008WR006802.

Gafurov A. and Bárdossy A. (2009) Cloud removal methodology from MODIS snow cover product.

Hydrol. Earth Syst. Sci., 13, 1361–1373.

Ghanbarpour M.R., Saghafian B., Saravi M.M. and Abbaspour K.C. (2007) Evaluation of spatial and temporal variability of snow cover in a large mountainous basin in Iran. Nordic Hydrol. 38(1), 45–58.

Godone D., Filippa G., Terzago S., Rivella E., Salandin A., Barbero S., Garnero G. and Freppaz M. (2011) - Snow cover Extent and Duration in MODIS Time Series: A Comparison with in-sity Measurements (Provincia Verbano Cusio Ossola, NW Italy). International Journal of Environmental Protection vol. 1 n.4: 7-11.

Hall D.K., Salomonson V.V. and riggs G.A. (2006) MODIS/Terra Snow Cover 8-Day L3 Global 500m Grid. Version 5. [Jan-Dec, 2001-2010]. Boulder, Colorado USA: National Snow and Ice Data Center.

Miller A. (1976) The climate of Chile. In “World Survey of Climatology, Vol. 12” (W. Schwerdtfeger, Ed.), pp. 113–145. Elsevier, Amsterdam.

Paudel K.P. and Anderson P. (2011) Monitoring snow cover variability in an agropastoral area in the Trans Himalayan region of Nepal using MODIS data with improved cloud removal methodology. Remote Sensing of Environment 115, 2011, pp. 1234–1246.

Pellicciotti F., Burlando P. and Vliet K.V. (2007) Recent trends in precipitation and streamflow in the Aconcagua River Basin, central Chile. IAHS Publ. 318, 2007.

Sther A., Debels P., Arumi J.L., Romero F. and Alcayaga H. (2009) Combining the Soil and Water Assessment Tool (SWAT) and MODIS imagery to estimate monthly flows in a data-scarce Chilean Andean basin. Hydrological Sciences, 54(6).

Verbunt M., Gurtz J., Jasper K., Lang H., Warmerdam P. and Zappa M. (2003) The hydrological role of snow and glaciers in alpine river basins and their distributed modeling. J. Hydrol. 282 (2003) 36–55.

Chapter 5

Remote sensing and interdisciplinary approach for studying glaciers

Published on J-READING (2014) by: Fea M., **Minora U.**, Pesaresi C., Smiraglia C.

Abstract

Remote sensing, which provides interesting input and approaches for multidisciplinary research and wide inventories, and which represents a very important tool in the strictly related fields of research and didactics, shows great potentialities in the specific area of the studies of glaciers (extension, balance and variations), glacier morphology and climate changes. In time, remote sensing applications for the analysis of glaciers and climate change have considerably increased, using different methodologies and obtaining significant results. In this paper, after a synthesis of some basic elements, we provide a detailed literary review, which sets out to underline the steps and results achieved and also to stimulate didactical considerations and hypothesis of work. Successively, we resume the main characteristics of specific glaciers, for which the European Space Agency (ESA-ESRIN) has provided images ad hoc and for each glacier we propose an interpretative analysis of these images. According to the scheme proposed by Fea and others (2013), the principal aim is to define research of referral and some interpretative guidelines useful for interdisciplinary frameworks focussed on glaciers, where geography can play the role of collector between different sciences with the support of various geotechnologies.

1. Introduction

The modern knowledge of the planet Earth describes it as an integrated system of six basic components, namely atmosphere, cryosphere, hydrosphere, geosphere, biosphere and anthroposphere, each of them in a permanent and complex interaction with all the others. The evolution of the Earth is characterised primarily by this interactivity, even if in the medium- and long-term an important role is played by external forces, such as solar wind and cosmic rays, and sometimes by sudden interplanetary events, for instance by the impact of a celestial body.

Nowadays, major scientific challenges are concerned with the apparent acceleration of the evolution of the Earth's climate, the increased occurrence of extreme meteorological events and atmospheric global warming. The real concern comes, in particular, from the actual impact that is caused to the above-mentioned natural evolution by the parallel exponential increase of the world population and human activities.

Specifically, two terms have become very popular: climate change and global warming, implying in reality with them the impact on natural phenomena (climate variability and atmospheric greenhouse effect) of human activities. Therefore, climate change and global warming are now first priority targets (among others, of course) for scientific research and world-wide operational observing systems. General and specific phenomena and parameters have been identified for an effective monitoring through measurements and observations at all scales and with all means, from ground devices to airplane and satellite instruments.

In the above context, the accurate monitoring of the cryosphere plays a very important role, as ice in all its forms, such as sea-ice, permafrost, glaciers, icebergs, snow cover and so on, has a fundamental role in the variability of key physical and chemical parameters, like for instance temperature, albedo, sublimation, pollution. Therefore, glaciers are very important scientific and operational indicators, as will be shown and demonstrated in the next chapters.

One last consideration concerns remote sensing, that is to say methodology, procedures and tools for observing a target without getting into physical contact with it. It uses devices (sensors) that measure the electromagnetic energy irradiated by the observed targets in different parts (spectral bands) of the electromagnetic (e.m.) spectrum, defined by their related wavelengths. The most common bands used to observe the Earth's surface are the Visible (VIS, which contains all the colours of a rainbow), Near-, Medium- and Far Infrared (NIR, MIR and FIR), the Thermal Infrared (TIR) and the Microwaves (MW).

The energy measured in each spectral band carries a different type of information about the observed target: for example, in the Visible the physical input is the fraction of sunlight (albedo) reflected by the target surface towards the sensor. Simultaneous use of different VIS bands provides information that is very useful to "recognise" the observed target and, therefore, to "classify" it through a multispectral observation. Each spectral band used by an observing instrument has a number assigned, specific to that instrument; the same band with a different instrument could have a

different number. The data are then visualised on a screen by inserting the values measured in a spectral band in one of the three colour channels (Red, Green and Blue) that drive the screen; the visualisation model is then identified by specifying RGB and the band numbers used to visualise the band values: for example, RGB 321 indicates that the data acquired by the sensor in the spectral band No. 3 of the used instrument are shown in Red colour tones on the screen.

Visualisation in natural (or true) colours means inserting into the RGB channels of the screen respectively the values measured by the sensor through the spectral bands of the corresponding red, green and blue colours of the rainbow in the Visible bands. Any other combination would provide a false colour image on the screen. Natural colour images provide a “human” view of the scene; false colours are very much used to help the interpretation of the data or to quickly identify a specific target (thematic images).

This paper, conducted on the basis of the scheme proposed by Fea and others (2013), focusses the attention on specific elements that would help to better understand the potentialities of remote sensing in the double and strictly related fields of research and didactics, resuming the methods and results of many studies carried out on different glaciers and examining various glaciers under a geographic, glaciological and geomatic point of view.

2. Remote sensing for the study of mountain glaciers. A literary review and some didactical considerations

International literature has shown many interesting and useful functions and applications regarding remote sensing for the study of glaciers (extension, balance and variations) and glacier morphology, also providing input for the analysis of climate change. In fact, there is a very large amount of research which has focussed the attention on different glaciers, providing important estimates regarding the dimensions and variations recorded over a number of years or decades. For example, the glaciers of the Himalayas and the Alps are precious sources of information and data because they have been analysed considering many aspects and points of view. In other cases, remote sensing has been used as a support for the assessment of hazards from glacier lake outbursts and for the origination of potential ice avalanches and debris flows and also for the evaluation of permafrost-related hazards in high mountains (Huggel and others, 2002; Kääb and others, 2005; Frey and others, 2010).

In order to collect a set of images that are explanatory and of considerable use both in research and didactics, it is very important to have images obtained over a period with a reduced blanket of snow and without cloud cover; similarly, in terms of evolution analysis, it would be recommended to make comparisons among images taken in the same month in different years so as to permit maximum comparability.

For some decades now many papers have underlined the potential added value of remote sensing for the study of glaciers, highlighting particular aspects and providing relevant contributions for different kinds of analysis, and in the last ten years an intense proliferation of studies has been

recorded, stimulating the need to define synthetic frameworks of knowledge and results.

As affirmed by Berthier and others In 2004, mountain glaciers can be considered a reliable indicator of climate change and remote sensing can provide “a suitable way to increase the number of monitored glaciers, especially in remote areas”. Focussing the attention on the Mer de Glace, the largest glacier in the French Alps, as “test area”, the approach used has adapted “the geodetic method to satellite images. The first step calculates the DEMs. Some adjustments and corrections are needed to reduce the biases between the DEMs. The mean thickness change is then extracted for each altitude interval on the glacier” (p. 1). Considering two time intervals (1994-2000 and 2000-2003), the study has made it possible to “show a rapid thinning of the Mer de Glace during the last 10 years below 2500 m” (p. 4).

A couple of years later, Bolch and Kamp stated that: “Glaciers are sensitive climate indicators and thus subject to monitoring of environmental and climate changes. Remote sensing techniques are often the only way to analyze glaciers in remote mountains and to monitor a large number of glaciers at the same time” (2006, p. 37). Their study has shown “the capability of accurate glacier mapping using multispectral data, digital elevation models (DEMs), and morphometric analysis for the Bernina Group in the Swiss Alps and for the northern Tien Shan in Kazakhstan and Kyrgyzstan” (p. 38).

Another interesting investigation regarding glacier variation was conducted using data from Indian Remote Sensing satellites by Kulkarni et al. in 2007. “This investigation was carried out for 466 glaciers in the highly glaciered Himalayan basins, namely Baspa, Parbati and Chenab” and “has shown overall 21% reduction in glacial area from the middle of the last century. Mean area of glacial extent was reduced from 1.4 to 0.32 km^2 between 1962 and 2001”. Nevertheless, “the number of glaciers has increased between 1962 and 2001” (due to fragmentation), but the “total areal extent has reduced” (pp. 73-74).

In the same year, glacier changes in the Alps were observed by satellite in research conducted by Paul and others and the “qualitative analysis of multispectral satellite imagery revealed clear but indirect evidence of massive glacier down-wasting in the European Alps since 1985. The changes can easily be detected with animated multitemporal false colour images which only require relative image matching” (2007, p. 120).

Furthermore in 2007, the old topographic maps of Svalbard and a modern digital elevation model were compared by Nuth and others to study the glacier geometry and elevation changes on Svalbard (seven regions for a total of about 5,000 km^2) over a long time interval (54 years), showing a significant area decrease and loss of mass for the 1936-1990 period.

Still in the same year, starting from the consideration that “Alpine glaciers dynamics may serve as an indicator of Climate Change”, the results of research aimed at developing “a true temporal GIS able to manage, visualize and analyse” different type of data which require a synthesis were exposed by Villa and others Particularly, the aims to create a complex and articulated geodatabase

were resumed in an “analysis of mass balance in relation to geographic parameters (aspect, slope, bedrock morphology, ice thickness), moraines mapping and analysis to support field reconstructions, mapping of different kind of features (seracs and crevasses i.e.) to support glacier dynamics analysis. Furthermore, it can be a useful base point for a web-mapping use of this data (environmental paths, geosites descriptions etc.). Moreover a more integrated quantitative analysis can be carried out by the use of a geosensors network” which can be defined as a system of tools “to acquire different kind of spatio-temporal data. GPS, total stations, digital cameras, laser scanners can be therefore defined as geosensors. GIS will be able to integrate this network of several sensor data type, offering to the research an added value in terms of a common ground for the fusion of data and in a forecasting perspective” (2007, p. 103).

Then in 2008, Malinverni and others “developed a study process to analyse the status of some Alpine glacier groups (Adamello, Ortles-Cevedale and Bernina) localised in the North of Italy, the ‘water tower’ of Europe. The investigation was based on a set of three multi-temporal Landsat scenes acquired with the sensors MSS, TM and ETM+ combined with other types of information (2D, 3D and thematic data). The GIS based analysis, supported by remote sensing processing, allowed the extrapolation of the meaningful parameters for the glacier dynamism in the temporal displacement of observation” (p. 120). They showed that: “More refined classification methods, principal components analyses and image rationing can produce a classification which is supported by a rigorous accuracy assessment and can facilitate the production of accurate maps of glacier extension useful for glacier inventory, for change detection studies and also for analysing the influence of climate change and global warming. The acquired location and the extent of each glacier derived by remote sensing techniques can update the data-base, adding information about the accumulation and ablation areas from which the accumulation area ratio (AAR) can be derived. Furthermore, the integration of the digital elevation model with the dataset could facilitate the derivation of some other important glacier inventory attributes” (pp. 130-131).

One year later, Knoll and Kerschner applied a “new approach to glacier inventory, based on airborne laser-scanner data”, to South Tyrol (Italy): “it yields highly accurate results with a minimum of human supervision. Earlier inventories, from 1983 and 1997, are used to compare changes in area, volume and equilibrium-line altitude. A reduction of 32% was observed in glacier area from 1983 to 2006. Volume change, derived from the 1997 and 2006 digital elevation models, was –1.037 km^3” (p. 46). So, modern Earth-observation methods and technologies (laser-scanning and radar remote sensing) have shown their importance for estimating and monitoring variations recorded in areas and volume, offering interesting “opportunity to investigate glacier changes” (2009, p. 50).

In 2010, Bolch and others provided “a comprehensive multi-temporal glacier inventory for British Columbia and Alberta, a region that contains over 15,000 glaciers, for the years 1985, 2000 (for about half of the area) and 2005, generated in a time frame of less than 1 year”. Regarding the technologies and tools used, they worked with satellite imagery, DEM and digital outlines of

glaciers from 1985 and the results showed that: “Glacier area in western Canada declined 11.1±3.8% between 1985 and 2005. The highest shrinkage rate in British Columbia was found in the northern Interior Ranges (−24.0±4.9%), the lowest in the northern Coast Mountains (−7.7±4.6%). The continental glaciers in the central and southern Rocky Mountains of Alberta, shrank the most (−25.4±4.1%). However, the shrinkage rate is mostly influenced by glacier size. Regional differences in ice loss are smaller when glaciers of any given size class are examined [...]. The shrinkage rates have possibly increased across the study area in the period 2000–2005, with the highest increase in the Rocky Mountains” (pp. 135-136).

Recently, in the study conducted by Negi et al. “Gangotri glacier [Himalaya, India] was monitored using Indian Remote Sensing (IRS) LISS-III sensor data in combination with field collected snow-meteorological data” for the period 2001-2008 (2012, p. 855), testing the potentialities and add value of the satellite remote sensing for a temporal interval of seven years. “The observed changes in snow cover area and snow characteristics were validated using field collected snow-meteorological data and field visit” (p. 864). The results of the investigation underlined an “overall decreasing trend in the areal extent of seasonal snow cover area (SCA)” (p. 855) and confirmed “the retreat of Gangotri glacier” (p. 864). Moreover: “This study has shown that the changes on glacier surface are due to climatic and topographic (local geomorphology) factors, which decreased overall glaciated area by 6% between 1962 and 2006” (p. 864).

Another contemporary paper, using also false colour images which have demonstrated their importance both in snow mapping and in identifying various glacial landforms, presented “the results obtained from the analysis of a set of multitemporal Landsat MSS, TM and ETM+ images for the monitoring and analysis of Gangotri Glacier main trunk change”. The investigation and data analysed by Haq and others have shown an overall significant reduction in glacier area between 1972 and 2010 (2012, p. 259).

Owing to its relevance and numerous applications, it is worth noting the “GLIMS” project (Global Land Ice Measurements from Space) coordinated by Jeffrey S. Kargel and finalised “to monitor the world’s glaciers primarily using data from optical satellite instruments, such as ASTER (Advanced Spaceborne Thermal Emission and reflection Radiometer)” (http://www.glims.org).

In fact, the main applications of GLIMS concern (http://www.glims.org/About):

- *Global Change Detection* and “GLIMS’ mission to establish a global inventory of ice will provide the community with data for later comparison. Monitoring glaciers across the globe and understanding not only the cause of those changes, but the effects”, the project will provide important steps “to a greater understanding of global change and its causes”;
- *Hazards Detection and Assessment* because “outburst floods, landslides, debris flows, and debris avalanches can destroy property and take lives in a sudden rush of water, ice, sediment, rock, soil, and debris”, provoking relevant problems and damages to the communities exposed to risk;

- *Glacier Monitoring* and "through the long-term monitoring of the world's glaciers" the GLIMS project has also the purpose to "build a base of historical data, detect climate changes early, and predict and avoid hazards to human communities living in the proximity of glaciers".

The GLIMS project "has implemented a database of glacier outlines from around the world and other information about glaciers that includes the metadata on how those outlines were derived" (http://www.glims.org/glims blurb.html). The GLIMS database is thought "to be a logical extension of the World Glacier Inventory (WGI) of the World Glacier Monitoring Service (WGMS)" (http://nsidc.org/glims/). For more than a century, WGMS and other predecessor organizations "have been compiling and disseminating standardized data on glacier fluctuations". Particularly, "WGMS annually collects glacier data through its scientific collaboration network that is active in more than 30 countries" (http://www.wgms.ch/).

Moreover, as supplementary element, the Randolph glacier inventory (RGI 3.2) was produced, which is a global inventory of glacier outlines (http://www.glims.org/RGI/randolph.html).

However, we have to remember that interesting input and considerations for the study of glacier variation based on remote sensing were already being carried out at the end of the 70s and 80s (Rabagliati and Serandrei Barbero, 1979; Della Ventura and others, 1982, 1983; Dozier, 1984), when for example remote sensing and geotechniques for the automatic analysis of digital images were applied to evaluate the glacier surfaces of Mount Disgrazia (Alpi Retiche, Italy) and to estimate fluctuations over time (between 1975 and 1980) (Della Ventura and others, 1985). Therefore, papers like these represent "guide studies" which have provided elements and input useful for future research and developments in the general framework of knowledge.

New interesting contributions successively produced in the 90s when:

- Landsat Thematic Mapper (TM) data of some glaciers in the eastern Alps of Austria were acquired every two years (in 1984, 1986, 1988 and 1990) and studied in detail in order to observe and quantify the glacier variations (Bayr and others, 1994, p. 1733);
- a specific algorithm was developed to map global snow cover using Earth Observing System (EOS) Moderate Resolution Imaging Spectroradiometer (MODIS) data (Hall and others, 1995, p. 127);
- the capability and potentialities of Spaceborne Imaging Radar-C/X-band Synthetic Aperture Radar (SIR-C/X-SAR) to map seasonal snow covers in alpine regions were tested (Shi and Dozier, 1997, p. 294);
- the SIR-C/X-SAR was used to map snow and glacial ice on the rugged north slope of Mount Everest (Albright and others, 1998, p. 25823).

Also at the beginning of 2000 a great amount of increasingly detailed research on these topics was published and relevant contributions were for example focussed on the Swiss and Austrian Alps.

Particularly, in 2000 a methodology based on remote sensing for analysing the distribution of glacier mass-balance was presented by Hubbard and others as far as concerns Haut glacier d'Arolla (Valais, Switzerland, between September 1992 and September 1993).

In 2001 aerophotogrammetric techniques and data and DEMs were used by Kääb to reconstruct a 20-year mass-balance curve (1973-1992) of Grubengletscher (Swiss Alps).

In 2002 a trend analysis of glacier area between 1969 and 1992 was conducted by Paul for 235 glaciers in the Tyrol (Austria), using Landsat Thematic Mapper (TM) imagery and data from the Austrian glacier inventory and the results showed that: "The total loss in area in this period is about 43 km^2 or -18.6% of the area in 1969 (230.5 km^2). Glaciers smaller than 1 km^2 contribute 59% (25 km^2) to the total loss although they covered only one-third of the area in 1969" (p. 787).

In the same year, a new Swiss glacier inventory was compiled from satellite data for the year 2000 and the most important tasks described by Paul and others were: "(1) an accuracy assessment of different methods for glacier classification with Landsat Thematic Mapper (TM) data and a digital elevation model (DEM); (2) the geographical information system (GIS)- based methods for automatic extraction of individual glaciers from classified satellite data and the computation of three-dimensional glacier parameters (such as minimum, maximum and median elevation or slope and orientation) by fusion with a DEM" (2002, p. 355). This work, applying different glacier-mapping methods, has shown the relevant role obtained by the synergic interaction between remote sensing and GIS in a context where the digital elevation model can provide other useful information and offer almost two main functions: "the orthorectification of the satellite imagery, and the derivation of three-dimensional glacier parameters within a GIS" (p. 358).

And then again in 2002, another study connected with the previous one and conducted by Kääb and others concluded that: "The new Swiss Glacier Inventory 2000 confirms the clear trend in area-loss of Alpine glaciers. A drastic acceleration of retreat since 1985 can be observed for the entire glacier sample analysed here (< 10 km^2). Although this drastic area loss of small glaciers is not equivalent to drastic volume loss with respect to the total ice volume [...] it has significant effects on processes involved in surface energy balance, hydrology or landscape evolution. The behaviour of the small glaciers shows a high spatial and temporal variability which can completely be assessed only by remote sensing methods".

Regarding aerophotogrammetric techniques applied to glacier inventory and studies on relationships between glacier changes and climate evolution, two recent studies combining registered colour orthophotos with differential GPS (DGPS) field measurements described the evolution of the two most glacialized Italian regions (Aosta Valley and Lombardy). Diolaiuti and others recorded a mean area loss of Aosta Valley glaciers during 1975-2005 of about -27% (-9% per decade) (2012a, p. 17). In Lombardy glaciers' area reduced from 1991 to 2003 by 21% and glaciers "smaller than 1 km^2 accounted for 53% of the total loss in area" (Diolaiuti and others, 2012b, p. 429).

To add some other recent results based on remote sensing methods, it must be remembered that

Mihalcea and others tested in 2008 the possibility of using ASTER satellite and ground-based surface temperature measurements to derive supraglacial debris cover and thickness patterns on debris-covered glaciers. “The comparison between field and remotely sensed data serves four purposes: 1) to compare different temperature data sources, assessing their reliability and accuracy; 2) to assist in the interpretation of the spatial variations of surface temperature on a debris-covered glacier; 3) to develop a method for mapping supraglacial debris cover distribution and thickness from ASTER data; 4) to assess the validity of the satellite-derived debris thickness map using field debris thickness measurements” (p. 342). The results obtained on Miage glacier confirmed the “validity of ASTER-derived surface temperatures of debris-covered” (p. 353).

Moreover, a contribution to analyse some particular glacier evolutions (i.e. the “Karakoram anomaly”, where a situation of general stability has been recently depicted) has been added by Minora and others in 2013. They focussed “the attention upon the glacier evolution within the Central Karakoram National Park [...] to assess the magnitude and rate of such anomaly”. Using remote sensing data (for example Landsat images), they “analyzed a sample of more than 700 glaciers” and “found out their area change between 2001 and 2010 is not significant (+27 km^2 ±42 km^2), thus confirming their stationarity” (p. 2892).

To sum up, literary review shows that remote sensing is a powerful tool for the study of glaciers from many points of view and it can be used in a synergic approach with GIS, GPS and other geospatial technologies.

It also represents a very useful didactical tool making it possible to:

- understand mountain and glacial environments and recognize peculiar forms and elements which in many cases would require lot of direct experience acquired during field surveys to be acknowledged;
- see with one’s “own eyes” the changes recorded over time in terms of areas affected by glaciers;
- search for common points and different elements among mountain environments and glaciers;
- understand the hazards related to particular aspects of glacier environment in high mountains;
- visualize images with strong “visual impact” which can capture the attention, stimulating hypothesis, considerations, dynamic participation in class and lively discussions with classmates and teachers;
- promote laboratorial and professional didactics, a kind of start-up of research in didactics and research for didactics, which represent crucial points, an essential symbiosis to show and spread the “real face” of modern geography.

From the didactical perspective, some examples of image visualizers from the air and satellites for the study of mountain environments, which highlight the differences between various contexts, have been given by De Vecchis and Pesaresi in 2011 (pp. 79-90), also comparing this kind of images with topographic maps and simulating a geography cycle of geography lessons which can be supported by these very interesting iconographic materials.

New perspectives can moreover be opened up by the function of ArcGIS Online which can be added to ESRI's GIS software. In fact, thanks to this modality, it is possible to visualize many images and applications already made to be shared, satisfying relevant didactical aspects concerning: the availability of the images; the overlay of related layers which use different sources or referred years, permitting the monitoring of glacier retreats and variations; the observation of prepared elaborations which can also provide input for similar elaborations and for new research in other contexts; the possibility of uploading one's own elaboration to share with other users, giving enthusiasm and increasing the sense of responsibility of single students and the group working on the research. Further important applications can be obtained by the integration between satellite images and GIS, importing georeferenced images in a GIS software able to re-elaborate, analyse and compare the acquired images. Thus, by the combined use of various geotechnologies it is possible to undertake many interesting didactical investigations, promoting and supporting innovative interdisciplinary studies, where specific methodologies and tools can be tested.

3. Miage glacier

The Miage glacier is a typical debris-covered valley glacier of the upper Veny Valley (Aosta Valley, Italy), that drains the southwest slope of the Mont Blanc massif. A valley glacier means that the ice body has such a long tongue as to flow along a valley. A debris-covered glacier means a glacier where part of the ablation zone has a continuous cover of supraglacial debris across its full width. Some authors apply a more rigorous definition of debris cover over at least 50% of the ablation zone (Kirkbride, 2011). This can greatly influence ablation values all over the glacier. In particular, a thin and dispersed layer of supraglacial debris is able to enhance ice melting above clean or uncovered ice rates because low-albedo rock surfaces absorb much of the incoming short-wave radiation (Kirkbride, 2011). On the contrary, under a continuous clast thick cover, exceeding a "critical value" (Mattson and others, 1993), heat transfer to the debris-ice interface is reduced due to the low thermal conductivity of the void-rich debris layer (Kirkbride, 2011; Nakawo and Rana, 1999; Adhikary and others, 2000; Mihalcea and others, 2006; Mihalcea and others, 2008; Scherler and others, 2011). With its 11 km^2 of surface, Miage represents the largest glacier of the Italian side of the Mont Blanc, and the third in Italy (after the Adamello and Forni glaciers).

The Miage glacier can be divided into three distinct zones: i) the upper part, characterized by numerous steep and narrow ice confluences, ii) the central part, almost flat, where the glacier tongue is canalized between steep slopes, and iii) the lower part, which flows into the Veny Valley, flanked by the Little Ice Age lateral moraine system.

The main flow line goes linearly North-West to South-West, bending in the very last portion to become parallel to the valley profile (SW-NE). The glacier extends from around 4,800 m a.s.l. (top of Mont Blanc) down to 1,770 m a.s.l.

The supraglacial debris cover of the Miage glacier mainly derives from landslides, and it is then redistributed by ice flow and snow avalanches all over the ablation tongue. Debris thickness increases from a few centimeters of dispersed cover on the upper tongue to >1 m at the terminus at 1,770 m a.s.l., although debris cover is patchy or absent in localized areas of crevasses (Brock and others, 2010; Diolaiuti and others, 2005; Deline, 2005). The different distribution and thickness of the supraglacial debris cause an increase of the so-called “differential ablation” (i.e. the ratio between the melt rate of debris-free ice and that occurring at debris-covered ice at the same elevation). Debris distribution (together with its different size and lithology) can lead to peculiar geomorphological features of the glacier surface. Among others, medial moraines, glacier tables, dirt cones, and cryoconites are the most common epiglacial features found on the Miage glacier (Smiraglia and Diolaiuti, 2011).

A marginal ice-contact lake is also present, near the southern extremity of the Miage glacier. The ice-water contact increases calving rates of the glacier cliffs, possibly leading to flood hazards and consequently calving waves. Thus, lake monitoring is very important for visitors’ safety, as it represents a popular tourist destination. For this purpose, we recall the tragedy that was avoided of 1996, when 11 tourists close to the lake got seriously injured because of a calving wave generated by an enormous ice wall which suddenly separated from the glacier and fell into the water below.

3.1 Analysis of the Miage glacier satellite images

The sector of the Western Alps where the Miage glacier is located is illustrated in this satellite medium resolution image (Figure 1), acquired on 18 April 2013 by the Operational Land Imager (OLI) instrument, carried by the Landsat-8 satellite, and visualized in natural colours. The dendritic appearance of the French, Swiss and Italian valleys in the North-Western Alps is well depicted in greenish-brownish colours. The Landsat scene covers an area of 180x180 km^2 , from lake Geneva (top-left) to almost Turin (bottom-right), where the Aosta Valley rising from Turin towards the centre of the image and the opposite valley of the river Arve rising from Geneva arrive from opposite directions to the Mont Blanc massif in the center-left of the image. The Miage glacier can be recognised in this winter image as a very narrow white oblique line NW-SE between the end of the two valleys (zooming electronically the image would facilitate the analysis).

The same Landsat-8 multispectral image but in a different band composition is shown in Figure 2. Here, the false colours come from the RGB 753 visualization, that is to say by displaying the Band 7 (Short Wavelength Mid Infrared [MIR] at 2.100-2.300 μm in Red colour, the Band 5 (Near Infrared [NIR] at 0.845-0.885 μm) in Green colour and the Band 3 (Green Visible at 0.525 – 0.600 μm) in Blue colour. This false colour combination has the advantage of showing ice in tones of light blue (that means no Red nor Green colours, therefore very little reflected radiation by MIR and NIR

spectral bands), thereby giving an immediate idea at first glance about ice and snow (white) coverage in the area and their topography. In this image, the Miage glacier can be recognised as a bright light blue segment in the NW-SE direction between the two valleys mentioned above.

Focusing on the glacier itself, an ALOS multispectral satellite image, acquired during the summer season on 31 August 2009 and visualised with band combination 431, is analysed (Figure 3). The scene includes all the glaciers belonging to the Mont Blanc massif, both on the Italian side and the French one. Figure 3 is a FCC (False Composite Colour) image, namely a combination of two visible (3, 1), and one NIR (Near InfraRed) (4) satellite bands in the RGB colour model (i.e. R=4; G=3; B=1). The resulting colours are:

i. red for vegetation (as visible wavelengths are highly absorbed by plants and NIR (band 4) radiometric values are visualized in the Red channel);

ii. greysh-blueish for rocks (and debris) (the latter making the distinction between debris covering ice and debris without ice below not so easy) , and very dark blue for water (see supraglacial small lakes and the ice contact lake) (because the latter has high absorption for the radiation in these three spectral bands);

iii. light blue for ice (well detectable on the ice falls or seracs);

iv. white for snow (i.e. total reflection, both for visible and NIR wavelengths) (only small avalanches patches on both the flanks of the valley and the upper zones of the ice confluences).

The Miage glacier is immediately recognizable owing to its peculiar shape (see in particular the three lobes of the terminus) and for being the unique glacier to be almost totally covered by debris. It is in fact one of the largest debris-covered glacier in the Alps (Deline, 2005). Moreover, in Figure 4 the absence of a real and large accumulation basin in its upper section can be clearly seen, while its accumulation is mainly based on the avalanches deriving from numerous narrow ice tongues (Mont Blanc, Dome, Bionassay, Col du Miage, Tète Carrée) flowing into the main ice body. Those characteristics make it easy to define the Miage glacier as a Himalayan-type glacier. Clearly visible are the medial moraines, which below form tributary confluences between 2,500 and 2,600 m a.s.l., and then develop into continuous debris cover below 2,400 m a.s.l., which has a varied lithology dominated by schists and granites on the western (dark grey on the image) and eastern sides (light grey) of the tongue, respectively. It is easy to observe that the glacier surface has not significantly retreated with respect to the Little Ice Age maximum, as attested by the lateral moraines, much less than at nearby debris-free glaciers owing to the insulating effect of the debris cover.

At the southern limit of the glacier, just where the ice stream turns sharply toward North-East, the ice contact lake (Miage lake) is also well visible. In the image the lake appears to be composed of two distinct parts.

The one in contact with the glacier is light blue, is almost empty and supplied by glacier melting

water.

The colour depends on its turbidity, which absorbs only a little quantity of sunlight, thus strongly reflecting it back to the satellite sensor. The southern part of the lake appears dark blue instead, due to the absence of the direct ice melting water supply. That is to say, a turbid water is more reflective than clear water at all visible and near infrared wavelengths (Moore, 1980). Moreover, the different colours of the two parts of the lake indicate there is likely to be no connection between the two zones.

In facts, bathymetric surveys showed that the lake consists of two basins separated by a largely submerged moraine (Diolaiuti and others, 2005). The lake is characterised by rapid drawdown episodes that have occurred with varying frequency in its history. The last rapid draining event (September 2004) was probably caused by sudden and temporary failure in the ice floor (Masetti and others, 2009).

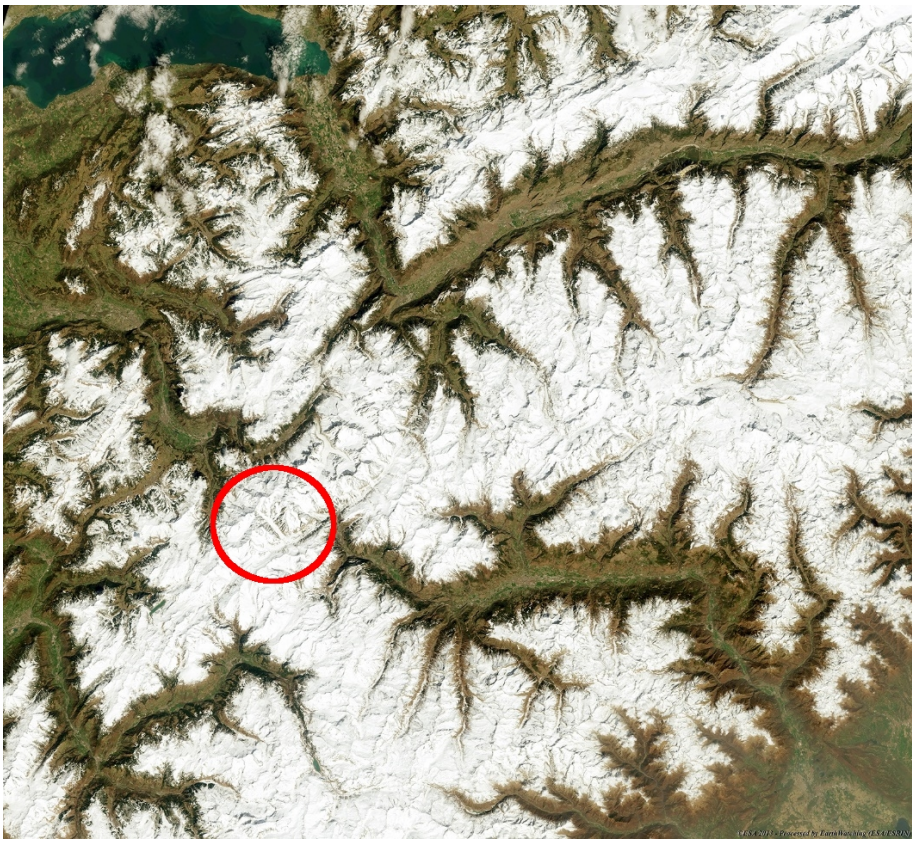

Figure 1: Landsat-8 multispectral image acquired on 18 April 2013 (RGB 432). Source: ESA.

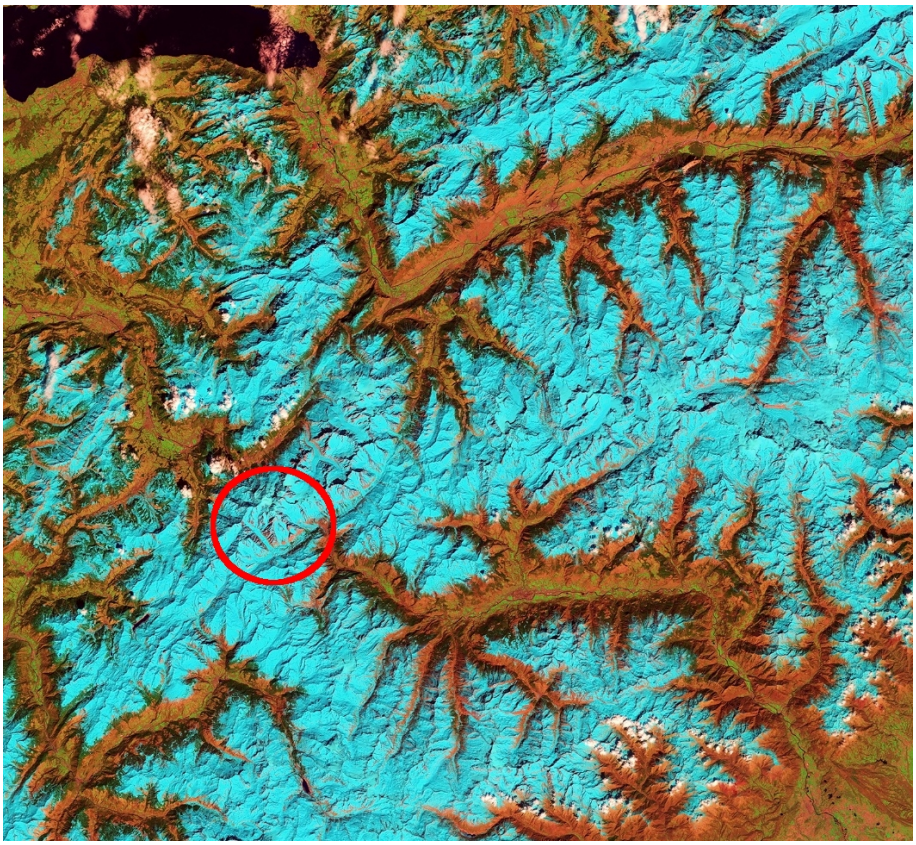

Figure 2: Landsat-8 multispectral image acquired on 18 April 2013 (RGB 753). Source: ESA.

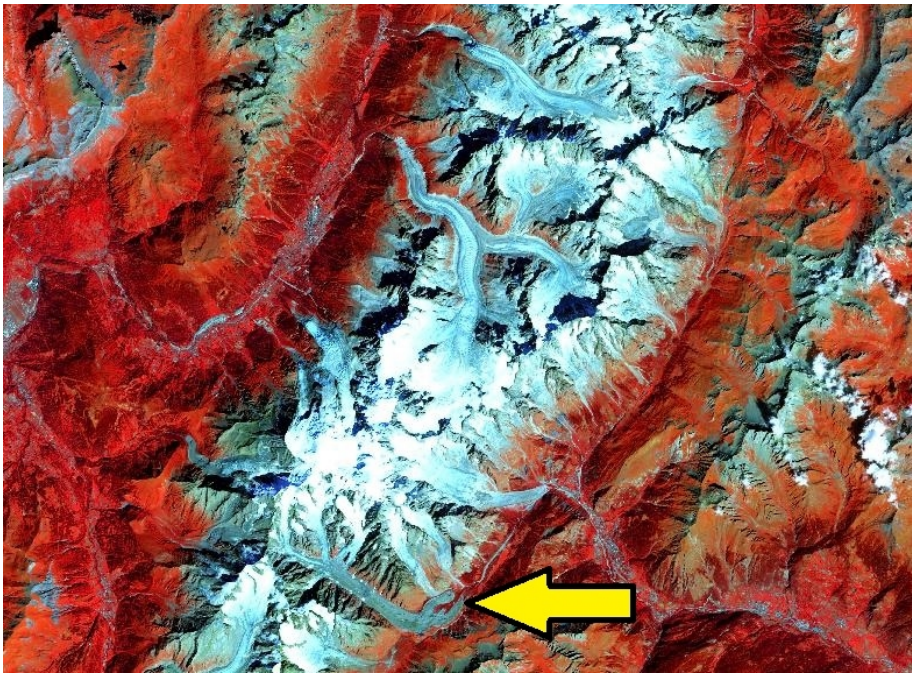

Figure 3: ALOS multispectral image acquired on 31 August 2009 (RGB 431). Source: ESA, JAXA (Japan Aerospace Exploration Agency).

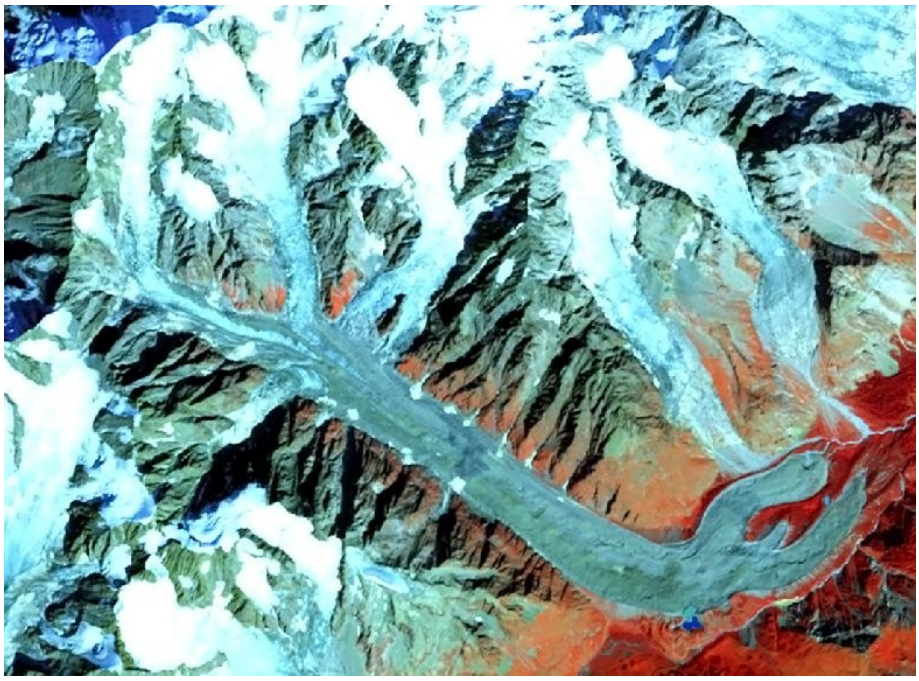

Figure 4: Zoom of Figure 3 on Miage glacier. Source: ESA, JAXA.

4. Freney glacier

The Freney glacier is a steep mountain glacier of the Mont Blanc massif (Graian Alps), in the upper Veny Valley, close to Courmayeur (Aosta Valley, Italy). A mountain glacier, contrary to a valley glacier is a glacier type that has no tongue or only a short one and does not flow down enough to reach the main valley. The Freney flows down the southern side of Mont Blanc de Courmayeur, between the ridge of Peuterey and the ridge of Innominata, along a deep narrow hanging valley. The ridge of Innominata separates it from the twin glacier of Brouillard, that flows parallel to it. Not far from the Freney glacier, the two main debris-covered glaciers of the Italian Mont Blanc massif (Miage southwestward) and Brenva (northeastward) extend their long black tongues. The discharge waters of these glaciers together feed the Dora di Veny River, which flows into the Dora Baltea River and finally into the well-known Po river.

The Freney glacier covers a surface of about 1.4 km^2 and its length is of 2.3 km ca. It extends from 3,700 m to around 2,400 m a.s.l. Above, within a small cirque, there is a glacieret (a very small glacier or ice masse of indefinite shape in hollows which has little or not movement for at least two consecutive years) which discharges ice into the Freney glacier below feeding it and until the 1970s was still connected with the main trunk. Even during the peak of the Little Ice Age the Freney glacier did not reach the main bottom valley of Val Veny and its snout remained hanging on a steep rock belt. At present the snout is very thin and flows down up to a few score meters from the rock step where a small frontal moraine has been deposited. The entire surface of the glacier is broken and dissected by a grid of crevasses and seracs. The Freney could represent a significant sample of

small size glacier (around 1 km^2); concerning this type of glaciers, one debated argument is about their fate in the forthcoming decades in the context of climate change. Italian glaciers underwent a generalized retreat in the 20^{th} century (Citterio et al., 2007) and in particular the Aosta Valley glaciers lost 44.3 km^2 during 1975-2005, i.e. ca. 27% of the initial area (Diolaiuti and others, 2012a). Small glaciers contributed considerably to total area loss; in fact the smaller the glacier the faster the reduction in size, so their extintion is more than a mere conjecture. On the other hand, glaciers flowing down along a narrow valley in steep mountain topography, such as the Freney, are subject to a slightly stronger shading. So, these shrinking glaciers are becoming less sensitive to climatic change and might thus be able to stabilize their extent. In any case, the southward aspect and the climatic forcing on one hand, and the protecting shading effect of vertical peaks on the other hand, could play opposite roles in the Freney glacier fate, and therefore it is hard to make any prediction.

4.1 Analysis of the Freney glacier satellite images

The Freney glacier is located very close to the Miage glacier, so that in the Landsat-8 images used to illustrate this alpine region (Figures 1 and 2), it can be identified almost parallel to it, just on the right hand side of the latter, after the Brouillard glacier, nearly touching the north-western end of the Aosta Valley, not too far from Courmayeur.

The image used here to describe the Freney glacier is the same one utilized for the Miage glacier, namely an ALOS (Advanced Land Observing Satellite) scene acquired on 31 August 2009 (Figure 5, left part). In Figure 5, glaciers are represented in light blue colour and snow in white, while rocks (and debris) are grey and vegetation is red. This colour contrast is due to the RGB combination of bands 431 of the AVNIR-2 (Advanced Visible and Near Infrared Radiometer type 2) sensor, and this allows an easy identification of glacier bodies.

It is not difficult to identify the snow line that divides the accumulation basin (the white narrow upper cirque) from the ablation basin (the light blue tongue): note the grey debris cover on the lowest part of the ablation basin, which has increased in the last decade, due to more effective cryogenic processes on the granite bare rock walls of Mont Blanc. The debris cover is quite complete and diffused on the lower zone of the ablation basin, while in the medium zone of the glacier it is reduced to two lateral active moraines, supplied by the debris production of the lateral rock walls.

In spite of the quite similar colour of debris still covering ice, of deposited debris and rocks, it is not particularly difficult to detect the exact glacier terminus position; the different grey tone of supraglacial debris (darker because of the higher humidity) and the evident ice step of the snout makes the glacier lower limit easily identifiable. The convex features of the terminus are also evident due to differential ablation (i.e. the ratio between the melt rate of bare or debris free ice and the melt rate occurring at debris-covered ice at the same elevation). The ablation gradient is opposite to that due to altitude, and the ice melt rate is smaller at lower altitude than that of the bare

ice at higher altitude; therefore supraglacial convex morphologies began to develop and are well detectable on satellite images.

Although Landsat satellites are more utilized for glacier studies, ALOS has a higher spatial resolution (10 m against 30 m of the NASA satellites), and therefore is more suitable to study such a small glacier as the Freney one. Otherwise spatial resolution would not make it possible to recognize glacier outlines properly.

As said above, the fate of the Freney glacier is uncertain, therefore the study of remotely sensed high resolution images taken at periodic intervals is necessary to monitor its state (also taking into account the difficulty or even the impossibility of collecting reliable field data).

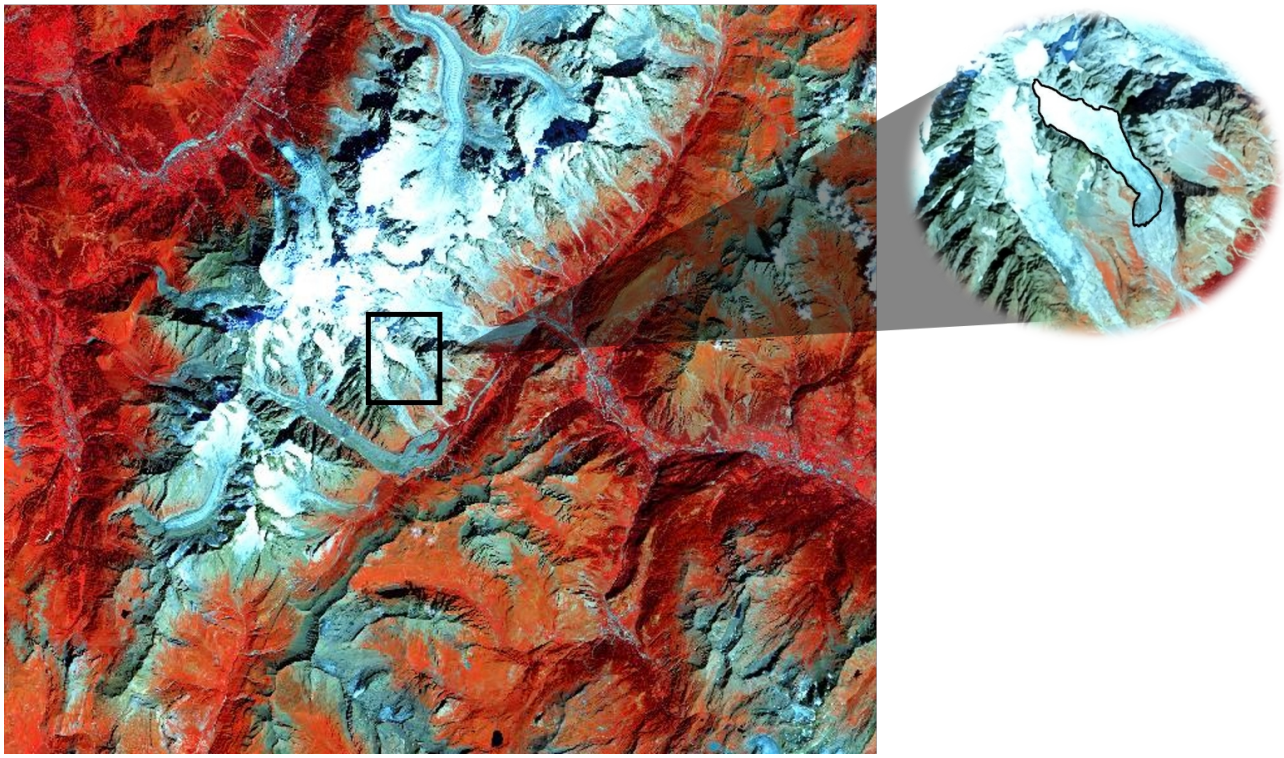

Figure 5: ALOS scene of 31 August 2009 showing the study area of the Freney glacier (left) and a zoom with black glacier outlines. Band combination is 431. Source: ESA, JAXA.

5. Kilimanjaro glaciers

Kilimanjaro is the Africa's highest peak (5,895 m) (the "white roof of Africa"). It is a huge dormant stratovolcano located close to the Kenya-Tanzania border, 370 km ca south of the Equator and about the same distance from the Indian Ocean (Kaser and others, 2004). It consists of three volcanic centers, active in sequence from the Pleistocene: Shira, Mawenzi and Kibo, the latter being the highest. The summit of Kibo forms quite a flat caldera, where along the southern scarp the Uhuru Peak, the highest point of the volcano, is found and which emerges from the flat plain with its snow capped iconic bulk. Snow and glaciers of Kilimanjaro were discovered in 1848 by the German

explorer Johannes Rebmann, but English geographers were incredulous about its snowcap until 1889, when Hans Meyer climbed the summit and made the first observations of glaciers.

At present, glaciers only exist on Kibo, with an extent of 1.76 km^2 in 2011, roughly half of that remaining on the continent (Hardy, 2011). The majority of the glacier bodies are bunched within two main ice fields, namely the Northern Ice Field (NIF, the largest ice body), and the Southern Ice Field (SIF). Even if from a glaciological point of view this classification (Ice Field) is now rather incorrect, it is still diffused and traditionally accepted. Kilimanjaro's glaciers may be distinguished in plateau or horizontal (>5,700 m) glaciers and slope (<5,700 m) glaciers. The first group on the Kibo summit has flat surfaces unbroken by crevasses; their margins are vertical or near-vertical and are fluted. The slope glaciers extend down from the crater of Kibo in only a few cases (among which Kersten glacier represents the largest remaining one, Mölg and others, 2009). They are all inclined at 30-40° and are all remnants of the former Southern Ice Field; their surface is today quite dirty, due to the wind-blow dust.

The area extent of the glaciers just prior to Meyer's observations has been estimated to be about 20 km^2 (Osmaston, 1989). So they have shrunk by more than 90 percent in little more than a century and become a global-warming poster child. The break up of ice bodies had just begun very likely at the end of the 19th century and the drastic shrinkage continued throughout the 20th century and the beginning of the 21st century. During the last Pleistocene glaciation the extent of moraines on Kibo and Mawenzi suggests that a large ice cap blanketed the mountain, covering an area of at least 150 km^2 (Osmaston, 1989).

In spite of air temperatures always below freezing, areal reduction of plateau glaciers is caused mainly by melt on vertical walls that characterize their north and south margins, induced by solar radiation (Mölg and others, 2003; Cullen and others, 2006). The beginning of the retreat of the glaciers at the end of the 19 th century can be attributed to an increase in net shortwave radiation, accompanied by a decrease in cloudiness and snowfall (Hastenrath, 2006). It appears likely that by mid-century the plateau glaciers will disappear from the mountain summit (Kaser and others, 2004; Cullen and others, 2012).

5.1 Analysis of Kilimanjaro glacier satellite images

A recent Landsat-8 satellite image dated 27 August 2013 is here used to describe the Kilimanjaro glaciers. Bands 742 are combined in the RGB model to emphasize ice and snow in the scene. In this way glaciers are indeed brought out by a bright light blue colour, in contrast with the other elements of the image (lava flows of different ages, vegetation, dry zone). In fact, Kilimanjaro's glaciers are immediately recognizable in the middle-right part of Figure 6, right in and around the volcano's crater, easily visible in the complete extent of the Landsat scene, even if it is not possible to distinguish the features of both the types of glaciers and to diversify snow from ice. The acquisition time is 11 am and afternoon clouds are coming to encircle the north-western and the southwestern slopes of the massif. This atmospheric phenomenon is more pronounced during the dry seasons and

it protects ice from direct solar radiation. Thus, ablation is more apparent on the eastern margins of the cliffs than on the western ones (Kaser and others, 2004).

Figure 7 is a zoom in the crater zone, where glaciers are situated. North-West of the crater there is the NIF, while SIF is South-East. The recent longitudinal fracture of the NIF is easily detectable, splitting the ice cap in two totally separate portions. Various slope glaciers are also present down to the slopes, especially southward, ice bodies derived from the fragmentation of the SIF. NIF and SIF tall ice cliffs, and slope glaciers are very sensitive to melt/no-melt cycles. In fact, during the boreal (austral) summer north-facing (south-facing) cliffs are irradiated by direct sunlight during daytime, which provides enough energy to initiate melting at the cliff faces although the air temperature is below freezing. In contrast, during the boreal (austral) winter north-facing (south-facing) cliffs are irradiated by direct sunlight only at very low angles, thus reducing ablation significantly (Kaser and others, 2004).

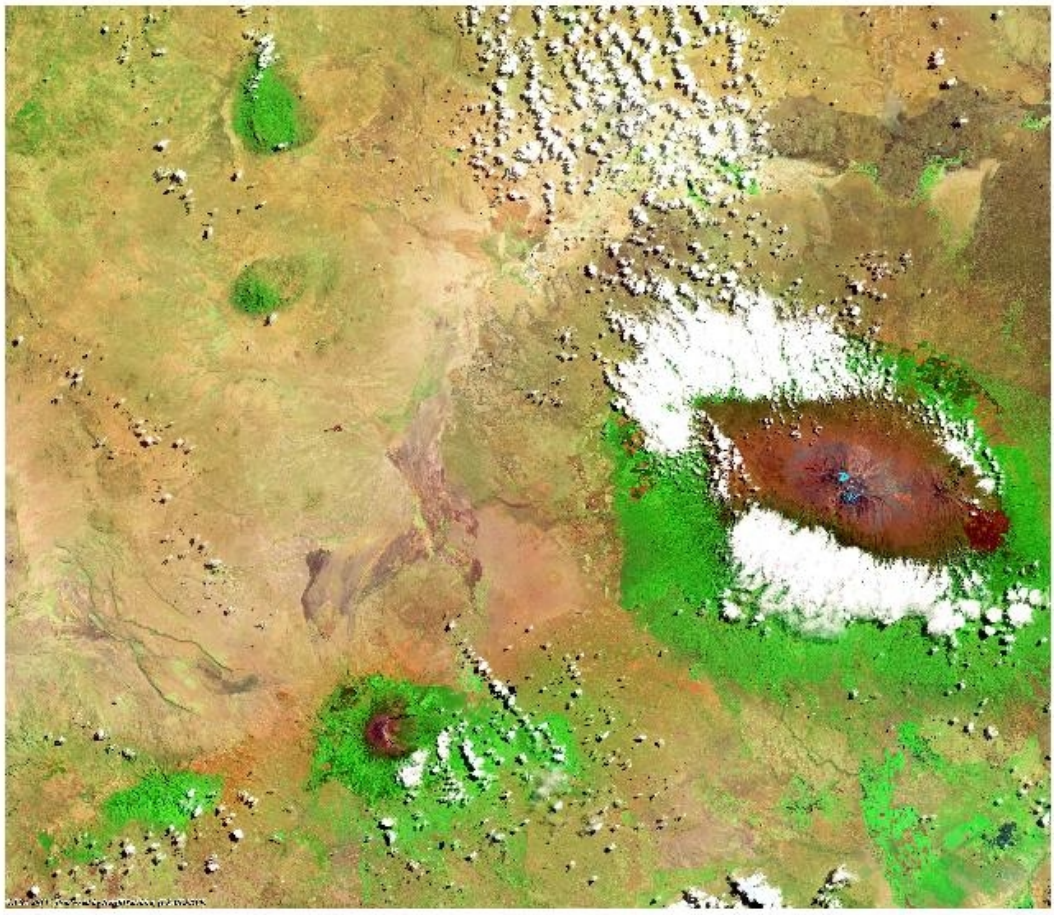

Figure 6: Area of Kilimanjaro, Operational Land Imager, Landsat-8, 27 August 2013, RGB 742. Source: ESA.

Figure 7: Kibo's crater and glaciers therein, Kilimanjaro. Source: ESA.

6. Harding Icefield

The Harding Icefield is the largest of the icefields in the Kenay Mountains (Kenay Peninsula, Alaska) and the largest icefield entirely contained within the boundaries of the United States.

An icefield is defined as a mass of glacier ice, usually smaller than an ice cap and lacking a dome-like shape (http://nsidc.org/cgi-bin/words/glossary.pl).

The Harding Icefield is about 80 km long (northeast-southwest) and 50 km across. Including the outlet glaciers, it covers an area of about 1,800 km^2 . Slightly more than half of the icefield lies within the present boundary of the Kenai Fjords National Park; the remainder lies within the Kenai National Wildlife Refuge. At least 38 glaciers of different sizes and types flow from the Harding Icefield, terrestrial and tidewater (i.g. glaciers that terminate in the sea, http://www.swisseduc.ch/glaciers/glossary/index-en.html); the most important being the Bear glacier, Exit glacier, Skilak glacier, Tustumena glacier and the Chernof glacier (Aðalgeirsdóttir et al., 1998).

Amongst them, lake- and land-terminating glaciers are present in the west side, where the two huge lakes of Skilak and Tustunena drain some glaciers, while tidewater glaciers lie in the east. Some of

the latter flow at high speed continuously (as much as 35 meters per day). Moreover, they may advance and retreat periodically, independently of climatic variation (as the surging glaciers, Jiskoot, 2011). Nowadays, recent studies have found that most of the glaciers in the Harding Icefield have receded (since 1973), some dramatically (Hall and others, 2005).

6.1 Analysis of Harding Icefield satellite images

The visible colour Landsat image is shown below where northeastward the smaller Sargent Icefield and southwestward the Harding Icefield are visible. Along the coast the plumes from the light grey glacial sediment are detectable as well. As the surface of the Harding Icefield is so large (1,800 km^2), Landsat resolution (30 m), is suitable for the purpose of glaciological studies in this area, even if it is impossible to describe the local morphological features such as the medial moraines. In the lower-left part of Figure 8, the Harding Icefield is well recognizable, with its tidewater glaciers on the eastern side touching the Gulf of Alaska waters. Here, the Pacific Ocean provides copious precipitation in the form of snow. On the opposite side, at the same (or higher) altitude, snow is still present but less. This is visible looking at the snow patches getting smaller as we move downward (or westward), towards the major lakes. In general, the Harding Icefield receives at least 10 meters of snow each year (http://www.kenai.fjords.national-park.com).

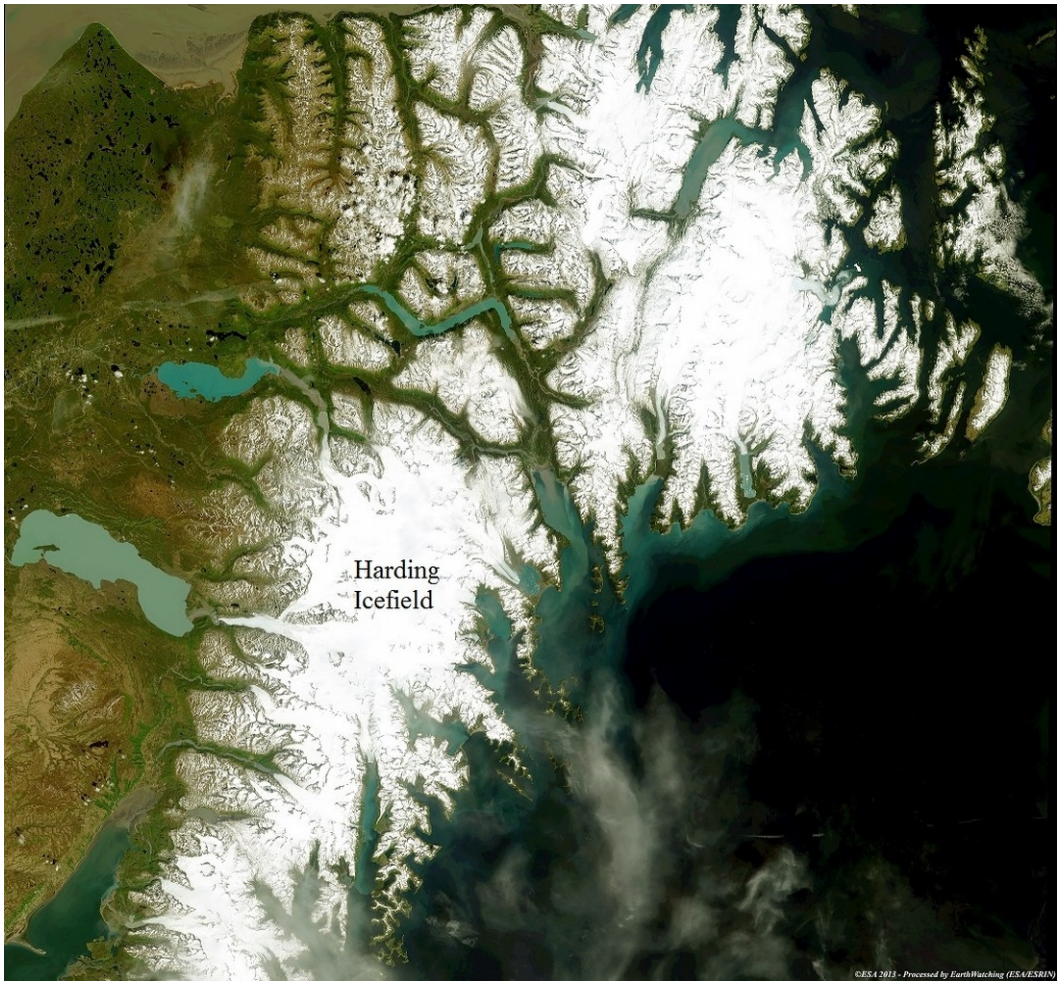

Figure 8: Landsat-8 scene of 11 June 2013 showing the Harding Icefield in the lower-left part. Source: ESA.

7. Aletsch glacier

The Aletsch glacier with a length of 23 km, surface area of about 80 km^2 and a maximum thickness of about 900 m, is by far the longest, the largest and the deepest glacier in the Alps and the most important of the Berner Alps (Valais) in Switzerland. The volume of the Aletsch was roughly 15 km^3 in 1999, representing about 20% of the entire ice volume in Switzerland (Farinotti and others, 2009). It is a typical example of compound basin valley glacier, that is to say two or more individual valley glaciers (four in the case of the Aletsch) issuing from tributary valleys and coalescing (WGMS, 2012). They all converge in the Konkordia Platz, where the ice reaches its maximum thickness of 900 m and starts the huge curved tongue (Jouvet and others, 2011). The tributary glaciers (Grosser Aletschfirn, the bigger one, the Jungfraufirn, the Ewigschneefeld and the smaller one, the Grüneggfirn) flow down into the main tongue through steep ice fall (seracs), crossed by numerous crevasses. Along the sides of the hanging valleys joining the Aletsch tongue, there is also a great amount of surface debris forming lateral moraines, a result of accumulations of

debris falling from the sides due to freeze-thaw activity and glacier flow. Where the lateral moraines of these tributary glaciers join the lateral moraine of the Aletsch, medial moraines are formed, which give the glacier the appearance of being divided into neat lanes or black paths. Over the course of the twentieth century, such as most of the Alpine glaciers, the Aletsch, the largest Alpine glacier, receded by more than two km. During the Little Ice Age (between 1600 and 1860) the glacier reached its maximum area (145 km^2) and the tributary valley glaciers of Mittelaletsch and Oberaletsch still joined the main tongue. In 1957 its surface area reached 130 km^2 . Then the link with the Mittelaletsch was interrupted. According to the median climatic evolution, the actual Aletsch glacier is expected to lose 90% of its ice volume by the end of 2100 (Jouvet and others, 2011).

7.1 Analysis of the Aletsch glacier satellite images

The multitemporal image acquired in early Spring by Landsat-8 on 18 April 2013 (Figure 9) illustrates the southwestern part of the Central Alps, covered by snow, as a diagonal, dividing the Swiss territory on the left hand side from the Italian northwestern part of the Piedmont and Lombardy regions. The Aosta Valley penetrates the white alpine mountains from East to West just below the center of the image, whilst the Rhone Valley starts almost in the upper left corner, comes down towards the southwest and in the town of Martigny turns up to then enter lake Geneva in the area of Montreux. Mount Cervino (the Matterhorn) and Monte Rosa are located in the mid-right part of the image, and the Mount Blanc massif at one third along the south-west diagonal.

The same image, but in a false colour visualization RGB 542 (Figure 10), enhances the white alpine snow-ice coverage, the black water of the lakes and the reddish vegetated valleys.

The multispectral image acquired by ALOS on 31 July 2010 (RGB 321) (Figure 11) shows the entire Berner Alps (Swiss Alps) from the Brienzersee to the Rhone Valley, in particular the Jungfrau-Aletsch massif (a UNESCO World Heritage Site) in the center-left. Enclosed by the high summits of Aletschorn, Junfrau, Mönch and Fiescherhorn (amongst others), flows the huge Aletsch glacier with its “sword-like” shape, arriving at just some 20 km from the town of Brigue. Northeastward the other giant glaciers of the Berner Alps are well detectable with their valley tongues: Fiescher, Oberar and Unteraar (the last two with their long artificial lakes). The complex structure of accumulation basin of the Aletsch is clearly observable. Actually it is formed by four accumulation basins: clockwise the Grosser Aletschfirn represents the bigger one, then the Jungfraufirn, the Ewigschneefeld, and the smaller one, the Grüneggfirn, follow. Together they converge in the Konkordia Platz forming a semicircle, then flowing along the big curve of the ablation tongue (changing the main direction from southwestward to southeastward). They reach the glacier snout separated the one from the other by medial moraines, well visible in the ALOS image; these moraines run along the ablation tongue like railways tracks, slightly enlarging toward the terminus, quite parallel to the lateral moraines. A visible grey line (trim-line) (Figure 12a) follows the border of the ablation tongue, indicating the limit between well-vegetated terrain that has remained ice-free for a long time and scarcely vegetated terrain that until recently (at least from

the Little Ice Age) laid under glacier ice.

This image was taken in the summer period (31 st of July, 2010), to limit the covering effect of the snow as much as possible. Using band combination 431 (Figure 12b) as RGB (that is to say by combining the NIR channel with two visible bands), a major colour contrast between snow (in bright white), and ice (in light blue), makes it possible to distinguish between these two features much more easily than simply looking in natural colour. Detecting the approximate position where ice makes room for snow is only possible using the FCC image (on the right of Figure 12b), while there is no way to do the same for the natural colour image (Figure 12a, on the left), because there is no change in colours. The reason why this occurs is because light is all reflected back by the albedo effect of snow and there is no radiation (colour), absorption in both images (i.e. pixel colour is white). On the other hand, ice is very weakly absorptive in the visible but has strong absorption bands in the near infrared. Thus the resulting FCC image has a greater colour contrast between snow and ice, making it possible to detect their boundary quite well. This is not only true for snow and ice, but also for the enhanced capacity to recognize glacier boundaries in the accumulation zone, or (for instance), for distinguishing mountain ridges.

Figure 9: The western part of the Central Alps imaged by Landsat-8 on 18 April 2013 (RGB 432). Source: ESA.

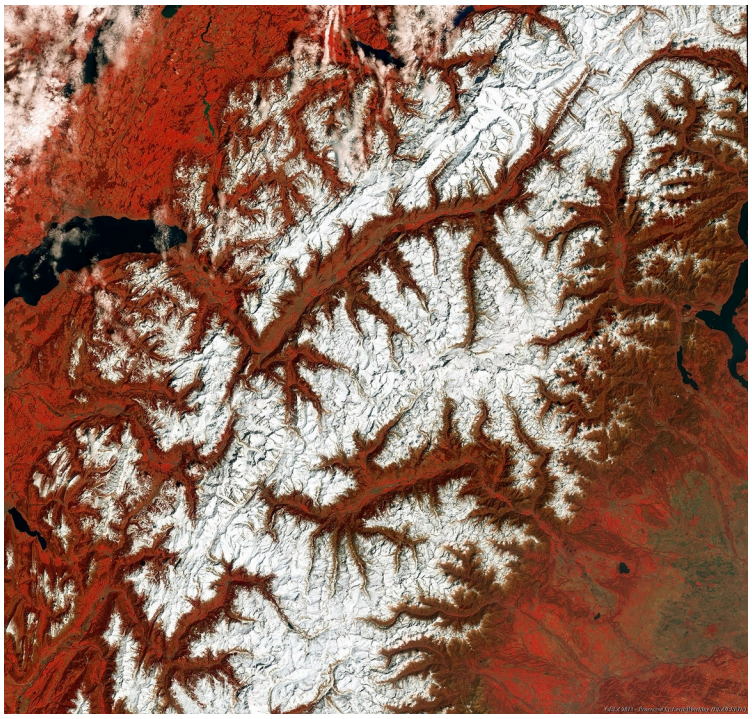

Figure 10: The same image as in Figure 9, but in a false colour visualization RGB (542). Source: ESA.

Figure 11: ALOS image acquired on 31 July 2010 (RGB 321). Source: ESA, JAXA.

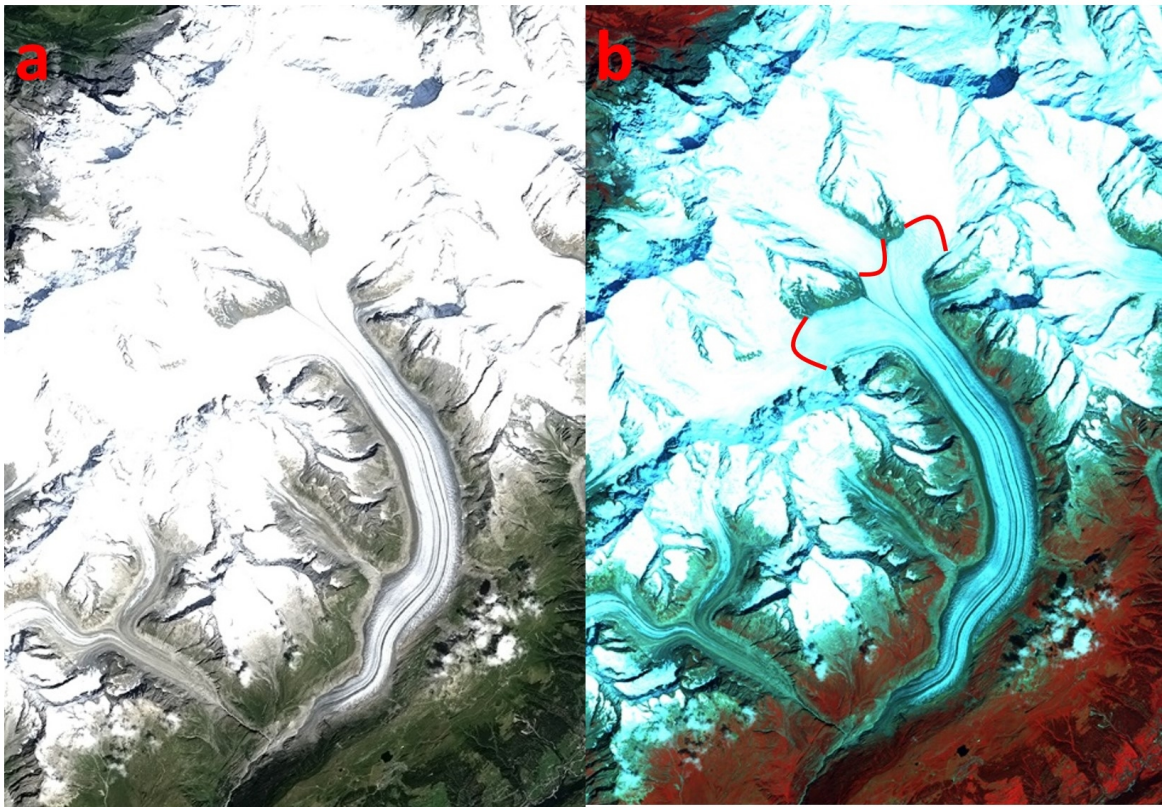

Figure 12: Aletsch glacier shown in two enlargements of the Figure 11, visualised in natural colours RGB 321 (a), and in false colours RGB 431 (b), respectively. Red lines in "b" are examples of snow-ice boundary detection. Source: ESA, JAXA.

8. Drygalski ice tongue

The Drygalski ice tongue is the floating seaward extension of David glacier, the largest outlet glacier in the Victoria Land part of the East Antarctic ice sheet, draining from the Talos and Circe Domes of the East Antarctic ice sheet (Frezzotti and Mabin, 1994).

An outlet glacier is a tongue of ice that extends radially from an ice dome; within the dome it can be identified as a rapidly moving ribbon of ice (an "ice stream"), while beyond the dome it occupies a shallow depression (Arora, 2011).

The David glacier – Drygalski ice tongue area covers a surface of about 224,000 km^2 (Frezzotti and Mabin, 1994). The grounding line (GL: the transition between the inner grounded ice and its outer floating counterpart, i.e. where the Drygalski ice tongue begins), is about 50 km inland from the coast.

The Drygalski ice tongue floats on the west side of the Ross Sea and forms the southern coastline of Terra Nova Bay. The Drygalski tongue is fed by a faster flow (580 m per year) coming from the Circe Dome and a second slower moving flow (300 m per year) coming from the Talos Dome.

These different and contrasting flow rates could probably be considered responsible for the characteristic rifts that open along the northern margin of the ice tongue (Frezzotti and Mabin, 1994).

As we move seaward starting from the David Glacier's grounding line (GL) the thickness decreases (from 1,500 to 150 m) (Tabacco and others, 2000).

The ice tongue plays a crucial role in the persistent development of the Terra Nova Bay polynya (area of open water surrounded by sea ice, Stringer and Groves, 1991). In fact, its formation and persistence is thought to be caused by the combined effect of the strong persistent offshore katabatic winds that prevent sea ice from forming in the bay, and the blocking effect of the Drygalski ice tongue, which stops sea ice from entering the Terra Nova Bay from the South (please, note the area of free ice water below the ice tongue in Figures 13 and 14) (Frezzotti and Mabin, 1994).

Outlet glaciers such as the David glacier, and in particular the Drygalski ice tongue, which is the part subjected to fast sea-contact dynamics, play a major role in the determination of the Antarctic ice sheet mass balance. The mass balance ablation components consist in calving and basal melting. A major calving event (calving is the process whereby masses of ice break off to form icebergs) occurred in December 1957, when the Drygalski ice tongue lost the outer 40 of its 110 km (estimated length from aerial photographs, Frezzotti and Mabin, 1994). Between 1997 and 2000 the Drygalski ice tongue advanced 2,200 m, increasing its area by almost 45 km^2 (Wuite and others, 2009). The basal melting rates (that is the melting at the base of the ice floating tongue) are higher close to the GL owing to thermoaline circulation by High Salinity Shelf Water. The basal melting rate is determined by the difference between net snow accumulation and ice discharge across the GL into the ocean (Frezzotti and others, 2000). About 90% of the snow that falls inland is drained by outlet glaciers and ice streams (Morgan and others, 1982). In 2005 and 2006 two huge icebergs coming from a calving of the Ross Ice Shelf collided with the ice tongue breaking off some large pieces.

8.1 Analysis of the Drygalski ice tongue satellite images

Figure 14 represents the Drygalski ice tongue as recorded by band 7 of the Landsat-8 satellite. That is to say that, it is the view of the same area as in Figure 13 (RGB 543), but filtered only through the Short Infra-Red wavelengths (from 2.11 to 2.29 μm). The result is an image where it is easier to distinguish the Drygalski ice tongue limits. Along the coast the sea ice is grey and darker with respect to the white floating ice tongues (the main Drygalski and the other minor ice tongues). The dark part of the medium Drygalski tongue and the many small other areas (that appear in light blue in Figure 13) are surfaces of the so called "blue ice", where the wind ablation is particularly active and the snow has been blown away. In the lower sector of both the images the polynya is well visible and its free ice open sea contrasts with large areas of sea ice, strongly fragmented, accumulated along the northern-side of the ice tongue. This sea ice can be also multi-year ice that often remains attached to the Drygalski ice tongue for many years and is carried out into the Terra

Nova Bay, giving the ice tongue the appearance of being several km wider than it really is.

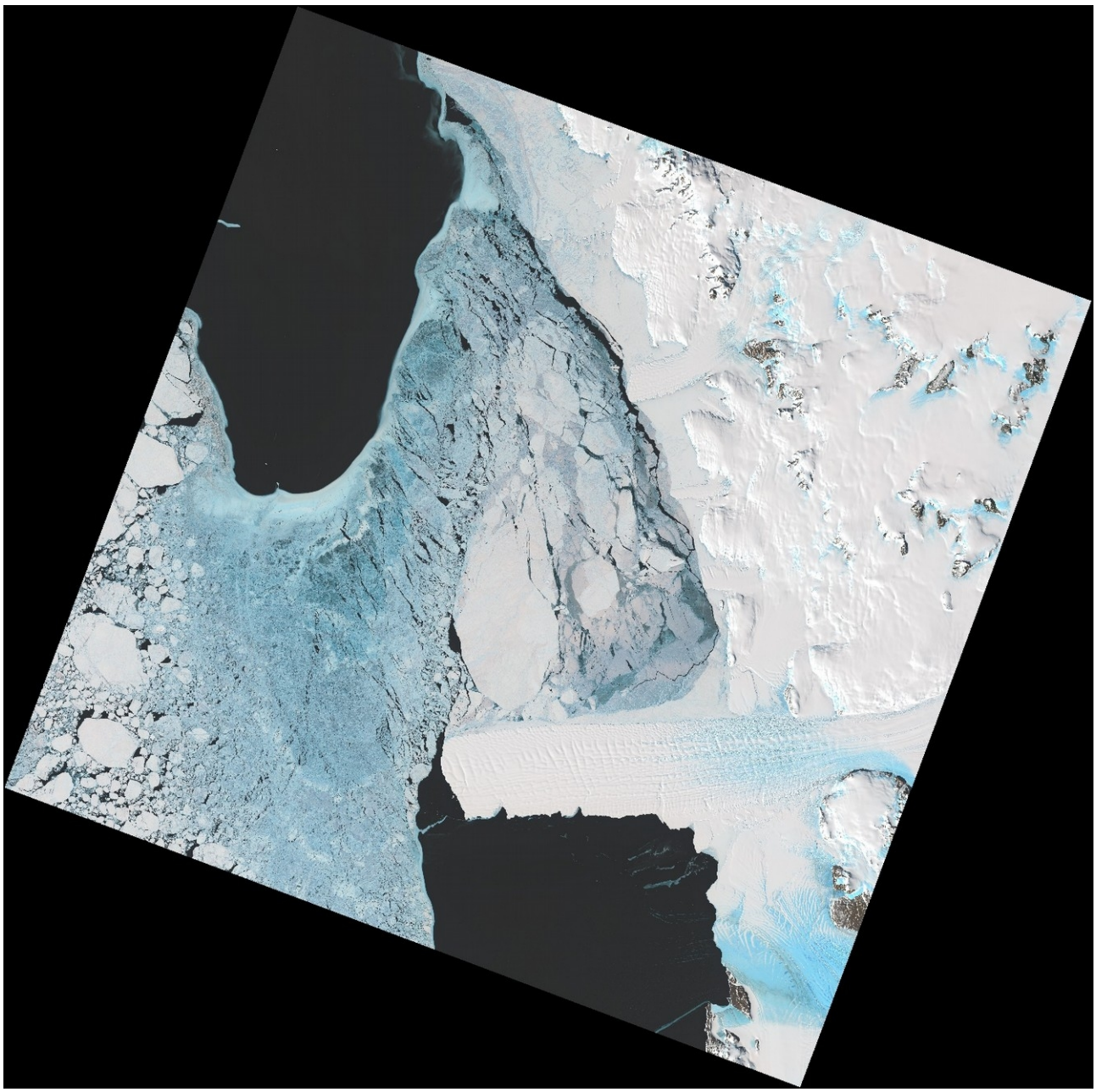

Figure 13: Landsat-8 scene of 26 November 2013 showing the Drygalski ice tongue (lower-right part). Multispectral band combination is 543. Source: http://earthexplorer.usgs.gov/.

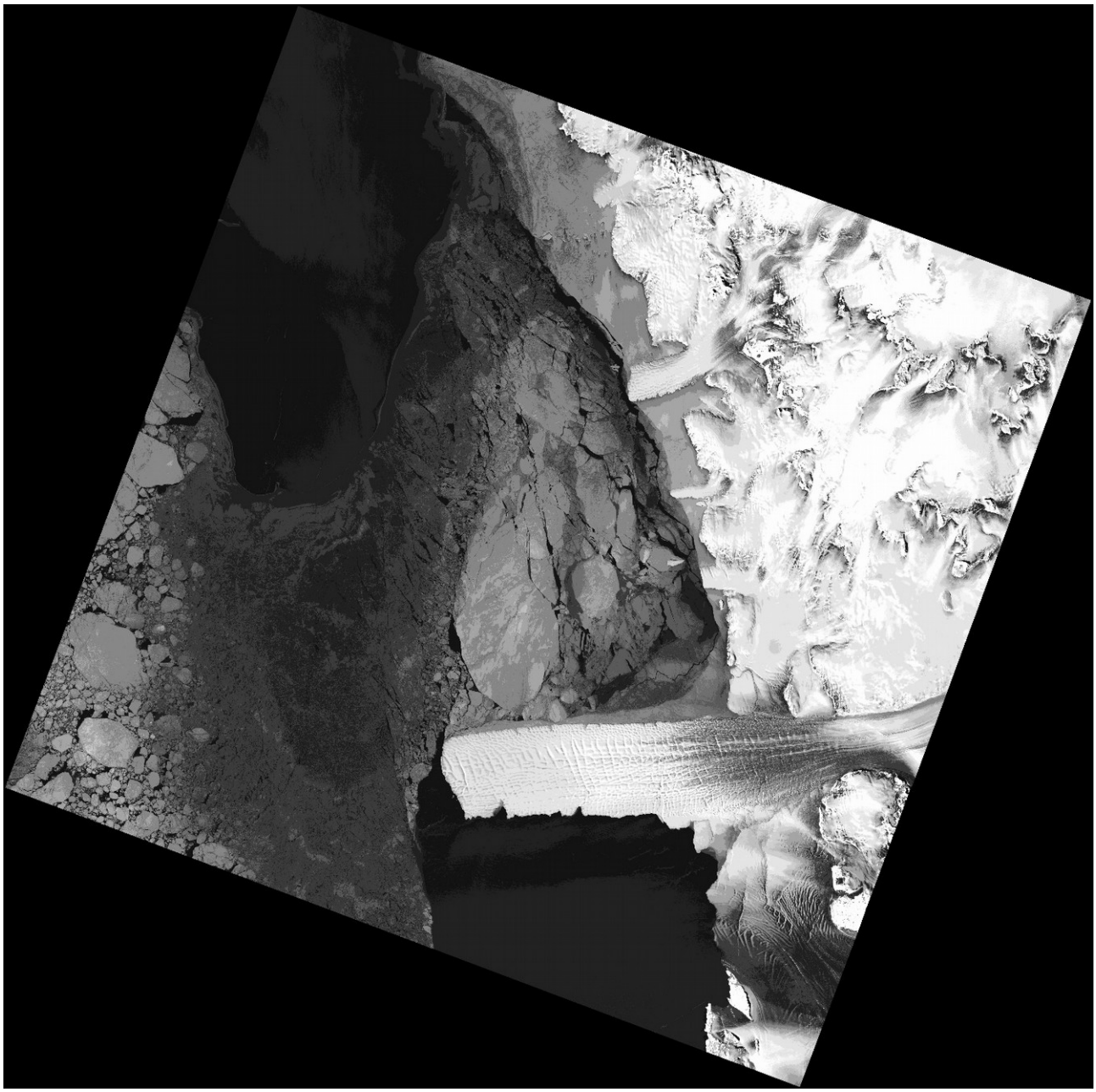

Figure 14: Single band (band 7 of Landsat-8) representation of the Drygalski ice tongue (lower-right part). Source: http://earthexplorer.usgs.gov/.

References

Aðalgeirsdóttir G., Echelmeyer K.A. and Harrison W.D. (1998) Elevation and volume changes on the Harding Icefield, Alaska, Journal of Glaciology, 44, 148, pp. 570-582.

Adhikary S., Nakawo M., Seko K. and Shakya B. (2000) Dust influence on the melting process of glacier ice: Experimental results from Lirung Glacier, Nepal Himalayas, IAHS Publ., 264, pp. 43-52.

Albright T.P., Painter T.H., Roberts D.A., Shi J.C., Dozier J. and Fielding E. (1998) Classification of surface types using SIR-C/X-SAR, Mount Everest Area, Tibet, Journal of Geophysical Research - B: Solid Earth and Planets, pp. 25823-25837.

Arora M., "Outlet glacier", in Singh V.P., Singh P. and Haritashya (Eds.) (2011) Encyclopedia of Snow, Ice and Glaciers, Dordrecht, p. 799.

Bayr J.J., Hall D.K. and Kovalick W.M. (1994) Observations on glaciers in the eastern Austrian Alps using satellite data, International Journal of Remote Sensing, 15, 9, pp. 1733-1742.

Berthier E., Arnaud Y., Baratoux D., Vincent C. and Rémy F. (2004) Recent rapid thinning of the 'Mer de Glace' glacier derived from satellite optical images, Geophysical Research Letters, 31, pp. 1-4.

Berthier E., Arnaud Y., Rajesh K., Sarfaraz A., Wagnon P. and Chevallier P. (2007) Remote sensing estimates of glacier mass balances in the Himachal Pradesh (Western Himalaya, India), Remote Sensing of Environment, 108, 3, pp. 327-338.

Bolch T. and Kamp U. (2006) Glacier Mapping in High Mountains Using DEMs, Landsat and ASTER Data, 8 th International Symposium on High Moutain Remote Sensing Cartography, Grazer Schriften der Geographie und Raumforschung, 41, pp. 37-48.

Bolch T., Menounos B. and Wheate R., (2010) Landsat-based Inventory of Glaciers in Western Canada, 1985-2005, Remote Sensing of Environment, 114, pp. 127- 137.

Bolch T. and others. (2012) The State and Fate of Himalayan Glaciers, Science, 336, 6079, pp. 310-314.

Brock B.W., Mihalcea C., Kirkbride M., Diolaiuti G., Cutler M.E.J. and Smiraglia C. (2010) Meteorology and surface energy fluxes in the 2005-2007 ablation seasons at Miage debris-covered glacier, Mont Blanc Massif, Italian Alps, Journal of Geophysical Research, 115, doi:10.1029/2009JD013224.

Citterio M., Diolaiuti G., Smiraglia C., D'Agata C., Carnielli T., Stella G. and Siletto G.B. (2007) The recent fluctuations of Italian glaciers, Geografiska Annaler, 89, A3, pp. 164-182.

Cullen N.J., Mölg T., Kaser G., Hussein K., Steffen K. and Hardy D.R. (2006) Kilimanjaro Glaciers: Recent areal extent from satellite data and new interpretation of observed 20th century retreat rates, Geophysical Research Letter, 33, doi:10.1029/2006GL027084.

Cullen N.J., Sirguey P., Mölg T., Kaser G., Winkler M. and Fitzsimons S.J. (2012) A century of ice retreat on Kilimanjaro: The mapping reloaded, The Cryosphere Discussion, 6, pp. 4233-4265.

De Vecchis G. and Pesaresi C. (2011) Dal banco al satellite. Fare geografia con le nuove tecnologie, Rome, Carocci.

Deline P. (2005) Change in surface debris cover on Mont Blanc massif glaciers after the 'Little Ice

Age' termination, The Holocene, pp. 302-309.

Della Ventura A., Rabagliati R., Rampini A. and Serandrei Barbero R. (1982) An application of ISIID: Remote Sensing Observation of Glaciers, Second Conference on Images Analysis and Processing, pp. 320-324.

Della Ventura A., Rabagliati R., Rampini A. and Serandrei Barbero R. (1983) Remote-sensing observation of glaciers towards their monitoring, Seventeeth International Symposium on Remote Sensing of Environment, pp. 723-733.

Della Ventura A., Rabagliati R., Rampini A. and Serandrei Barbero R. (1985) Controllo delle fluttuazioni dei ghiacciai alpini mediante telerilevamento da satellite, Geografia Fisica e Dinamica del Quaternario, 8, pp. 150-155.

Diolaiuti G., Kirkbride M.P., Smiraglia C., Benn D.I., D'Agata C. and Nicholson L. (2005) Calving processes and lake evolution at Miage glacier, Mont Blanc, Italian Alps, Annals of Glaciology, 40, pp. 207-214.

Diolaiuti G., Bocchiola D., Vagliasindi M., D'Agata C. and Smiraglia C. (2012a) The 1975-2005 glacier changes in Aosta Valley (Italy) and the relations with climate evolution, Progress in Physical Geography, 6, pp. 764-785.

Diolaiuti G., Bocchiola D., D'Agata C. and Smiraglia C. (2012b) Evidence of climate change impact upon glaciers' recession within the Italian Alps: the case of Lombardy glaciers, Theoretical and Applied Climatology, 109, pp. 429-445.

Dozier J. (1984) Snow reflectance from Landsat-4 Thematic Mapper", IEEE Transactions on Geoscience and Remote Sensing, pp. 323-328.

Farinotti D., Huss M., Bauder A. and Funk M. (2009) An estimate of the glacier ice volume in the Swiss Alps, Global and Planetary Change, 68, pp. 225-231.

Fea M., Giacomelli L., Pesaresi C. and Scandone R. (2013) Remote sensing and interdisciplinary approach for studying volcano environment and activity, Journal of Research and Didactics in Geography (J-READING), 1, 2, pp. 151-182.

Frey H., Huggel C., Paul F. and Haeberli W. (2010) Automated detection of glacier lakes based on remote sensing in view of assessing associated hazard potentials, Grazer Schriften der Geographie und Raumforschung, 45, pp. 261-272.

Frezzotti M. and Mabin M.C.G. (1994) 20th century behaviour of Drygalski Ice Tongue, Ross Sea, Antarctica, Annals of Glaciology, 20, pp. 397-400.

Frezzotti M., Tabacco I.E. and Zirizzotti A. (2000) Ice Discharge of eastern Dome C drainage area, Antarctica, determined from airborne radar survey and satellite image analysis, Journal of Glaciology, 46, pp. 253-273.

Gardelle J., Berthier E. and Arnaud Y. (2012) Slight mass gain of Karakoram glaciers in the early twenty-first century", Nature Geoscience, 5, pp. 322-325.

Hall D.K., Riggs G.A. and Salomonson V.V. (1995) Development of methods for mapping global snow cover using moderate resolution imaging spectroradiometer data, Remote Sensing of Environment, 54, pp. 127-140.

Hall D.K., Giffen B.A. and Chien J.Y.L. (2005) Changes in the Harding Icefield and the Grewingk-Yalik Glacier Complex, 62nd Eastern Snow Conference, Waterloo, ON, Canada, pp. 29-40.

Haq M.A., Jain K. and Menon K.P.R. (2012) Change Monitoring of Gangotri Glacier using Remote Sensing, International Journal of Soft Computing and Engineering (IJSCE), 1, 6, pp. 259-261.

Hardy D.R., "Kilimanjaro", in Singh V.P., Singh P. and Haritashya (Eds.) (2011) Encyclopedia of Snow, Ice and Glaciers, Dordrecht, pp. 672-679.

Hastenrath S. (2006) Diagnosing the decaying glaciers of equatorial East Africa, Meteorologische Zeitschrift, 15, pp. 265-271.

Hubbard A., Willis I., Sharp M., Mair D., Nienow P., Hubbard B. and Heinz B. (2000) Glacier mass-balance determination by remote sensing and high-resolution modelling, Journal of Glaciology, 46, 154, pp. 491-498.

Huggel C., Kääb A., Haeberli W., Teysseire P. and Paul F. (2002) Remote sensing based assessment of hazards from glacier lake outbursts: a case study in the Swiss Alps, Canadian Geotechnical Journal, 39, pp. 316-330.

Jiskoot H., "Glacier surging", in Singh V.P., Singh P. and Haritashya (Eds.) (2011) Encyclopedia of Snow, Ice and Glaciers, Dordrecht, pp. 415-428.

Jouvet G., Huss M., Funk M. and Blatters H. (2011) Modelling the retreat of Grosser Aletschgletscher, Switzerland, in a changing climate, Journal of Glaciology, 57, pp. 1033-1045.

Kääb A. (2001) Photogrammetric Reconstruction of Glacier Mass-Balance using a Kinematic Ice-flow Model. A 20-year Time-Series on Grubengletscher, Swiss Alps, Annals of Glaciology, 31, pp. 45-52.

Kääb A., Paul F., Maisch M., Hoelzle M. and Haeberli W. (2002) The new remote sensing derived Swiss glacier inventory: II. First results, Annals of Glaciology, 34, pp. 362-366.

Kääb A., Huggel C., Fischer L., Guex S., Paul F., Roer I., Salzmann N., Schlaefli S., Schmutz K., Schneider D., Strozzi T. and Weidmann Y. (2005) Remote sensing of glacier and permafrost-related hazards in high mountains: an overview, Natural Hazards and Earth System Science, 5, pp. 527-554.

Kaser G., Hardy D.R., Mölg T., Bradley R.S. and Hyera T.M. (2004) Modern glacier retreat on Kilimanjaro as evidence of climate change: observations and facts, International Journal of

Climatology, 24, pp. 329-339.

Kaufmann V. (2012) The evolution of rock glacier monitoring using terrestrial photogrammetry: the example of Äusseres Hochebenkar rock glacier (Austria), Austrian Journal of Earth Sciences, 105, 2, pp. 63-77.

Kirkbride M. “Debris-covered glaciers”, in Singh V.P., Singh P. and Haritashya (Eds.) (2011) Encyclopedia of Snow, Ice and Glaciers, Dordrecht, pp. 190-192.

Knoll C. and Kerschner H. (2009) A glacier inventory for South Tyrol, Italy, based on airborne laser-scanner data, Annals of Glaciology, 50, 53, pp. 46-52.

Kulkarni A.V., Bahuguna I.M., Rathore B.P., Singh S.K., Randhawa S.S., Sood R.K. and Dhar S. (2007) Glacial retreat in Himalaya using Indian Remote Sensing satellite data, Current Science, 92, 1, pp. 69-74.

Malinverni E.S., Croci C. and Sgroi F. (2008) Glacier Monitoring by Remote Sensing and GIS Techniques in Open Source Environment, EARSeL eProceedings, 7, 2, pp. 120-132.

Masetti M., Diolaiuti G., D’Agata C. and Smiraglia C. (2009) Hydrological characterization of an ice-contact lake: Miage Lake (Monte Bianco, Italy), Water Resources and Management, 24, pp. 1677-1696.

Mattson L.E., Gardner J.S. and Young G.J., (1993) Ablation on debris-covered glaciers: an example from the Rakhiot Glacier, Punjab, Himalaya, IAHS Publ., 218, pp. 289-296.

Mihalcea C., Mayer C., Diolaiuti G., D’Agata C., Smiraglia C. and Tartari G. (2006) Ice ablation and meteorological conditions on the debris covered area of Baltoro Glacier (Karakoram, Pakistan), Annals of Glaciology, 43, pp. 292-300.

Mihalcea C., Brock B.W., Diolaiuti G., D’Agata C., Citterio M., Kirkbride M.P., Cutler M.E.J. and Smiraglia C. (2008) Using ASTER satellite and ground-based surface temperature measurements to derive supraglacial debris cover and thickness patterns on Miage Glacier (Mont Blanc Massif, Italy), Cold Regions Science and Technology, 52, pp. 341-354.

Minora U., Bocchiola D., D’Agata C., Maragno D., Mayer C., Lambrecht A., Mosconi B., Vuillermoz E., Senese A., Compostella C., Smiraglia C. and Diolaiuti G. (2013) 2001-2010 glacier changes in the Central Karakoram National Park: a contribution to evaluate the magnitude and rate of the ‘Karakoram anomaly’”, The Cryosphere Discussion, 7, pp. 2891-2941.

Mölg T., Hardy D.R. and Kaser G. (2003) Solar radiation-maintained glacier recession on Kilimanjaro drawn from combined ice-radiation geometry modeling, Journal of Geophysical Research, 108, p. 4731.

Mölg T., Cullen N.J., Hardy D.R, Winkler M. and Kaser G. (2009) Quantifying Climate Change in the Tropical Midtroposphere over East Africa from Glacier Shrinkage on Kilimanjaro”, Journal

of Climate, 22, pp. 4162-4181.

Moore G. (1980) Satellite remote sensing of water turbidity, Hydrological Sciences-Bulletin des Sciences Hydrologiques, 25, 4, pp. 407-421.

Morgan V.I., Jacka T.H., Ackerman G.J. and Clarke A.L. (1982) Outlet glaciers and mass-budget studies in Enderby, Kemo and Mac. Robertson lands, Antarctica, Annals of Glaciology, 3, pp. 204-210.

Nakawo M. and Rana B. (1999) Estimate of ablation rate of glacier ice under a supraglacial debris layer, Geografiska Annaler, 81A, 4, pp. 695-701.

Negi H.S., Thakur N.K., Ganju A. and Snehmani (2012) Monitoring of Gangotri glacier using remote sensing and ground observations, Journal of Earth System Science, 121, 4, pp. 855-866.

Nuth C., Kohler J., Aas H.F., Brandt O. and Hagen J.O. (2007) Glacier geometry and elevation changes on Svalbard (1936–90): a baseline dataset, Annals of Glaciology, 46, pp. 1-11.

Osmaston H. “Glaciers, glaciations and equilibrium line altitudes on Kilimanjaro”, in Mahaney W.C. (Ed.) (1989) Quarternary and environmental research on East African mountains, Rotterdam, Balkema, pp. 7-30.

Paul F. (2002) Changes in glacier area in Tyrol, Austria, between 1969 and 1992 derived from Landsat 5 Thematic Mapper and Austrian Glacier Inventory data, International Journal of Remote Sensing, 23, 4, pp. 787-799.

Paul F., Kääb A., Maisch M., Kellenberger T. and Haeberli W. (2002) The new remote-sensing-derived Swiss glacier inventory: I. Methods, Annals of Glaciology, 34, pp. 355-361.

Paul F., Kääb A. and Haeberli W. (2007) Recent glacier changes in the Alps observed by satellite: Consequences for future monitoring strategies, Global and Planetary Change, 56, pp. 111-122.

Paul F., Barrand N.E., Baumann S., Berthier E., Bolch T., Casey K., Frey H., Joshi S.P., Konovalov V., Le Bris R., Mölg N., Nosenko G., Nuth C., Pope A., Racoviteanu A., Rastner P., Raup B., Scharrer K., Steffen S. and Windswold S. (2013) On the accuracy of glacier outlines derived from remote-sensing data. Ann. Glaciol. 54 (63).

Rabagliati R. and Serandrei Barbero R. (1979) Possibilità d’impiego del remote sensing da satellite per il controllo annuale dei ghiacciai, Geografia Fisica e Dinamica del Quaternario, 2, pp. 35-40.

Racoviteanu A.E., Williams M.W. and Barry R.G. (2008) Optical Remote Sensing of Glacier Characteristics: A Review with Focus on the Himalaya, Sensors, 8, pp. 3355-3383.

Scherler D., Bookhagen B. and Strecker M. (2011) Spatially variable response of Himalayan glaciers to climate change affected by debris cover, Nature Geoscience, 4, pp. 156-159.

Shi J.C. and Dozier J. (1997) Mapping seasonal snow with SIR-C/X-SAR in mountainous areas, Remote Sensing of Environment, 59, 2, pp. 294-307.

Smiraglia C. and Diolaiuti G., “Epiglacial Morphology”, in Singh V.P., Singh P. and Haritashya (Eds.) (2011) Encyclopedia of Snow, Ice and Glaciers, Dordrecht, pp. 262-268.

Stringer W.J. and Groves J.E. (1991) Location and Areal Extent of Polynyas in the Bering and Chukchi Seas, Arctic, 44, pp. 164-171.

Tabacco I.E., Bianchi C., Chiappino M., Zirizzotti A. and Zuccheretti E. (2000) Analysis of bottom morphology of the David Glacier-Drigalski Ice Tongue, East Antartica, Annals of Glaciology, 30, pp. 47-51.

Villa F., Sironi S., DeAmicis M., Maggi V., Zucca F. and Tamburini A. (2007) Integration of Different Kind of Remote Sensing Data as a Tool for Quantitative Analysis of Glacier Evolution, 9th International Symposium on High Mountain Remote Sensing Cartography, Grazer Schriften der Geographie und Raumforschung, 43, pp. 103-108.

WGMS (compiled by Zemp M., Frey H., Gärtner-Roer I., Nussbaumer S.U., Hoelzle M., Paul F. and Haeberli W.) (2012) Fluctuations of Glaciers 2005-2010, vol. X, Zurich, Switzerland, ICSU(WDS)/IUGG(IACS)/UNEP/UNESCO/W MO, World Glacier Monitoring Service.

Williams R.S. and Ferrigno J.G. (Eds.) (2012) Satellite Image Atlas of Glaciers of the World. State of the Earth’s Cryosphere at the Beginning of the 21st Century: Glaciers, Global Snow Cover, Floating Ice, and Permafrost and Periglacial Environments, U.S. Geological Survey, Professional Paper 1386–A, Washington, United States Government Printing Office.

Wuite J., Jezek K.C., Wu X., Farness K. and Carande R. (2009) The velocity field and flow regime of David Glacier and Drygalski Ice Tongue, Antarctica, Polar Geography, 9, pp. 111-127.

Chapter 6

Conclusions

Glaciers are sensitive climate indicators because they adjust their size in response to changes in climate (e.g. temperature and precipitation). The attention paid by the scientists to mountain glacier change is increasing as there is robust evidence of a global glacier shrinkage over the past five decades, which in turn is the consequence of global warming. Understanding the glacier response to climate change is of tremendous importance not only for improving scientific knowledge, but also to predict and manage water resources and natural hazard risks for the people living in mountain areas in the short (e.g. glacier lake outburst floods), and long term (e.g. droughts).

This doctoral dissertation focused on different applications of remote sensing to studying the cryospehere. In particular, two major case studies were presented: the evolution of the glaciers in the Central Karakoram National Park (CKNP) in Northern Pakistan, and the snow cover variability of eighteen mountain watersheds of the Chilean central Andes.

The main aims of the present work were to provide a complete and detailed glacier inventory of the CKNP, and to study the evolution of glaciers therein during 2001–2010. As the glaciers in the Karakoram region are famous for being ones of the few in the world in stable condition on average —from here the term “Karakoram Anomaly”—, this work investigated on the causes of such uncommon behaviour. To this regard, it was necessary to assess the recent climate change of the region, and to relate it to the glacier change.

Then, a model to evaluate ice ablation both at debris-free and debris-covered areas was proposed, to quantify the amount of freshwater due to ice melt at the glacier surface. The effect of a debris cover on the actual glacier melt was considered and evaluated in the model. To the author's knowledge, this is the first such model which combines usability (few and easily obtainable inputs), applicability (different scales and locations), and precision at the same time.

Finally, a methodology to study SCA variability was implemented for eighteen watersheds of central Chile, and then it was applied in the CKNP area as well.

In chapter 2 the focus was initially on the compilation of the CKNP glacier inventory. Glacier outlines were drawn manually over different Landsat images using a GIS. An automatic approach was not suitable in this case because the supraglacial-debris (which is abundant in the study area) is too similar (spectrally) to the glacier surroundings, and so the existing methods still fail to recognize the actual glacier outlines properly and would need major efforts for manual corrections afterwards. The glacier outlines were obtained for the years 2001 and 2010. All the glaciers in the CKNP were mapped, for a total of 711 glacier bodies covering about 4600 km^2.

The next focus of chapter 2 was to analyze the glacier change occurred during the two reference years. The area change during 2001–2010 was +0.4 ± 202.9 km^2 over 4605.9 ± 86.1 km^2 in 2001, evidence of a certain stability. This is in accordance with the Karakoram Anomaly. The possible causes of glacier stability were then analyzed in view of the ongoing climate change. A slight

increase in late summer SCA during 2001–2010 was observed from MODIS snow data. At the same time, the available weather stations revealed an increase of snowfall events and a decrease of mean summer air temperatures since 1980, which would translate into more persistent snow cover during the melt season. These results support an enhanced glacier preservation in the ablation areas due to a long-lasting snow cover, and stronger accumulation at higher altitudes, pushing towards positive net balances. Nevertheless, linking these observations to the analysis of glacier area changes is not unambiguous, since there is a delay of the glacier area response to climate change depending on glacier size, with usually longer response times (even several decades) for larger glaciers (Bolch and others, 2012).

In chapter 3, a model to evaluate ice melt over the ablation area of the same CKNP glaciers was described. It is a distributed model able to evaluate both debris-covered and debris-free ice ablation below 5200 m a.s.l. (elevation of the equilibrium line altitude of Baltoro glacier). It is made up of two main parts: an enhanced T-index part for the debris-free areas (Pellicciotti and others, 2005), and a conductive heat flux part for the debris-covered ones (Mihalcea and others, 2008). The model was calibrated and validated using two sets of an ablation dataset collected in the field in the CNKP. Snow melt was neglected since snow data in the study area was not systematically available. The model was run against the peak ablation season (23 July–9 August 2011), when meltwater is largely derived from ice melt, with snow thaw playing a minor role (Soncini and others, 2015). Glacier features (i.e. surface area, supraglacial-debris occurrence and thickness), were estimated from remote sensing analysis as in chapter 2. Meteorological input data were distributed starting from data acquired at Askole automatic weather station, located within the CKNP. The meteorological distribution was validated by comparison with data from other two AWS in the same park limits (Urdukas and Concordia). The modeled ablation data were in strong agreement with measurements collected in the field during 2011 on Baltoro glacier, which is representative of CKNP glaciers.

The total freshwater from the ablation areas of CKNP glaciers estimated by the model was 1.963 km^3 (0.109 km^3 d^{-1} on average). The meltwater from the debris-covered parts was 0.223 km^3 (on average, 0.012 km^3 d^{-1}; min–max 0.006–0.016 km^3 d^{-1}), and 1.740 km^3 (on average, 0.097 km^3 d^{-1}; min–max 0.041–0.139 km^3 d^{-1}) from debris-free sectors. The estimated total freshwater corresponds to 14% of the water contained in a large strategic dam along the Indus River, of which all the CKNP glaciers are tributaries.

The proposed model requires only a small number of input data, such as air temperature and SW_{in} (recorded by most of the standard AWS), a DEM, and debris thickness measurements collected in the field. It should provide portability to other regions, although adjustments of the parameters against field measurements are necessary. In particular, (1) the lapse rate to distribute the air temperature should be locally evaluated; (2) the use of a constant albedo value might require adjustment to fit the actual local characterization of the glacier surface (e.g. in case of debris-free ice affected by dust and black carbon deposition, Azzoni and others (2014)); (3) the debris effective thermal resistance (DR) estimation requires debris-covered ice ablation and debris surface

temperature data collected in the field.

Finally, the sensitivity tests suggest that melting will increase largely if summer air temperature increases. Also, any increase in the extent of debris coverage (which will likely occur due to augmented macrogelivation processes and rockfall events), will affect melt depending on new debris thickness.

The aim addressed in chapter 4 was to implement a methodology to analyze the snow cover variability over a large time- and spatial-scale. In particular, the methodology was implemented to study the SCA variation over eighteen mountain watersheds of the central Andes in Chile during 2008–2011. Because of the computational limit to analyze the study area in its entirety (it is more than 200,000 km^2), the zone was divided into three major sub-zones (Northern, Central, and Southern). The proposed methodology uses the MOD10A2 snow product (derived from MODIS sensor from the NSIDC), to extract snow maps on a daily basis, discarding those days with too much cloud cover (the threshold was set to 30% as a best trade-off between data quality and availability). The method combines some GIS geoprocessing tools with the Python programming language for automation purposes.

Overall, SCA decreased during the four considered years. The maximum SCA was found in the Central Zone, while the topographic and climatic features (i.e. lower altitudes in the South, and a drier climate in the North), limited snow deposition elsewhere. The snow line was found higher in the Northern zone due to the presence of the plateau, while it decreases southwards. In the Northern Zone the minimum SCA was reached sooner than elsewhere, and it lasted for a longer period (November to March), probably because of the drier climate. West aspects showed the maximum of SCA in all zones throughout the study period.

As said, the same methodology to analyze SCA variation in Chile proposed in chapter 4 was adopted for the CKNP region, for investigating the climate change occurred during 2001–2010.

Finally, chapter 5 described some examples of remote sensing applied to glaciers of various typology, size, and localization. Here, six case studies were shown, amongst which there are three alpine glaciers (Miage, Freney, Aletcsh), equatorial glaciers (the Kilimanjaro glaciers), the Harding Icefield in Alaska, and an Antarctic glacier (the Drygalsky Ice Tongue).

As for the Freney glacier, it was discussed how for such a small glacier the pixel resolution of the Landsat 8 satellite (30 m) was not sufficient as in the other glaciers to recognize its features properly. Moreover, in the section dedicated to the Drygalsky Ice Tongue, the benefit from having a broad wavelength of the electromagnetic spectrum being registered by the OLI sensor of the Landsat 8 satellite was evident: the short infra red band (band 7, from 2.11 to 2.29 μm), facilitated the individuation of the actual limits of the ice tongue compared to the other bands, because of the enhanced difference between the emissivity of the solid and liquid water at this frequency compared to the other wavelengths. This permitted to easily distinguish between snow and ice in the satellite image.

References

Azzoni R.S., Senese A., Zerboni A., Maugeri M., Smiraglia C. and Diolaiuti G. (2014) A novel integrated method to describe dust and fine supraglacial debris and their effects on ice albedo: the case study of Forni Glacier, Italian Alps. Cryosphere Discuss., 8, 3171–3206 (doi: 10.5194/tcd-8-3171-2014)

Bolch T., Kulkarni A., Kääb A., Huggel C., Paul F., Cogley J.G., Frey H., Kargel J.S., Fujita K., Scheel M., Bajracharya S. and Stoffel M. (2012) The state and fate of Himalayan glaciers. Science 336: 310-314.

Mihalcea C., Mayer C., Diolaiuti G.A., D'agata C., Smiraglia C., Lambrecht A., Vuillermoz E. and Tartari G. (2008) Spatial distribution of debris thickness and melting from remote-sensing and meteorological data, at debris-covered Baltoro glacier, Karakoram, Pakistan. Ann. Glaciol. 48: 49-57.

Pellicciotti F., Brock B.W., Strasser U., Burlando P., Funk M. and Corripio J.G. (2005) An enhanced temperature-index glacier melt model including shortwave radiation balance: development and testing for Haut Glacier d'Arolla, Switzerland. J. Glaciol., 51, 573–587 (doi: 10.3189/172756505781829124)

Soncini A., Bocchiola D., Confortola G., Bianchi A., Rosso R., Mayer C., Lambrecht A., Palazzi E., Smiraglia C., Diolaiuti G. (2015). Future hydrological regimes in the upper Indus basin: a case study from a high altitude glacierized catchment, J. Hydrometeorology, 16(1):306-326.

Curriculum Vitae

Umberto Minora earned the Master's degree in “Sciences of Nature” on Febraury 2012 (grade: 110/110 cum laude) at the University of Milan, under the supervision of professor Claudio Smiraglia and prof Guglielmina Diolaiuti. He started his PhD career at the department of Earth Sciences “Ardito Desio” (University of Milan), the same year under the guide of the same tutors, and professor Mauro Guglielmin of the Insubria University. On July 2015 he started working at One Team srl as a GIS specialist and consultant.

His main interest is the analysis of cryospheric processes by means of remote sensing and field campaigns. His research involves data retrieval through remote sensing (multispectral images) and quality check; collection of field samples; production of glacier inventories, of snow and permafrost maps. He acquired experience in the advanced use of GIS and image processing softwares (e.g. ENVI), that are essential to his research. His work entails the production and use of Python scripts which recall GIS functionalities to produce (e.g.) annual global radiation maps, or to mask specific land features over an image (such as clouds, shadows, snow, etc.). He uses MATLAB/GNU Octave to produce physical models — requiring remote sensing and weather station data as inputs, and the field samples for calibration and validation — for the analysis of the evolution of the cryosphere through time. In particular, during his PhD program he has been focusing on the areas of the Karakoram and Himalayan Ranges, studying on site and in lab the processes driving glacier and snow melt, in presence or absence of a supraglacial debris.

List of Publications

1. Fea M., **Minora U.**, Pesaresi C., Smiraglia C. (2014) Remote sensing and interdisciplinary approach for studying glaciers, Journal of Research and Didactics in Geography (J-READING), 2, 2, pp.115–142, DOI: 10.4458/2379-10

2. **Minora U.**, Bocchiola D., D'Agata C., Maragno D., Mayer C., Lambrecht A., Mosconi B., Vuillermoz E., Senese A., Compostella C., Smiraglia C. and Diolaiuti G. (2013) 2001-2010 glacier changes in the Central Karakoram National Park: a contribution to evaluate the magnitude and rate of the "Karakoram anomaly", The Cryosphere Discussion, http://www.the-cryosphere-discuss.net/7/2891/2013/tcd-7-2891-2013.html, 2013

3. **Minora U.**, Senese A., Bocchiola D., Soncini A., D'Agata C., Ambrosini R., Mayer C., Lambrecht A., Vuillermoz E., Smiraglia C. and Diolaiuti G. (2015) A simple model to evaluate ice melt over the ablation area of glaciers in the Central Karakoram National Park, Pakistan, Annals of Glaciology, Vol.56, N.70,pp.202–216(15)

4. **Minora U.**, Godone D., Lorenzini S., D'Agata C., Bocchiola D., Barcaza G.S., Smiraglia C. and Diolaiuti G. (2016) 2008–2011 snow covered area (SCA) variability over 18 watersheds of the central Chile through MODIS data, Geografia Fisica e Dinamica Quaternaria, Vol.38,Issue 2, pp.169–174, DOI: 10.4461/GFDQ.2015.38.15

5. **Minora U.**, Bocchiola D., D'Agata C., Maragno D., Mayer C., Lambrecht A., Vuillermoz E., Senese A., Compostella C., Smiraglia C., Diolaiuti G.Glacier area stability in the Central Karakoram National Park (Pakistan) in 2001–2010 — the "Karakoram Anomaly" in the spotlight, *under revision*

6. Smiraglia C., **Minora U**., Diolaiuti G. (2014) L'evoluzione recente delle coste antartiche. Il Caso del Drygalsky Ice Tongue (DIT), Terra Vittoria Settentrionale. Studi Costieri, 22, pp. 171-178.

Abstracts:

1. **Minora U.**, Mayer C., Bocchiola D., D'Agata C., Maragno D., Lambrecht A., Mosconi B., Vuillermoz E., Smiraglia C., Diolaiuti G.: The recent changes of the supra-glacial debris cover in the Central Karakoram National Park (CKNP, Pakistan), Geophysical Research Abstracts, Vol. 15, EGU2013-14192, EGU General Assembly 2013.

2. **Minora U.**, Mayer C., Bocchiola D., D'Agata C., Maragno D., Lambrecht A., Vuillermoz E., Smiraglia C., Diolaiuti G.: Is supraglacial debris actually playing a role in driving the Karakoram Anomaly?, Geophysical Research Abstracts, Vol. 16, EGU2014-14206, EGU General Assembly, 2014.

3. **Minora U.**, Mayer C., Bocchiola D., D'Agata C., Maragno D., Lambrecht A., Vuillermoz E.,

Smiraglia C., Diolaiuti G.: Mapping distribution and thickness of supraglacial debris in the Central Karakoram National Park: main features and implications to model glacier melt water, Geophysical Research Abstracts, Vol. 16, EGU2014-14258, EGU General Assembly, 2014.

International conferences:

- ✓ **Alpine Glaciology Meeting**

2013 *2001–2010 glacier changes in the Central Karakoram National Park: a contribution to evaluate the magnitude and rate of the "Karakoram anomaly"*, poster presentation, 14 February 2013, Grenoble, France.

2014 *2001–2010 glacier changes in the Central Karakoram National Park: a contribution to evaluate the magnitude and rate of the "Karakoram Anomaly"*, oral presentation, 27 February 2014, Innsbruck, Austria.

2015 *The state of the glaciers in the Central Karakoram National Park, Northern Pakistan*, oral presentation, 7–9 May 2015, Milan, Italy.

- ✓ **European Geosciences Union, General Assembly**

2013 *The recent changes of the supra-glacial debris in the Central Karakoram National Park (CKNP, Pakistan)*, poster presentation, 10 April 2013, Vienna, Austria.

2014 *Mapping distribution and thickness of supraglacial debris in the Central Karakoram National Park: main features and implications to model glacier meltwater*, poster presentation, 27 April–2 May 2014, Vienna, Austria.

- ✓ **Pakistan Water Summit 2014**: *Ongoing processes in Karakoram glaciers: recent findings from field observations and ground based monitoring networks*, oral presentation, 19 March 2014, Islamabad, Pakistan.

Field campaigns:

2012a. Changri Nup glacier expedition (Sagarmatha National Park, Nepal), SHARE-PAPRIKA project under the umbrella of EvK2-CNR committee.

2012b. Remote sensing consultant at *Dirección General de Aguas* (Chilean Ministry of Public Works, Santiago de Chile, Chile), *Chile-Action Plan For The Conservation Of Glaciers To Climate Change* project, promoted by the Inter-American Bank for the Development, the EvK2-CNR committee, and the University of Milan.

2013. Baltoro glacier expedition (Shigar Valley, Pakistan) SHARE-PAPRIKA and SEED projects, promoted by the EvK2-CNR committee and coordinated by the University of Milan.

2014. Khumbu expedition (Sagarmatha National Park, Nepal), KHUMBU HYDROLOGY project, promoted by the EvK2-CNR committee and coordinated by Politecnico di Milano.